UNIVERSITÀ DEGLI STUDI DI ROMA "TOR VERGATA"

Macroarea di Scienze Matematiche, Fisiche e Naturali

Corso di Laurea Magistrale in Fisica

Tesi di Laurea

Validation of a New Bunch Crossing Identification Decision Logic for the ATLAS Level-1 Calorimeter Trigger using Saturated Pulser Runs

Validazione di una nuova logica di decisione per il Bunch Crossing Identification per il trigger calorimetrico di livello 1 di ATLAS.

CANDIDATO

Francesco Maria Follega

RELATORI

Prof.ssa Anna Di Ciaccio

Prof. Hans-Christian Schultz-Coulon

Anno Accademico 2015/2016

Riassunto della Tesi

Il rivelatore ATLAS è uno dei quattro principali esperimenti al *Large Hadron Collider* (LHC) di Ginevra. Quest'ultimo accelera due fasci di protoni, organizzati in *bunches* da $1.5\text{x}10^{11}$ protoni ciascuno. LHC può accelerare contemporaneamente fino a 2800 *bunches* e produce collisioni attualmente ad un energia di 13 TeV nel sistema del centro di massa. L'istante dell'incrocio tra due *bunches* viene chiamato chiamato *Bunch Crossing* (ogni 25 ns). Nelle interazioni tra i protoni hanno luogo numerose collisioni sovrapposte (eventi di pile-up). Le particelle si propagano dai differenti vertici di interazione in tutte le direzioni e vengono rivelate dal detector.
Nelle collisioni al *Large Hadron Collider*, solamente in una piccola frazione degli eventi vengono prodotte particelle con alto impulso trasverso, corrispondenti a eventi di *hard scattering* tra i costituenti dei protoni, i quark. Questi eventi di interesse vengono filtrati da un sistema chiamato trigger. Il trigger di ATLAS è formato da vari livelli: il *Livello 1* e un secondo livello chiamato *High Level Trigger* (HLT). Il primo livello di trigger è diviso a sua volta in vari sottosistemi, uno dei quali è il trigger calorimetrico di livello 1, chiamato *Level-1 Calorimeter Trigger* (L1Calo). Questo sistema è stato progettato per utilizzare l'informazione proveniente dai due calorimetri di ATLAS e separare e ricostruire l'energia dei numerosi eventi di pile-up prodotti in un singolo bunch crossing. Infatti, il segnale analogico prodotto dalle particelle che si propagano nelle celle calorimetriche dura tipicamente il tempo di 5-6 *bunch crossings*, pari a 125-150 ns. Pertanto si rende necessario associare il segnale misurato al *bunch crossing* nel quale è avvenuta l'interazione che l'ha prodotto.
Una componente fondamentale di L1Calo è il preprocessore, un modulo del sistema che provvede principalmente alla sincronizzazione dei segnali analogici provenienti dalle celle calorimetriche, alla digitalizzazione con frequenza 40 MHz di questi ultimi e all'identificazione del bunch crossing, *Bunch Crossing Identification*(BCID). Il bunch crossing viene identificato all'interno di questo modulo mediante due algoritmi: il *PeakFinder* e il *Saturated BCID*. Entrambi gli algoritmi lavorano a 40 MHz, ma sono progettati per l'analisi di segnali con caratteristiche molto diverse. Il primo è in grado di identificare il *bunch crossing* di segnali a medio bassa energia, mentre il secondo è un algoritmo specializzato per segnali altamente saturati. Poichè gli algoritmi sono due, ma la decisione sul

corretto *bunch crossing* è unica, esiste una logica di decisione che di volta in volta sceglie uno dei due algoritmi, in base a determinati criteri. In questo lavoro di tesi è stata studiata, ottimizzata e convalidata una nuova logica di decisione per alte energie (> 1.5 TeV). La nuova logica permette ai due algoritmi per l'identificazione del bunch crossing di lavorare contemporaneamente, in due differenti regioni di energia. Per stabilire tali regioni di confidenza è stata considerata una nuova variabile: il livello di saturazione del segnale. Con questo nuovo set-up, in uso, sono stati raggiunti ottimi risultati e una buona copertura angolare per entrambi i calorimetri. Il funzionamento della logica è stato studiato attraverso run di calibrazione chiamati *pulser runs*, iniettando segnali di test.
Poichè alcuni segnali ad altissima energia rimangono al di sopra delle soglie del *Saturated BCID* a 40 MHz, è stato provato un nuovo algoritmo chiamato Saturated BCID a 80 MHz. Essenzialmente questo algoritmo è uguale al precedente, ma lavora con il doppio della frequenza di digitalizzazione del segnale. In questo modo le curve di salita dei segnali sono misurate con più precisione e il corretto bunch crossing può essere identificato più facilmente. Non è stato possibile validare questo nuovo algoritmo attraverso i run di calibrazione, poichè ad altissime energie i segnali prodotti dal sistema di iniezione di cariche sono troppo diversi dai segnali ottenuti nelle collisioni p-p. Pertanto la futura validazione di questo nuovo algoritmo dovrà essere effettuata attraverso dati sperimentali raccolti nelle collisioni.

Abstract

The Level-1 Calorimeter Trigger (L1Calo) is one of the main trigger systems of the ATLAS detector. Its decision is based on reduced calorimeter granularity and is taken within a short fixed latency of less than 2.5 μs. L1Calo matches digitized calorimeter pulses to the corresponding bunch crossing of the LHC. This is done by two BCID algorithms. These are the PeakFinder algorithm, for non-saturated pulses, and a thresholding SatBCID algorithm, for saturated pulses. During the first long LHC shutdown the L1Calo hardware was upgraded and amongst other improvements the pile-up treatment has been enhanced. In this way the BCID efficiency for small signals was increased, but at the same time a very small inefficiency in the saturated pulses was introduced. The performances for saturated pulses were restored by the introduction of new decision logic in firmware which combines the PeakFinder and the SatBCID algorithms. Furthermore, studies of run-1 data showed that the SatBCID algorithm would not be able to perform efficiently up to the highest energies available in LHC run-2 in which the center of mass energy is increased from 8 to 13 TeV. Therefore a new SatBCID algorithm was introduced based on the upgraded ADCs which provide the digitized data at 80 MHz resulting in doubled pulse resolution. In this thesis both the performance of the new decision logic and of the Sat80 algorithm have been studied using calibration runs.

Contents

1 Introduction **9**

2 The Large Hadron Collider **13**
2.1 Main Machine Features 13
2.2 Physics at the LHC 14

3 The ATLAS Experiment **16**
3.1 The ATLAS Detector 16
3.1.1 Inner Detector 17
3.1.2 Calorimeters 17
3.1.3 Muon Spectrometer 20
3.1.4 Magnet System 22
3.2 The Trigger System 22
3.2.1 Level-1 Trigger 23
3.2.2 High-level Trigger and Data Aquisition 23

4 The Level-1 Calorimeter Trigger **25**
4.1 The Analog Input 25
4.2 The Pre-Processor Module 27
4.3 Bunch Crossing Identification Algorithms 28

5 Calibration Run Analysis **33**
5.1 Pulser Runs 33
5.2 Analysis Procedure 34
5.3 Pulser vs. Physics Shapes 37

6 The New Decision Logic **40**
6.1 The BCID Decision Logic 40
6.2 Validation Process 44
6.3 Results 45

7 The Updated Saturated BCID Algorithm **59**
7.1 The Algorithm Design 59
7.2 Validation Process 60
7.3 Results 62
7.4 Emulating the Algorithm 64

8 Conclusions **71**

A HAD layer of the LAr calorimeter **74**

B New Tile ADC correlation plots **83**

Bibliography **84**

Acknowledgements **86**

Chapter 1

Introduction

The High Energy Physics (HEP) is finalized to improve the understanding on the smallest constituents of the matter and their fundamental interactions. The most successful model in this field of the physics is the Standard Model, which describes the fundamental interactions of particles (except for the gravitational one): strong, weak and electromagnetic (Fig. 1.1). In 1967 Weinberg [15] and Salam [16] founded the unification of Quantum Electrodynamics (QED) and weak interaction, incorporating the Higgs mechanism in the Glashow's interaction [17]. The Quantum Cromodynamics (QCD) was suggested by Gell-Mann [19] in 1963. The unification of these two theories brought us to the Standard Model. It gave us a way to interpret the particle physics phenomena. Moreover, it creates the base for the investigation of modern physics fundamental issues, such as the origin of the mass, the preponderance of matter compared to antimatter, the existence of "dark matter" and the physics at the time of the Big Bang.
In the Standard model the fundamental particles are gathered in two groups: *fermions* and *boson*. The former have half-integer spin and they are divided in two categories: the *quarks* and the *leptons* (Tab.1.1); while the latter are the *bosons* with integer spin (Tab. 1.2).
The twelve fermions in the model can be used to describe all the ordinary matter. The bosons can be used to explain their interactions. These are represented by the symmetry group S(2)xU(1)xSU(3), where S(2)xU(1) describes the properties of the weak and electromagnetic interactions, whereas SU(3) describes the strong interaction. Therefore, photon and the Z and $W^{\pm}$ bosons refer to the subgroup S(2)xU(1), while eight gluons, whit color charge, refer to SU(3).
The model predicts the existence of an Higgs boson, introduced by Higgs and Englert, in order to explain the masses of the Z and $W^{\pm}$ bosons via the mechanisms

Fermions	Generation			Charge
Quarks	u	c	t	2/3
	d	s	b	-1/3
Leptons	e	μ	τ	-1
	ν_e	ν_μ	ν_τ	0

Table 1.1: Table of all quark and leptons of the different generations.

Force	Boson	Range (m)
Strong	8 gluons	10^{-15}
Weak	Z,$W^{\pm}$	10^{-18}
Electromagnetic	γ	∞

Table 1.2: Table of all the bosons predicted by the Standard Model.

of spontaneous symmetry breaking of SU(2)xU(1) (*Higgs mechanism*) [20].

Starting from this point, many high energy physics experiments were built in order to prove Standard Model predictions and search for new physics beyond it.
The collider experiments are largely used in this field of physics, because of the high energies and collision rate which they can achieve. In this category of experiments, the ATLAS detector, located in Geneva at the LHC ring, is very important (a detailed overview will be given in the next two chapters). Its main contribution concerned the detection of the Higgs boson in 2012 [7].
One of the challenge ATLAS has to face is the analysis of a great number of events

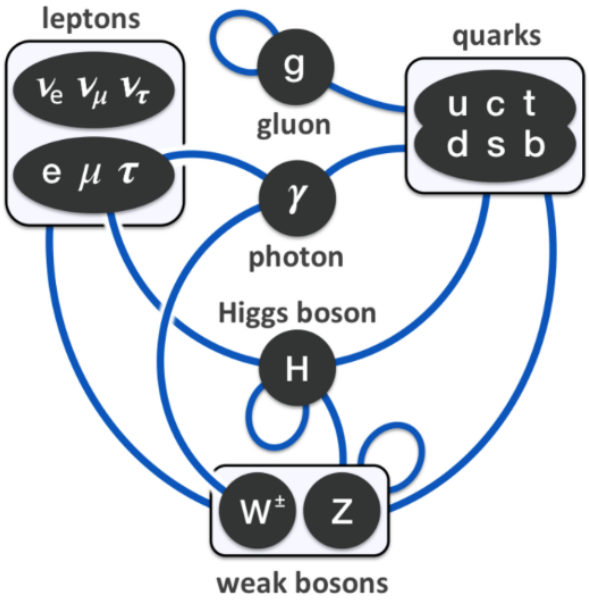

Figure 1.1: Schematic view of the interactions predicted by the Standard Model. The fermions are connected with blue lines which represent the bosons, that make them interact.

produced in a small fraction of time. The LHC produces one billion of events per second (a rate of $\approx$ 1 GHz), which should be analyzed by the detector. Because of this large number of events, the ATLAS detector needs a "trigger". A trigger is essentially a device that tells the whole detector whether an event is physically interesting or not. It is used in order to reduce the rate of events, which have to be processed, and at the same time the size of data, which have to be stored in the hard disks.

In this Master Thesis, the Level-1 Calorimeter Trigger of ATLAS has been studied. Many studies have been carried out by looking at special saturated calibration runs. They were focused on the validation of a new decision logic for the Bunch Crossing Identification algorithms. Moreover, a validation procedure of a new BCID algorithm has been tried, looking once again at calibration runs. The validation procedure has been performed using softwares (ATHENA and ROOT) developed for data analysis.

Chapter 2

The Large Hadron Collider

The Large Hadron Collider (LHC) is a particle accelerator and a collider built near Geneva. It is located in a 27 km long underground tunnel, built between 1984 and 1989 for the CERN LEP machine. In 1998, the CERN Council, thanks to the economic contribution of the member and non member-states, decided to build a machine able to accelerate particles from 0 up to 7 TeV in a circular ring using superconducting magnets. The designed ring purpose was to produce collisions with a large energy spectrum and make them available for the experiments located along the accelerating machine [13].

2.1 Main Machine Features

The CERN accelerator complex (Fig.2.1) has many accelerating rings connected by injectors. It accelerates particles up to 7 TeV by injecting the beams from an accelerating ring to a more energetic one. The LHC speeds up particles from 450 GeV to 7 TeV. The particles are accelerated by superconducting radio-frequency cavities that operate at 400 MHz and they are bent in circular trajectories by a 8.34 T magnetic field, produced by dipole magnets. Such a large magnetic field is provided by 1232 superconducting dipole magnets using niobium-titanium technology. In order to achieve superconductivity properties they have to be cooled down to 1.9 K. Moreover, focusing and defocusing quadrupoles and other correction magnets are placed along the ring.
In every collider experiment the number of events expected for a process with a cross section $\sigma_{process}$ is

$$N_{process} = L\sigma_{process}.$$

where L is a machine parameter called *luminosity*.

The LHC beams are formed by several bunches, each containing 1.15×10^{11} protons. These bunches are spaced approximately 7.48 m, which corresponds to 25 ns. This placement allows to store up to 2800 bunches in the LHC ring. When two bunches cross, the protons collide at an energy of approximately 13 TeV in the center of mass. The time intervel between two bunch collisions is called *bunch spacing*, it is 25 ns at the LHC.

In a bunch, particles follow a gaussian distribution. Therefore the luminosity $\mathcal{L}$ is given by

$$\mathcal{L} = \frac{N_b^2 n_b f \gamma_r}{4\pi\sigma_x\sigma_y}$$

where N_b is the number of particles in the bunch, n_b the number of bunches stored in the beam, f is the revolution frequency, $\sigma_{x,y}$ is the size of the beam along the x,y axis according to a gaussian distribution. The designed luminosity for LHC is $\mathcal{L} = 10^{34} cm^{-2} s^{-1}$. More precisely $\mathcal{L}$ is called *instantaneous luminosity*. We can indeed define another useful parameter, the integrated luminosity, defined as

$$L_{int} = \int \mathcal{L}(t) dt.$$

In our case it can be parametrized as

$$L_{int} = L_0 \tau_L [1 - e^{-T_{run}/\tau_L}]$$

where T_{run} is the total duration of the run, and τ_L is the characteristic luminosity lifetime. Hence, the luminosity L_{int} strongly depends on the ratio between the duration of the run and the characteristic luminosity lifetime. This parameter quantifies the number of collisions available for physics analysis. For Run 2, the LHC machine currently reached an integrated luminosity of $\approx 30\ fb^{-1}$ up to August 2016.

2.2 Physics at the LHC

The LHC has five main experiments placed along the ring. They are:

- ATLAS(A Toroidal LHC ApparatuS) [3] and CMS [6] (Compact Muon Solenoid). They are twin experiments working at $\mathcal{L} = 10^{34} cm^{-2} s^{-1}$ at most. They both investigate high energetic p-p collisions and explore physics at the Terascale;
- LHCb (LHC beauty experiment) [21] focuses on b-physics. It reaches its efficiency at a luminosity of $\mathcal{L} = 10^{32} cm^{-2} s^{-1}$, lower than the nominal one, in order to have mainly just one collision per event;
- TOTEM (Total Cross Section,Elastic Scattering and Diffraction Dissociation) [24] built for high precision measurements of p-p interaction cross sections and designed for a deep study of the proton inner structure. It works at a luminosity of $\mathcal{L} = 10^{29} cm^{-2} s^{-1}$;
- ALICE (A Large Ion Collider Experiment) [1] , working at a luminosity of $\mathcal{L} = 10^{27} cm^{-2} s^{-1}$. This experiment differs from the previous p-p ones because it makes use of ion beams. It is optimized for heavy ion collisions, such as lead-lead collisions, in order to study the physics of strong interacting matter at very high densities.

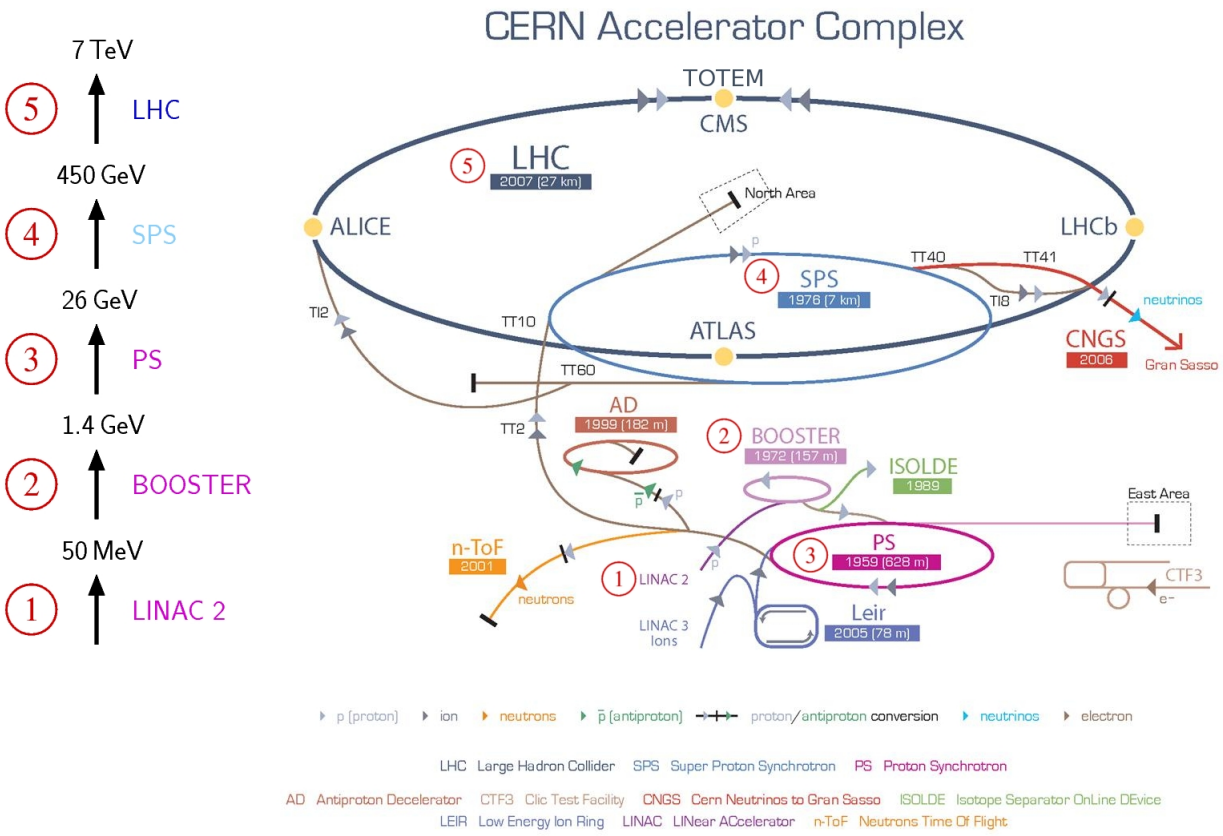

Figure 2.1: CERN Accelerator Complex and its main experiments [14].

Chapter 3

The ATLAS Experiment

3.1 The ATLAS Detector

In modern times it is very challenging to build a particle detector. Indeed, the high luminosity, the large energies achieved and the large number of produced particles in the collisions put strict requirements on the new detectors. In this thesis I am going to talk about one of the LHC experiments appointed to study the p-p collisions: the ATLAS detector. The ATLAS detector was built in five years (2003-2008) thanks to the collaborations and the studies of a large number of physicists and technicians. In order to work well the ATLAS detector has to fulfill many requirements:

- good space-time resolution and a great energy resolution for the calorimeters;
- high granularity in order to avoid overlapping events in particular due to pile-up;
- fast electronics and a good selection criteria in such a way to pick out only a small fraction of events and decrease the initial rate of ≈1 GHz down to 500-1000 Hz. which is the storage rate;
- radiation-hard components;
- a magnetic system in order to measure the momentum of charged particles;

The ATLAS detector is shown in figure 3.1. It has a cylindrical symmetry around the beam axis with 25 m in diameter and 45 m in length. It weighs 7000 tons ca and it is the largest experiment ever installed at CERN. The nominal coordinates are η and ϕ, the former longitudinal and the latter radial. The η coordinate is defined as

$$\eta = -\ln[\tan(\theta/2)]$$

where θ is the angle between the momentum $\vec{p}$ of the particle and the beam axis. The ϕ coordinate is simply the azimuthal angle, measured around the beam axis.
The ATLAS detector is divided in several parts: the *Inner Detector*, used to track and find vertices; the *Electromagnetic and Hadronic Calorimeters*, employed to measure the energy of the collision products; the *Muon System*, which detects muons [3].

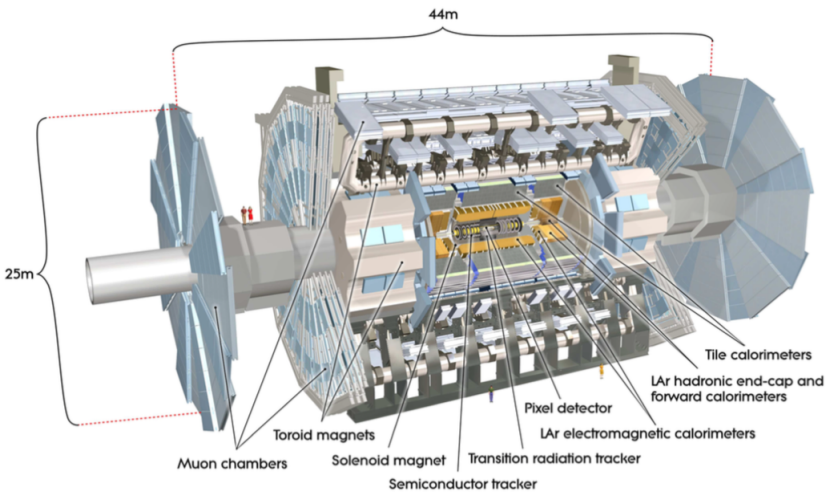

Figure 3.1: Picture of the ATLAS detector [3].

3.1.1 Inner Detector

The inner detector (ID), shown in Fig. 3.2, is used to track particles and reconstruct vertices. It contributes mainly to the identification of particles like electrons, photons and muons. The tracking procedure and the measurements of the transverse momentum and energy are possible thanks to the strong solenoid. It produce a field $B = 2T$ and consequently the charged particles trajectories are curved and the momentum p can be extracted by the bending radius ρ as follows [3]

$$p = \frac{qB\rho}{c}$$

where c is the speed of light and q the charge of the particle.
The ID extends between $-2.5 < \eta < 2.5$ and it has a symmetric structure in η and in ϕ . It is composed of many subsystems. Starting from the center they are:

1. the Pixel Detectors;
2. the semiconductor tracker (barrel and end-caps);
3. the transition radiation tracker (barrel and end-caps);

3.1.2 Calorimeters

There are two calorimeters in the ATLAS (Fig.3.3): the Electromagnetic Calorimeter and the Hadronic Calorimeter. Both of them are sampling calorimeters. The former is used for the detection of particles such as e, e^+, γ. It makes use of Liquid Argon technology using lead as absorber. The latter, instead, is used to measure hadrons, jets and taus. It uses scintillating tiles as active material and steel as absorber.
The calorimeters form two concentric layers covering a region between $-4.9 < \eta < 4.9$. Both of them have a good containment of the particle showers, in order to keep

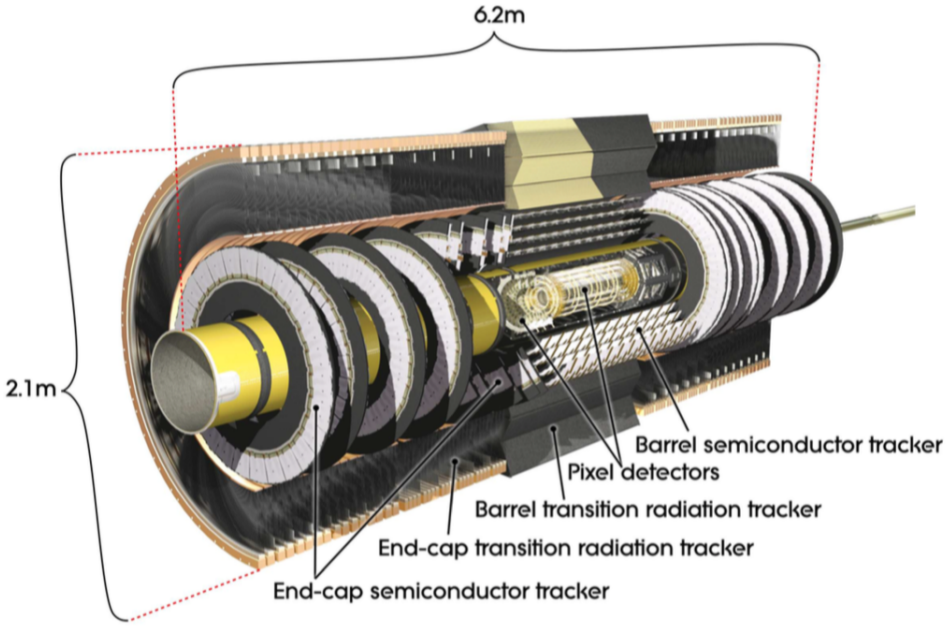

Figure 3.2: Picture of the ATLAS inner detector [3].

Calorimeter	η	$\Delta\eta$x$\Delta\phi$ granularity
Electromagnetic Barrel	$\|\eta\| < 1.475$	0.3 x 0.1
Electromagnetic End-Cap	$1.375 < \|\eta\| < 3.2$	0.1 x 0.1
Hadronic Barrel	$\eta\| < 1.0$	0.1 x 0.1
Hadronic End-Cap	$1.5 < \|\eta\| < 2.5$	0.1 x 0.1
	$2.5 < \|\eta\| < 3.2$	0.2 x 0.2
Forward Calorimeter	$3.1 < \|\eta\| < 4.9$	0.2 x 0.2

Table 3.1: The granularity in the different regions of the ATLAS calorimeters.

all the information of the interaction without losing energy resolution. Furthermore, they have different granularities depending on the η region as shown in Tab.3.1.

The LAr Caloriemter

The LAr calorimeter is a LAr-lead calorimeter with fine granularity and a very good angular coverage. The particle showers develop in the lead, ionize the LAr in between and the charges are collected on the kapton electrodes. This calorimeter has an inner structure: the *Electromagnetic Barrel* and the *Electromagnetic End-Cap Calorimeter*. The first one is composed of 16 identical modules. Each of them, in turn, is formed by three layers and a pre-sampler (in particular in the barrel). These layers are the *Front Layer*, the *Middle Layer* and the *Back Layer*. The granularity decreases from the Front Layer to the Back Layer.

The Electromagnetic End-Cap Calorimeter is composed of two disks arranged in

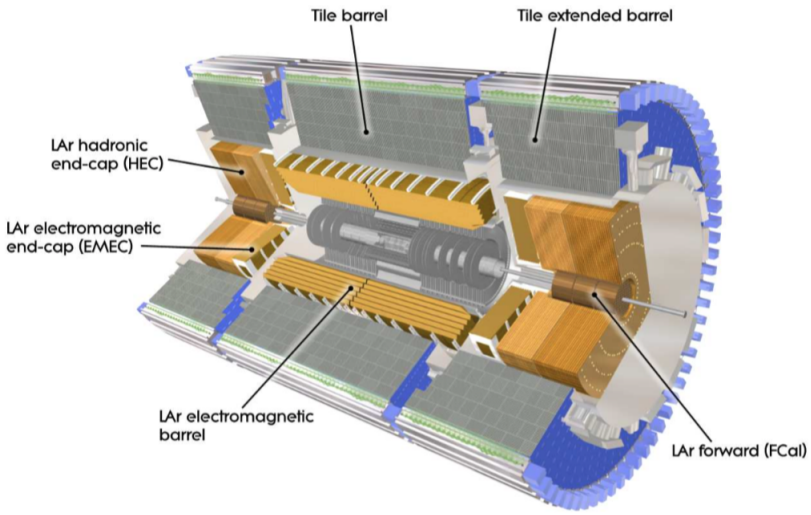

Figure 3.3: Cut-away view of the ATLAS calorimeters [3].

eight modules instead. They are always made by lead absorbers and LAr in between in order to collect charges. Unlike the barrel, the end-caps have absorbers that change thickness depending on the η coordinate, in order to keep the ϕ symmetry. All these features of the LAr calorimeter contribute to the energy resolution. The overall resolution achieved by the EM calorimeter of the ATLAS detector is [5]

$$\frac{\sigma(E)}{E} = \frac{10\%}{\sqrt{E}} \oplus 0.7\%$$

where the first term stands for the sampling term and the second term describes the detector imperfections.

The Hadronic Caloriemeter

The Hadronic calorimeter surrounds the electromagnetic calorimeter and it covers the same angular region. It is divided in three main blocks: the *Tile Calorimeter*, the *End-Cap Calorimeter* and the *Forward Calorimeter*.
The first one is divided in 64 modules (Fig.3.5), each of them with three layers. The active part are the scintillating tiles, 3 mm thick with a trapezoidal shape, placed in a steel container perpendicularly to the beam axis. When a particle passes through the tiles a scintillation light is produced. Then, it is shifted to the blue light by wavelength shifting fibers and brought to a PMT system.

The End-Cap Calorimeters are located in $1.4 < |\eta| < 3.2$. They are a system of four disks, two for each end-cap. They are all composed of 32 modules with 2 layers. They use of liquid Argon as active material, placed between two copper plates.
The LAr Forward Calorimeter (FCal) works at high $|\eta|$. Each of the end-caps is divided in three modules (FCAL1,FCAL2,FCAL3): FCAL1 is made of copper, FCAL2

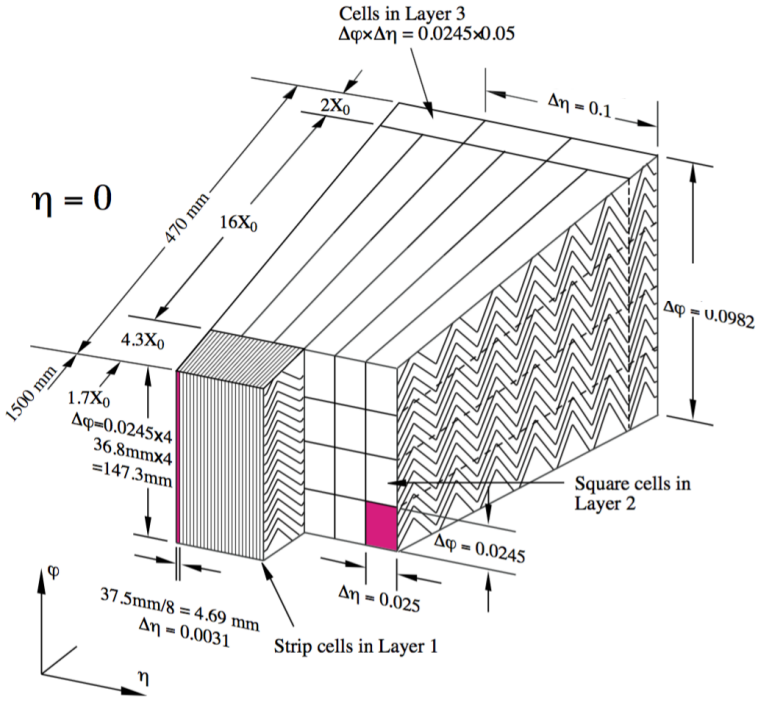

Figure 3.4: Picture of one of the EMB modules that composes the barrel [4].

and FCAL3 are made of tungsten. The first layer is for electromagnetic measurements , the other two are placed at the very high η in order to provide shower containment.

The energy resolution achieved by the hadronic calorimeter is [5]

$$\frac{\sigma(E)}{E} = \frac{50\%}{\sqrt{E}} \oplus 3\% \quad , \quad |\eta| < 3$$

$$\frac{\sigma(E)}{E} = \frac{100\%}{\sqrt{E}} \oplus 10\% \quad , \quad 3 < |\eta| < 5 \ .$$

3.1.3 Muon Spectrometer

The Muon Spectrometer is the system that ATLAS uses in order to detect muons, elusive particles otherwise very hard to catch. The fundament of the spectrometers is the magnetic system. ATLAS has very strong toroids able to bend fast muons, which allow their tracking and the measurement of their transverse momentum. The whole structure is symmetrical in η and so we will describe just the positive η regions.
The system makes use of different kind of detectors: the *precision-tracking chambers* and the *trigger chambers* (Fig. 3.6).
The precision-tracking chambers are the Monitored Drift Tubes (MDTs) and Cathode Strips Chambers (CSCs). They are used to track muons with high precision. The MTDs are placed at the border of the η range. They are arranged in three

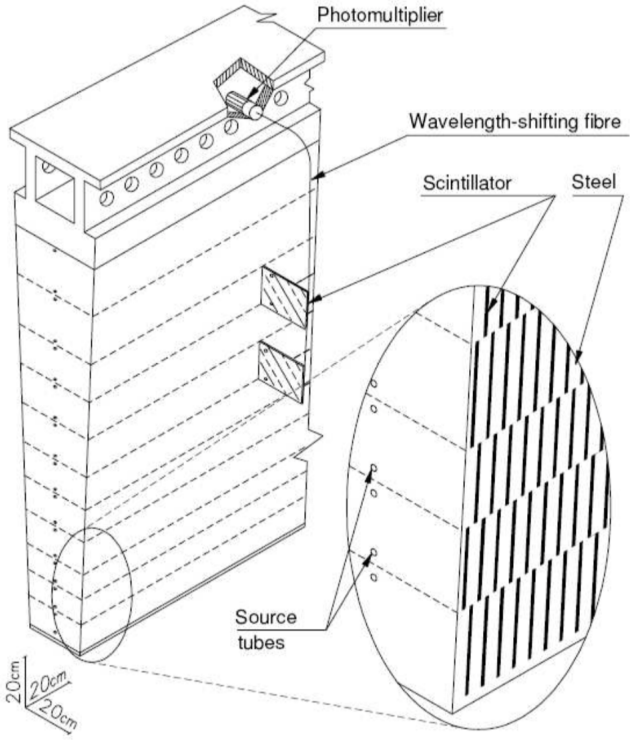

Figure 3.5: Picture of a Tile module [4].

barrels parallel to the beam axis and four wheels composed by eight layers of drift tubes. The dimension of the tubes is 30 mm in diameter. When a muon passes through the MTD, ionization charges are produced and collected on the electrodes, achieving the optimal spacial resolution.
The CSCs are used at $2 < \eta < 2.7$. They are multi-wire proportional chambers, with higher granularity than MTDs. They are used also because they collect charges very fast.

The trigger chambers are the Resistive Plate Chambers (RPCs) and the Thin Gap Chambers (TGCs). They are employed to trigger on muons. The former are used at low η (< 1) the latter are more distant to the interaction point, placed at $1 < \eta < 2.4$. The RPCs are gas detectors: a gas is located in a narrow gap between two plastic plates. When a particle passes through it, it triggers a localized avalanche. The charges are rapidly collected by the metal strips of the plates. The optimal configuration for the RPC is to place them in series in order to have more trajectory points and extrapolate a track.
The TGCs are multi-wire proportional chambers as the CSCs. They have a modified geometry that increases the time resolution. Their tasks are to contribute to the triggering on the detected particle and to estimate the azimuthal angle [3].

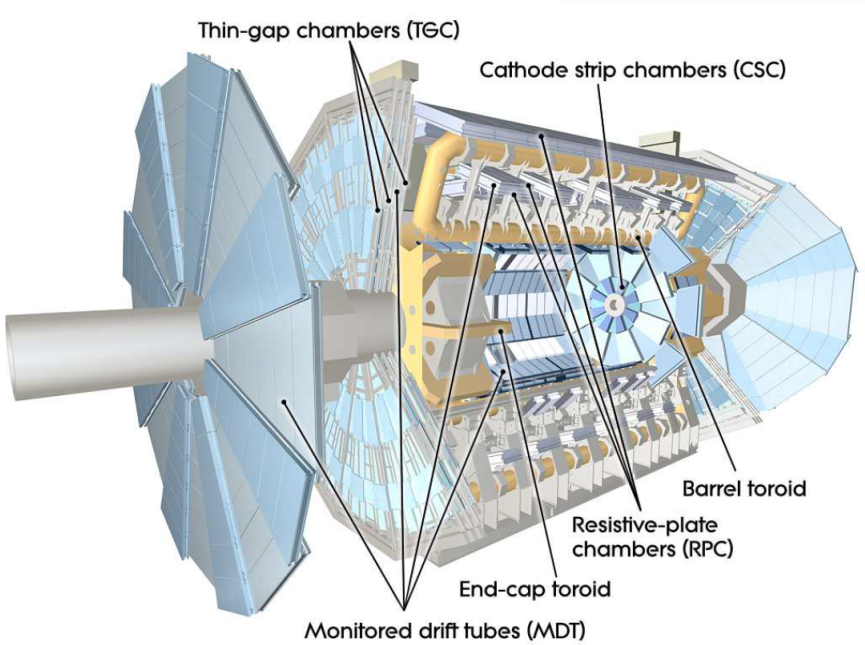

Figure 3.6: Picture of the ATLAS muon spectrometer [3].

3.1.4 Magnet System

The ATLAS detector is equipped with a system of four large superconducting Al stabilized NiTi magnets, as shown in Figure 3.7. With a dimension of 22 m in diameter times 26 m in length, it is placed in one of the underground cavern of the LHC and provide a volume of 12000 m^3 with a magnetic field ($0 < |\eta| < 2.7$). This magnet system consists of a *central solenoid* and of a *toroidal magnet*. The solenoid has a cylindrical symmetry around the beam axis and produces a field of 2 T on the x axis, the toroid is divided in a barrel and two end-caps and produces a toroidal field of 0.5-1 T. As shown in Figure 3.7, the central solenoid is composed of one coil held up by a cylindrical support. Since the central solenoid is inside the region contained by the calorimeters, the solenoid design is optimized in such a way that the material between the calorimeters and the interaction point is the least possible. Each of the three toroidal magnets is made with 8 coils instead. They are arranged radially in a symmetric way around the beam axis [3].

3.2 The Trigger System

The trigger system has two distinct levels: *Level-1* (L1) and the *High Level Trigger* (HLT) (Fig. 3.8). Each trigger level refines the decision made by the previous one by applying stricter selections. The first level uses a reduced amount of the information coming from the detectors (Calorimeters and Muon System) and reduces the initial rate to 100 kHz. After the L1 Trigger decision, the High Level Trigger adds more information and performs a stronger selection reducing the rate to 1 kHz. At the end of the trigger and storing procedure, each event has a size of approximately 1.3

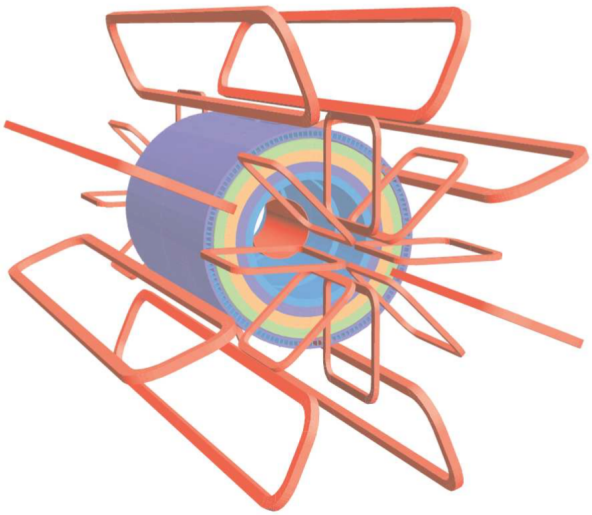

Figure 3.7: Cut away of the ATLAS Magnetic System [3].

Mbyte.

3.2.1 Level-1 Trigger

The Level-1 trigger is used to look for events with high transverse energy carried by charged particles, jets or photon. Its decision is based on the reduced information coming from the hadronic or electromagnetic calorimeters and from the muon spectrometer. The *Level-1 Muon* and *Level-1 Calorimeter Trigger* (L1Calo) information is processed by the central trigger processor. Furthermore, in each event, the L1 trigger defines one or more Regions-of-Interest, i.e. the η and ϕ coordinates where the trigger saw interesting physics. I will talk more in details about L1Calo in chapter 4.

3.2.2 High-level Trigger and Data Aquisition

The High Level Trigger uses the full calorimeter granularity information. It unites the previous L2 and the Event Filter systems and reduces the Level-1 trigger rate. At the end HLT needs just a small fraction of the total amount of the data stored $(3 - 5\%)$. After the decision of HLT the event is discarded or built. Then, offline algorithms perform finer selections when the event data is passed to the Event Filter of the HLT. The Event Filter is formed of approximately 3200 quad-core CPUs. If the Event Filter accepts the event, it is passed to the farm and then stored on disk [4].

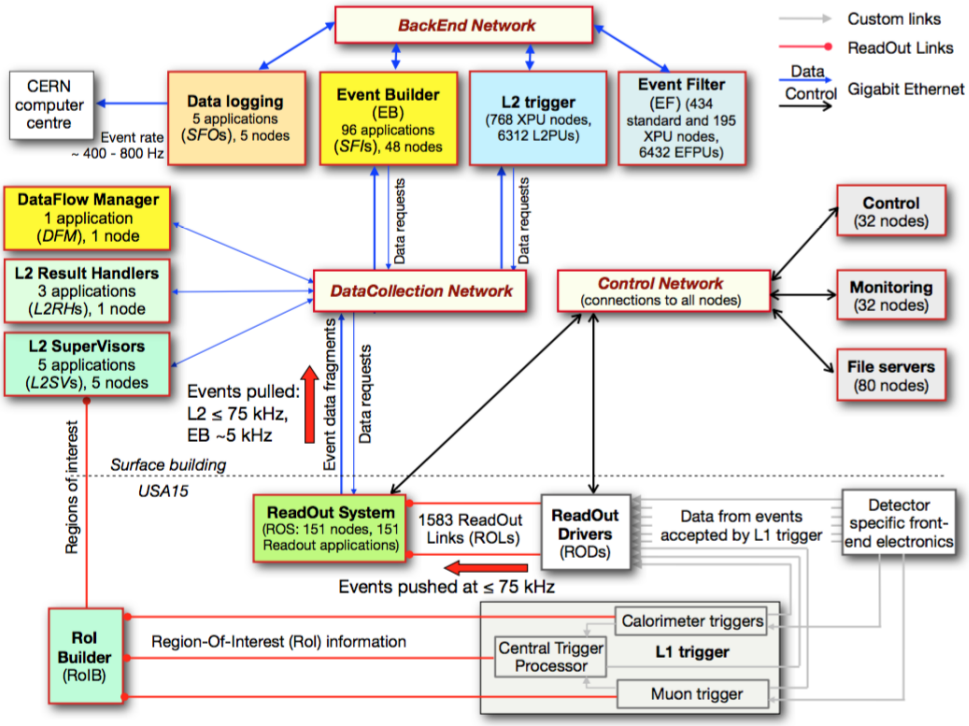

Figure 3.8: Block scheme of the Trigger and DAQ system [4].

Chapter 4

The Level-1 Calorimeter Trigger

The L1 Calorimeter Trigger (L1Calo) is part of the ATLAS trigger system. It analyzes the information from both the electromagnetic calorimeter and the hadronic calorimeter. This system was designed and built to scan the events coming from the collisions by looking at the energy deposits in the whole calorimeter, all within a fixed latency of 2.5 μs. In order to do that, it uses a reduced granularity. This reduced granularity is provided by the 7168 trigger towers, which supply a granularity of 0.1 x 0.1 (η x ϕ). The signal coming from the trigger towers is parallelized and processed by a customized electronics, which is highly specialized and which can handle the precise requirements of L1Calo.
The L1Calo system consists of three components: the *PreProcessor (PPr)*, the *Cluster Processor (CP)* and the *Jet Energy Processor (JEP)*. Each of them performs different tasks:

- the PPr is the first step of the signal processing path. It digitizes the trigger tower pulses and transforms them to GeV scale digital signals. Then this information is then sent to the next two processors;
- The CP looks for high energy clusters produced by an e^-, e^+, γ or τ and applies isolation requirements as well;
- The JEP uses coarser granularity (0.2 x 0.2) in order to find jet candidates and it provides energy sums and an estimation of the E_T^{miss}.

The PreProcessor works before the other two processors, which work in parallel (Fig. 4.1). The information coming from the last two is passed to the CMX (Common Merger Module eXtended) and then to the CTP (Central Trigger Processor) that combines them together with L1Muon [22] information and makes the final L1A decision (Level-1 Accept) based on selection criteria, namely the "trigger menus" [11].

4.1 The Analog Input

The analogue shapes produced in the trigger towers of the two calorimeters are very different. When particles fly into the calorimeter they deposit energy in the cells.

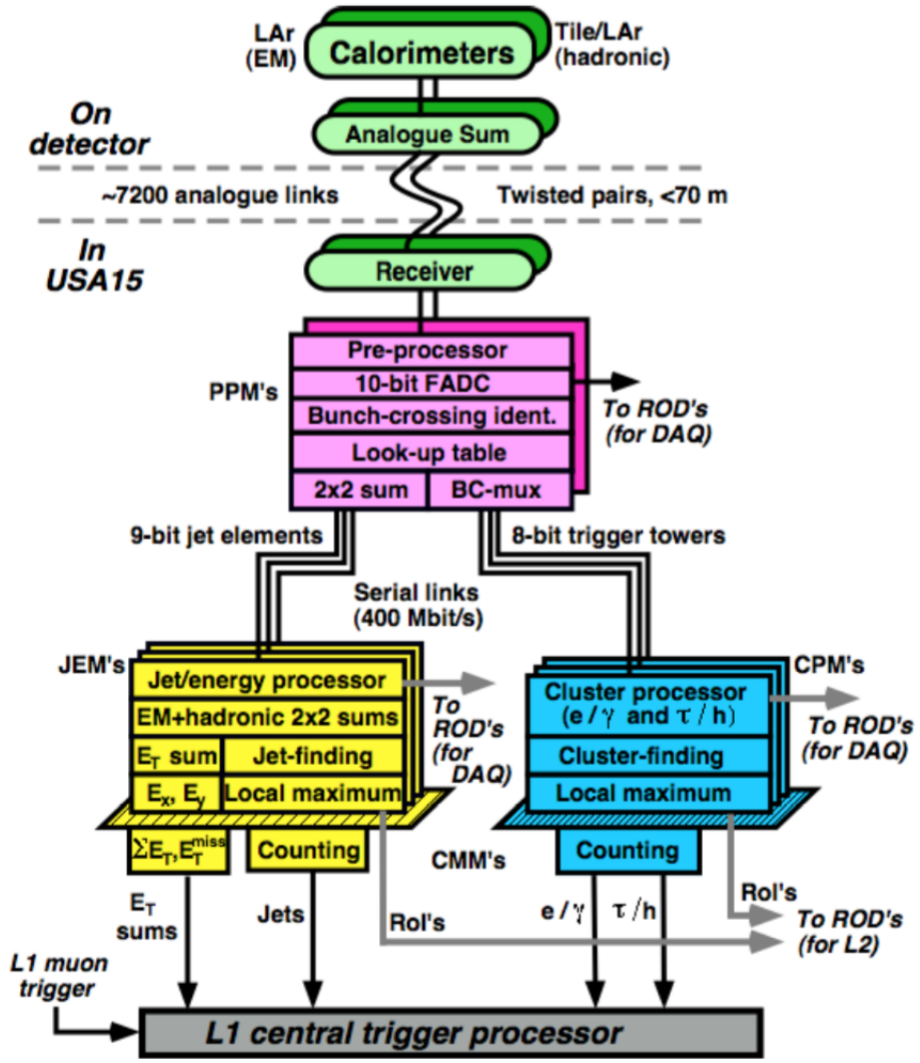

Figure 4.1: Architecture of the Level-1 Calorimeter Trigger [9].

Then a summation over different cells is performed in order to form trigger towers signals. The pulse of the LAr calorimeter (Fig. 4.2) has a very fast rise time (1 ns) produced by the fast ionization of charges and a linear fall down, representing the collection of the electrons. The Front-end electronics (FE) transforms these in pulses with a positive part, which is 5 BC long, and a negative part as well. For the Tile calorimeter the shaping of the signal is faster because it has PMTs connected to wavelength shifting fibers (Fig. 4.2). Therefore, a gain is applied on the signals in order to maximize the separation with the background. After that the signals from the LAr calorimeter, as well as the pulses coming from the Tile calorimeter, are sent to the Receiver Modules, which performs adjustments on the signals:

- summation for the towers in the overlap region between EMEC and EMB;
- A gain adjustment, assigning to each signals its correct voltage scale;
- A re-ordering of the signals in order to match L1Calo processors requirements.

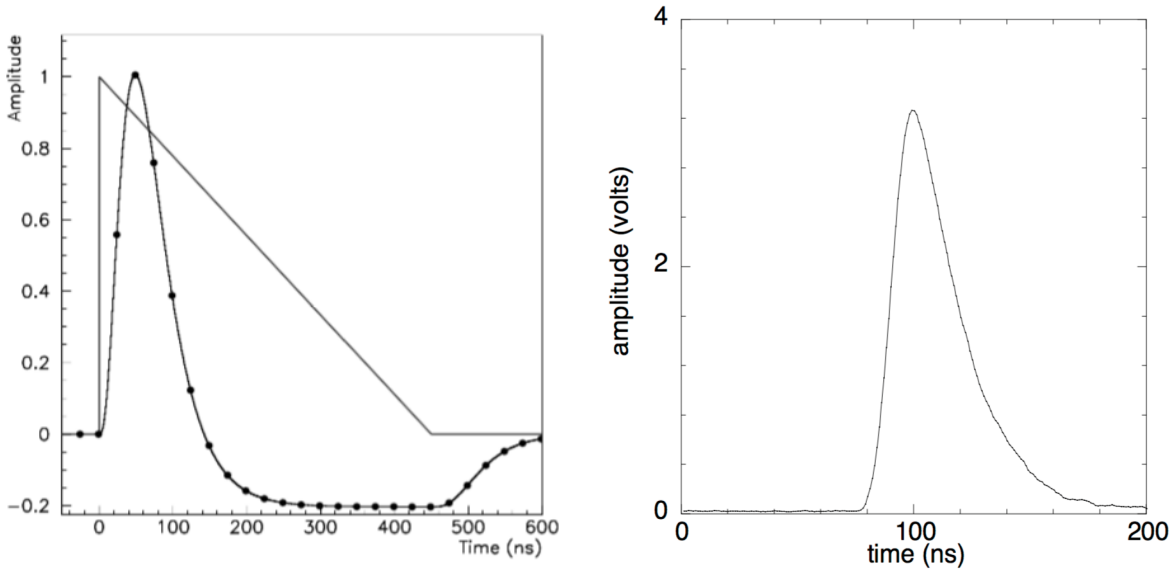

(a) (b)

Figure 4.2: LAr analog signal and trigger tower signal (a), and Tile pulse (b) [9].

After that the analogue signals are provided to the PreProcessor, which is the next stage of signal processing.

4.2 The Pre-Processor Module

The PreProcessor is a crucial stage for the signals coming from the calorimeters. It is divided in 124 PreProcessor Modules (PPM) (Fig. 4.3) that are located in 8 VME crates. These are divided in 4 crates which process the electromagnetic calorimeter signals and 4 are assigned to the hadronic calorimeter ones. We summarize the main pre-processing tasks performed by the PPr in this brief list:

- they digitize the analogue pulses in the Multi-Chip Modules (MCMs). Pulses are digitized by two dual-channel flash-ADC (FADC) in 80 MHz (double of LHC frequency) samples with 10-bit resolution, according to the LHC clock;
- since the cables connecting the calorimeters to the electronics have different length, the PPr synchronizes the trigger towers signals in time. This is done in an FPGA (Field Programmable Gate Array) together with the Bunch Crossing Identification(BCID). The latter consist in assigning a LHC bunch crossing to the correspondent E_T. Then, there is the E_T calibration, and the digital signal preparation for the next processor is performed by the PPr [12];

The PreProcessor logic saturates when the analogue signal is above $\sim$ 250 GeV, corresponding to 1024 ADCs counts. After that the signal is cut off.

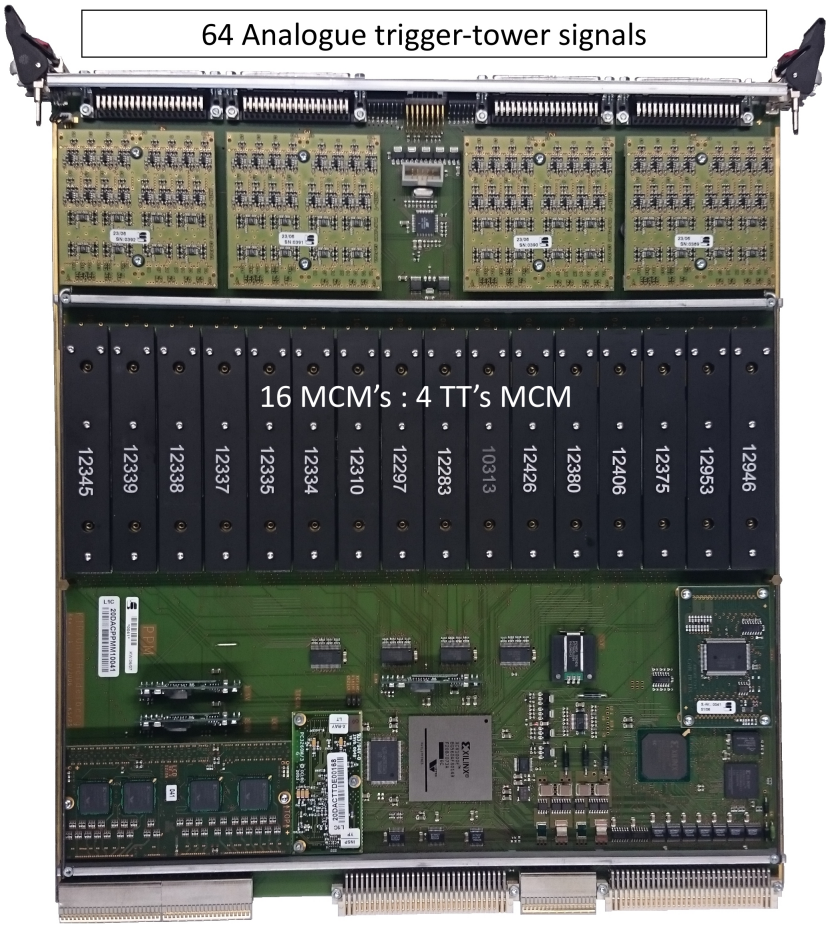

Figure 4.3: Photograph of a PreProcessor Module [3]. These modules host 16 MCMs where the main processing of the signal takes place.

4.3 Bunch Crossing Identification Algorithms

As mentioned before, the signals produced in a collision extend over several bunch crossings (Fig.4.4), but the event has to be assigned to one of them. Therefore a crucial task of L1Calo is the BCID. During this process the peak of the pulse, between all the digitized samples, and its corresponding bunch crossing are identified. This has to be done for every single trigger tower. It is a fundamental task because if the BC is misidentified the measured energy in that channel could be assigned to another event. Due to this missing information, the processing of the event leads to different results, in the worst case the system doesn't trigger and an interesting event could be lost.
The PPr logic responds linearly for energy between 0 and ≈ 255 GeV, after that the pulses are cut off because of saturation of the ADCs.
Because of this the BCID task is performed by two different algorithms: the *Peak-Finder* and the *Saturated BCID*, specialized in the BCID of saturated pulses.

1. PeakFinder takes five consecutive ADC samples in the pipeline and applies on the samples the FIR (Finite Response digital filters) coefficients. They are chosen and optimized to amplify the peak of the signal amongst the other

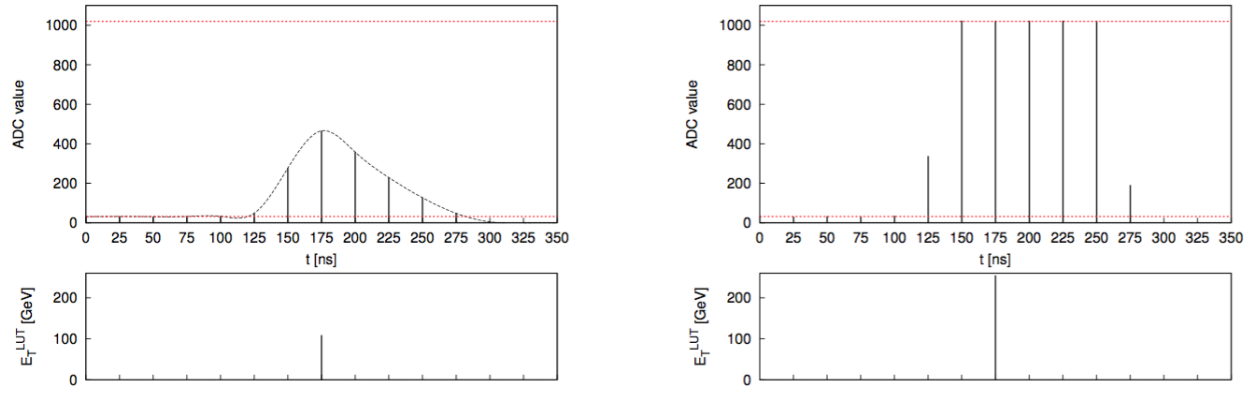

Figure 4.4: Examples of digitized trigger tower pulses, as seen in calibration run. The red line at 32 ADC counts is the pedestal and the red line at 1024 is the saturation. The vertical lines are the samples and their height corresponds to the value of the digitized pulse in that sample. The (a) is the normal sized pulse and the (b) is the saturated one [10].

samples. Therefore, the five samples are selected and the following sum is computed

$$S_m = \sum_{i=-2}^{2} F_i ADC_{(m+i)}$$

where m is the sample which we are looking at in order to know if it is the peak, the F_i are the set of FIR coefficients and ADC_i are the ADC counts. Then, following sum condition is checked

$$S_{n-1} < S_n \geq S_{n+1}.$$

If the condition is matched for n, n is the correct BC. The n sample is sent to the LUT and finally the E_T is calculated and sent to the other processors. This energy will be called "E_T^{LUT}" .
Since the different regions of the calorimeters have different responses, the FIR coefficients are different depending on the coordinates in the calorimeters and on the layer (Fig. 4.5). Currently there are two sets of coefficients:

- the *Matched FIR coefficients*. They are always positive and calculated on the pulse shapes, optimal for the white noise.
- the *Auto-Correlation coefficients*. They consider the correlation with noise and they are dependent on the pile-up. Because of that they can be also negative. They are optimal for pile-up noise.

2. The BCID algorithm for saturated pulses is the *SatBCID*. It is a thresholding algorithm based on the comparison between the leading edge of the pulse and two thresholds: the high threshold (HT) and the low threshold (LT)(Fig. 4.6). For this algorithm it is important identifying the position of the first saturated

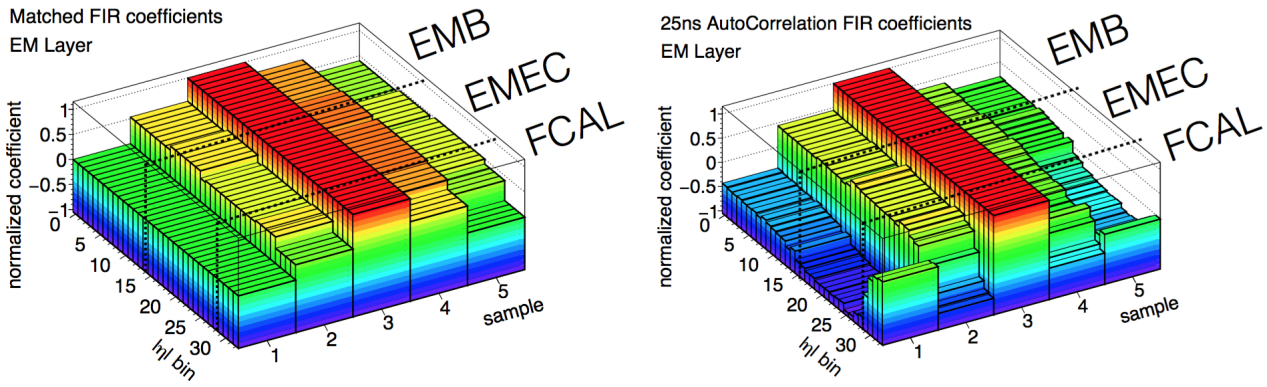

(a) (b)

Figure 4.5: Examples of the two sets of coefficients for the EM layer. In (a) there are the matched coefficients and in (b) the AC coefficients [8].

sample in a given pulse which is called s. Therefore, if the pulse is suitable with the following decision logic the BC is identified

- $ADC(s-1) > HT$ and $ADC(s-2) > LT$ then n=s
- else $n = s + 1$

where s-1 and s-2 are respectively one sample and two samples before the first saturated one. The thresholds can be adjusted tower by tower. When there is

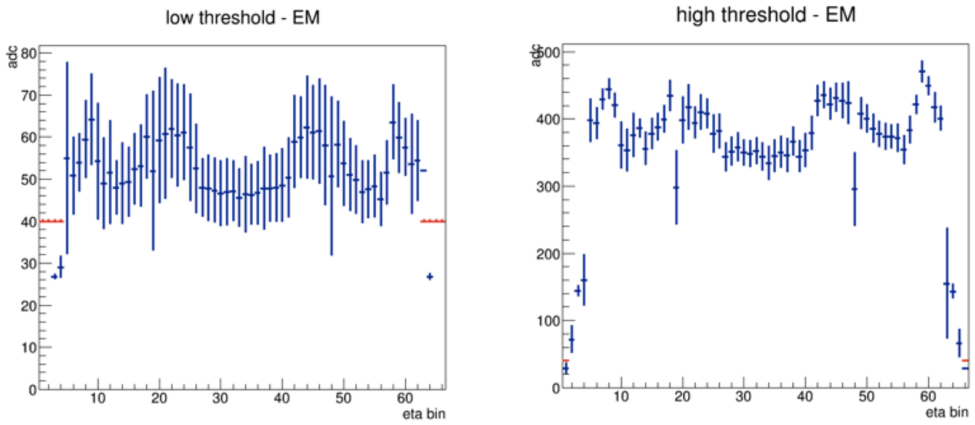

(a) (b)

Figure 4.6: Examples of the two average thresholds over the towers with the same η for the EM layer. In (a) there is low threshold and in (b) the high threshold [10].

at least one saturated sample in the digitized pulse (over 255 GeV) the system triggers automatically. Nevertheless the BCID is important in order to know the correct BC of the signal.

These algorithms are tuned in such a way that is possible that they work together. More detailed explanations about that will be given in the chapter

6.
As mentioned, after the recent ATLAS hardware upgrade we have capability to work also with 80 MHz digitized signals. Therefore a new algorithm was designed, the *Sat80*. It is able to work with 80 MHz samples, thus it can handle the BCID of signals even more saturated than the ones which SatBCID was designed for. More detail about Sat80 can be found in the last chapter.

Chapter 5

Calibration Run Analysis

The Tile and LAr calorimeters are equipped with a precise charge injection system and calibration boards that allows the calibration of the two systems by emulating a physical signal. This gives the possibility to adjust the parameters of the calorimeters in order to be well tuned by the time which physics collision take place.
In the case of the LAr electromagnetic calorimeter the pulses are directly injected into the input of the detector via injection resistors located in front of the detector cells. Figure 5.1 shows a schematic view of the calibration system for the cells of the LAr calorimeter.
The Tile calorimeter is calibrated in three independent calibration steps: one for the scintillators and fibers, one for photomultipliers and the last for the front-end electronics, which is responsible for the shaping and the digitization of the light signal. In the Tile calorimeter a charge injection system is used to calibrate the front-end electronics with high accuracy. The calibration is important for the whole system and it is done using special runs called *pulser runs*. Further details concerning this will be given in the next paragraphs.

5.1 Pulser Runs

Pulser runs are special calibration runs taken in order to test the Level-1 Calorimeter Trigger response. They are artificial signals injected in the calorimeters cells by the charge injection system. The advantage of the pulser runs is that one can test the L1Calo system independently of the luminosity provided by the Large Hadron Collider. Several steps in transverse energy can be chosen in order to check the system response over a large E_T spectrum: the system will inject a calibrated amount of charge so as to produce the effect of energetic events. Four 40 MHz pulses from the same pulser run are shown, with an increasing energy, in Figure 5.2 . They display increasing degrees of saturation. The pulses shown are signal windows of five consecutive samples taken around the peak sample, the signal analogue or real is indeed longer.

As one can notice these pulses are built in such a way that the peak sample is always the central one. The position of the peak sample is indeed determined by

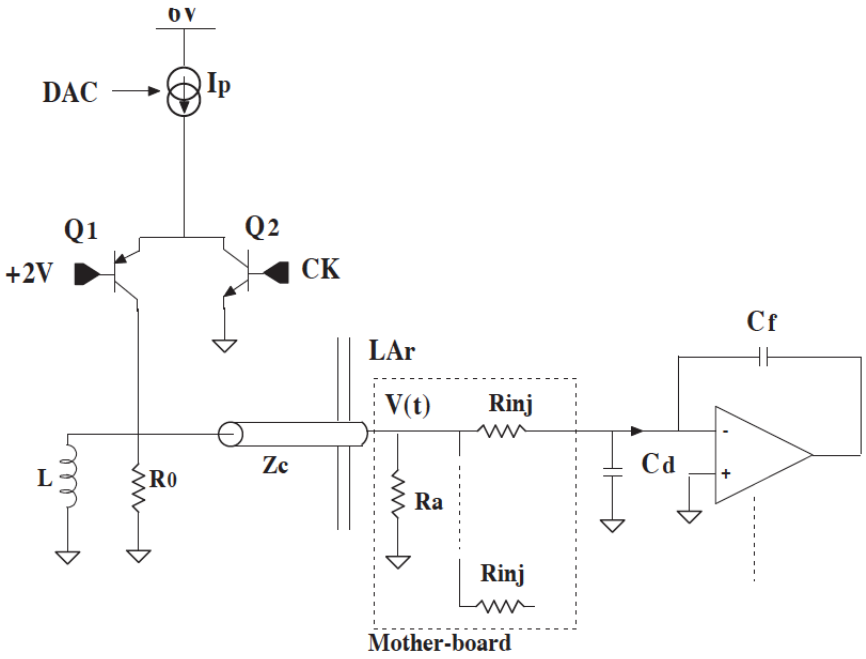

Figure 5.1: A schematic view of the charge calibration system of the LAr calorimeter is depicted in the figure. In the left part of the diagram there is the calibration board, the distribution of the signals in the cells of the calorimeter is represented on the right. This has been done using high precision resistors denoted with R_{inj}, which divide the charges in the calorimeter cells [3].

the calorimeter system. In this way we have more control over the BCID process and we can verify the L1Calo BCID decision against the real one.

5.2 Analysis Procedure

In this work, pulser runs were analyzed in order to test the behavior of the two BCID algorithms and their efficiency. The calibration runs produced by the ATLAS charge injection system were encoded in an EDM (Event Data Model). These are essentially a collection of classes and their relationships that together provide the representation of an event in ATLAS, stored in an easily usable way. They can be manipulated and used to know approximately every information acquired by the L1Calo system. In order to read and manipulate the pulses information, we used xAOD and a software framework called ATHENA (version 2.3.25). The xAODs are special EDM easy and fast to use, that can be used by both ROOT and ATHENA. The latter is the ATLAS off-line software framework, based on the GAUDI [18] architecture. It was originally developed by the LHCb experiment in order to support event data processing applications from the trigger online system to the final analysis.

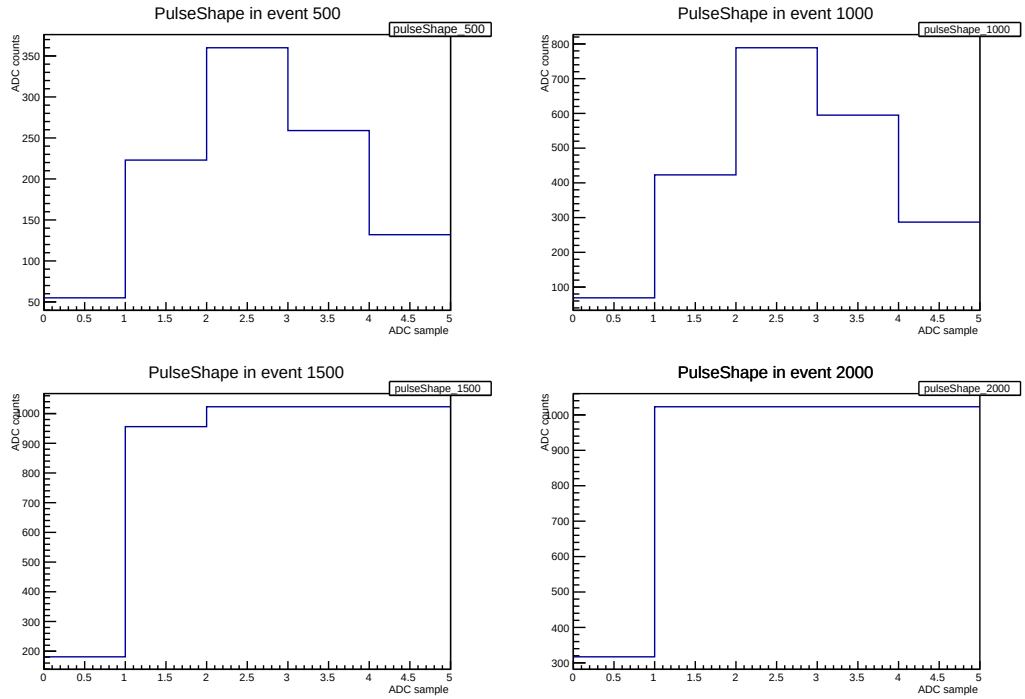

Figure 5.2: On the x axis there is the ADC sample number and on the y axis the corresponding ADC counts. The signal window extends over five bunch crossing (each 25 ns, since the pulse is taken at 40 MHz).

The ATHENA framework [2] is commonly used and developed within ATLAS project and its main advantages are:

- the abstract interfaces that allow an easy manipulation by the different groups of users;
- a large use of dynamic libraries and loadings that improves the GAUDI architecture;
- data and algorithms are well separated, the data are stored in packages set apart from the algorithmic code;
- a separation between transient and persistent data.

Many "pulser runs" with different energies were taken, for each of the two ATLAS calorimeter systems. For each xAOD file we usually had $\approx$ 2000 events, which covered a range up to 7-8 TeV. We had 10-11 energy steps that could be placed uniformly in the desired range. Figure 5.3 shows the spectrum of energies contained in one single xAOD of 2000 events.
Basically after every 200 events the charge injected into the calorimeter regions increases and this means a new step in energy. Therefore we could gather events belonging to the same step by looking at the energy.
The trigger towers of the calorimeters are the sensible units of the calorimeter and each of them might be independently analyzed. By knowing their coordinates we

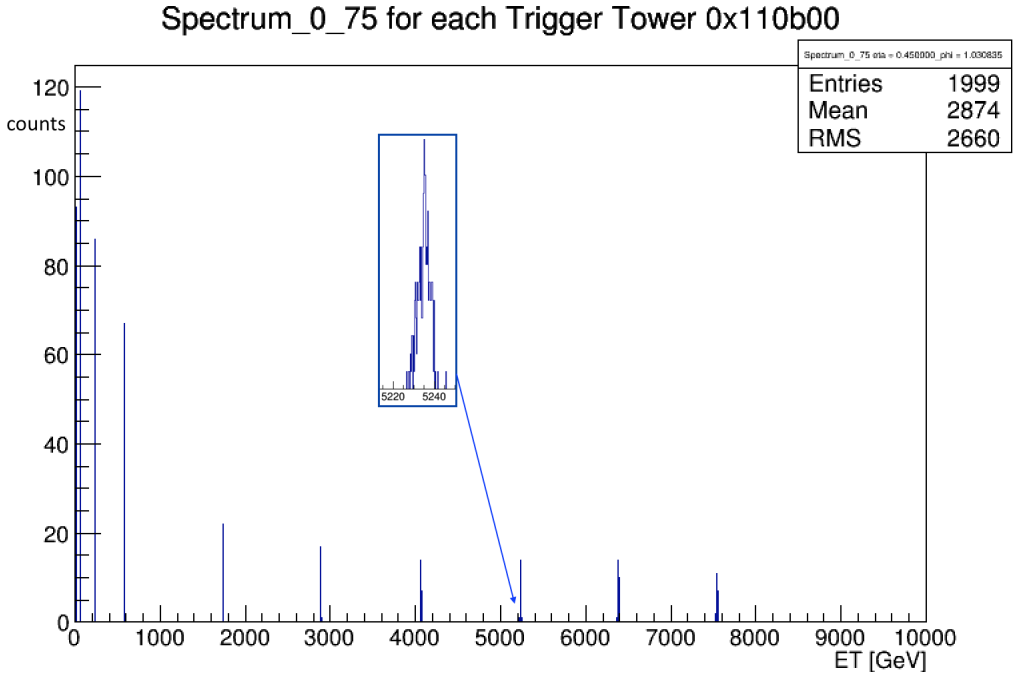

Figure 5.3: The energy spectrum of a calibration run taken for the LAr calorimeter (number of occurred events at the same E_T) for a single trigger tower. The distribution of events around the expected energy is represented in the zoomed square.

could indeed always refer to one of them or studying a group of them in a particular region.
The correlation between energy and ADC counts is expected to be linear and it was checked for the trigger towers ("at trigger tower level"). The "calibration curves", which have been done in order to check the linearity of the calorimeter response, are shown in the figure 5.4. Plotted against the Y-axis is the peak ADC count of the pulse, determined by looping over all the five samples and selecting the biggest one. Plotted against the X-axis is the so-called offline transverse energy ($E_T^{offline}$) - a more accurate energy value, in GeV, determined using calorimeter cell-level information. By looking at Fig. 5.4 it is clear that in the four trigger tower calibration curves we reach saturation after about 1 TeV. Basically it happens since after 250 GeV a single sample saturates, therefore roughly after 1-1.25 TeV all the samples start saturating. The peak sample is, of course, always the first sample that saturates. At low energies we have some points outside the linear behavior, which is an indication of the pulser imperfections in the taken run.

Furthermore we also checked the correlation between the ADC counts of the peak sample and the ADC counts of each sample, producing plots for each of the five samples in 40 MHz. In the following plots for the Tile calorimeter will be shown. As one can observe, there are two distinct shapes in the graphic shown in the figure 5.5. In fact, there is a leading shape approximately linear and a few points that deviate. These points are due to irregular pulses that are left-shifted by one sample, therefore the peak sample appears one sample before the central one. After these mistimed events were found, the code used for the analysis was updated so that they

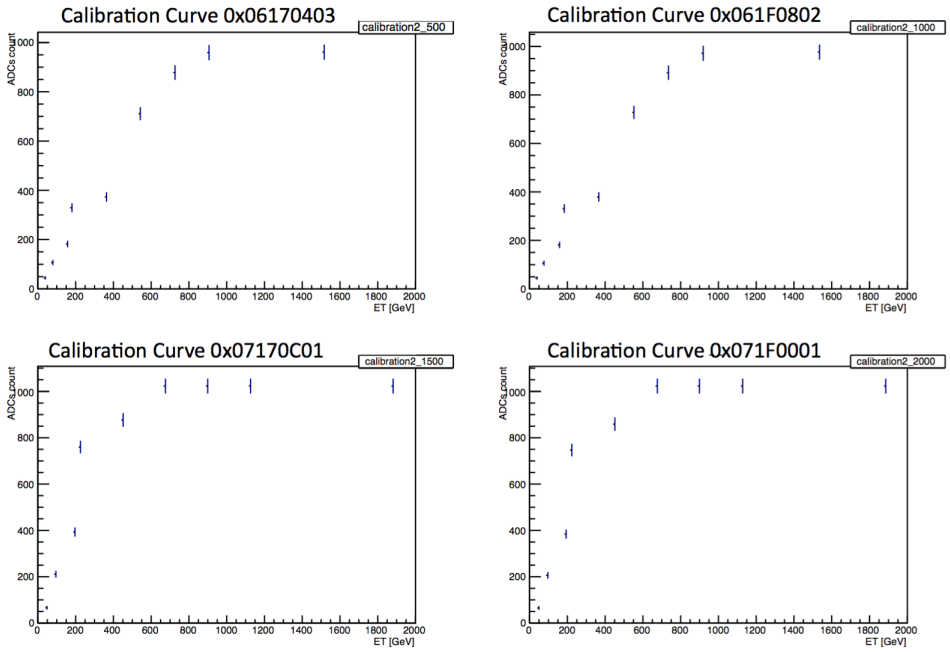

Figure 5.4: Calibration curves for four different trigger towers. On the plot titles there is the CoolID of the tower: a number which identifies the position of the tower in the calorimeters (layer, crate, module, etc).

could be discarded (Appendix B).

5.3 Pulser vs. Physics Shapes

As already mentioned the charge injection system produces pulses that mimics the physical pulses, however they are not exactly the same. In this paragraph some examples of normalized pulses (Fig. 5.6 and Fig. 5.7) are shown. By looking at the two pulse shapes overlaid one on the other, one can easily see the difference. They are normalized in order to wash out the energy dependence of the pulse shape. However one can still see the difference between pulser and physics in the two plots. Because of this, pulser runs results were sometimes different compared to the results coming form physical data.

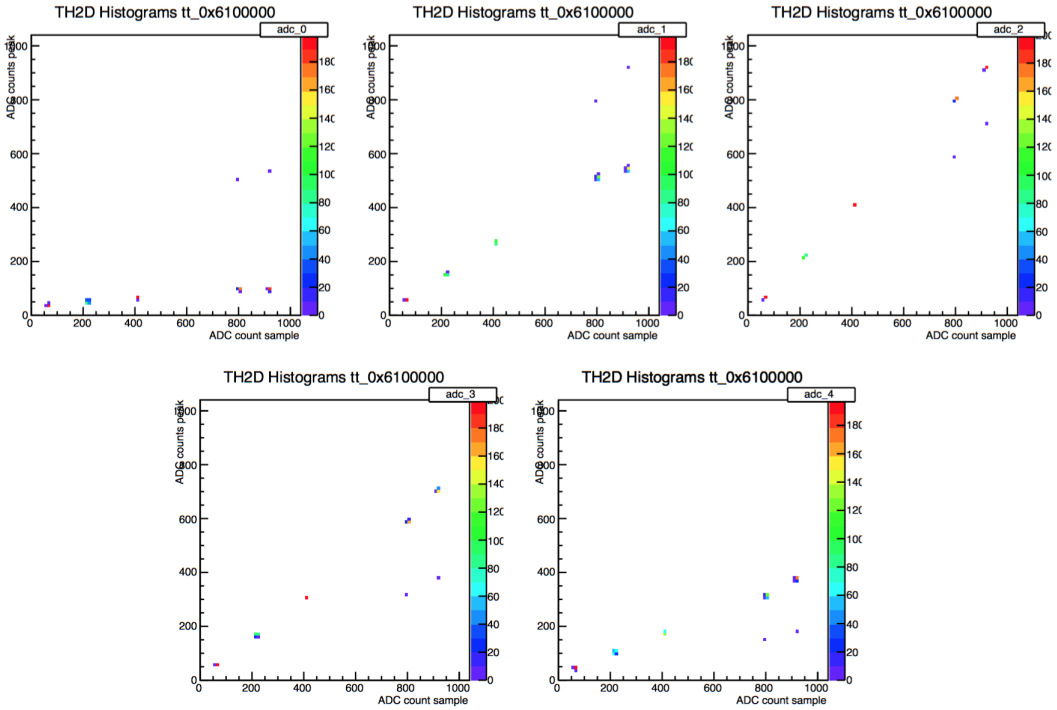

Figure 5.5: The curve of the ADC samples as a function of the energy in the peak sample, that is proportional to the energy of the pulse. The names in the frames (ADC_0, ADC_1, ADC_2...) indicate the position of the sample whose curve we are plotting. The color scale indicates the number of events contained in a certain bin of the two dimensional histogram.

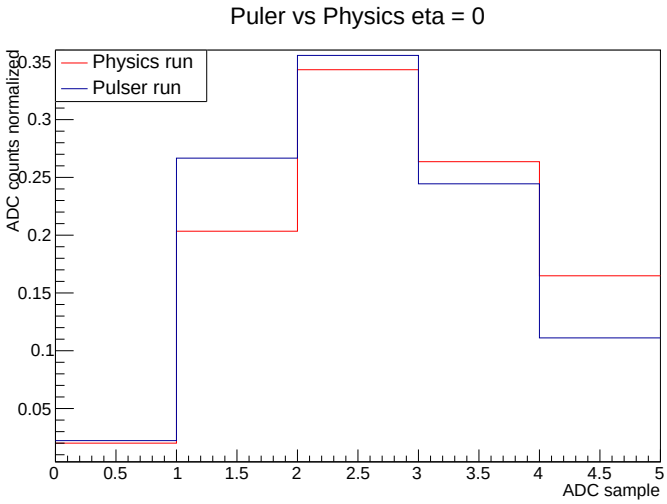

Figure 5.6: Normalized pulses for a trigger tower at $\eta = 0$ of the LAr EM layer are shown in the picture. These pulses point out the difference between physics and pulser runs.

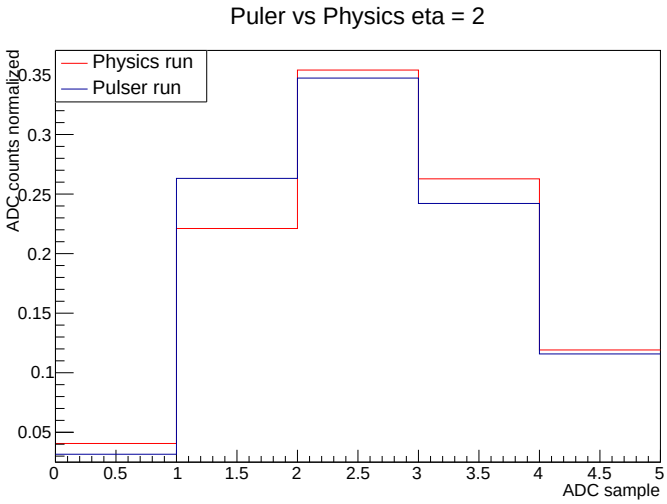

Figure 5.7: Similarly to Figure 5.6, normalized pulses for a trigger tower at $\eta = 2$ of the LAr HAD layer are shown.

Chapter 6

The New Decision Logic

After the first long LHC shutdown, pile-up treatment was enhanced for L1Calo and BCID algorithms were improved in that direction, in order to work up to higher energies. These studies led also to the introduction of the new AC coefficients. They replaced the old matched coefficients, which were not calibrated for high pile-up events. The efficiency for small energy signals was improved a lot thanks to the new AC coefficients, but a small inefficiency was introduced at the saturation energies. This happened because the Auto Correlation coefficients can also be negative in some cases, and that makes the peak finder trigger one bunch crossing earlier for high saturated pulses. For this reason a new decision logic was introduced, resulting in a better combination of the decisions of the different BCID algorithms.

6.1 The BCID Decision Logic

The "decision logic" represents the logic through which the decision between the PeakFinder and the SatBCID is taken, especially in case of conflict. It can happen indeed that for an event the two algorithms, which use different principles and different calibrations, identify two different bunch crossings. Therefore, the decision logic is used to choose which of the algorithms is more reliable for the current pulse. For each of the two algorithms there is a decision bit, which is assigned to the algorithm for every bunch crossing. If the algorithm has taken a decision, the bit is set to 1, otherwise it is set to 0. Thus, after each bunch crossing the bits are checked and their values are sent to the decision logic block that combines them and takes the final decision (Fig. 6.1). The first decision logic was based on the following two points:

- defined energy regions in which an algorithm performs better than the other;
- in case of conflict between the algorithms, the one that fires first takes the decision.

During the first year of Run-2 (2015), the decision logic simply considered the difference between saturated pulses and non-saturated pulses:

- the SatBCID would be used if the signal had at least one saturated sample;

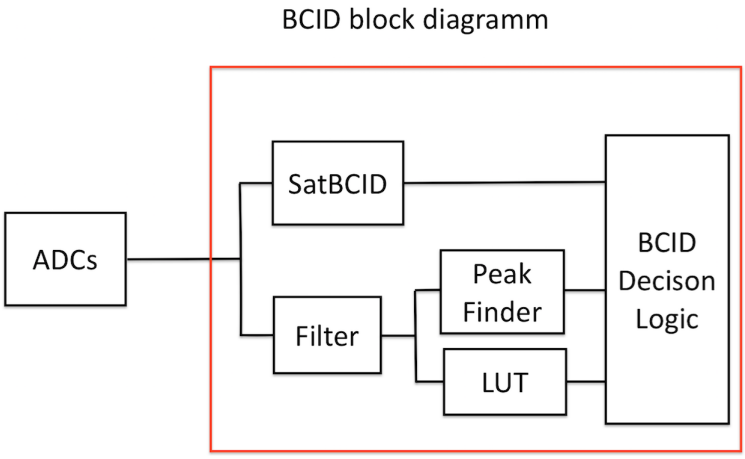

Figure 6.1: The block diagram of the decision logic is shown in the figure. After the digitization of the signals (ADCs), the samples are passed to the algorithms and their decision bits are given as an input to the decision logic, which takes the final decision.

- the PeakFinder was used for all the energies. Therefore, for saturated pulses, it worked together with the SatBCID.

This set-up was based on the matched filters as used during Run-1. It was observed that for highly saturated pulses the PeakFinder fires later than SatBCID and it is therefore ignored (SatBCID is trusted). In Fig. 6.2 examples of pulse shapes as a function of the energy are shown. One can see the way of operating of this decision logic for different digitized pulses. As shown in the figure, the SatBCID decision trigger earlier than the PeakFinder. Therefore, the final decision is taken by the SatBCID.
After the LHC upgrade, the previous decision logic was too trivial to identify the correct bunch crossing over all the wide energy range. After the introduction of the autocorrelation coefficients for pile-up treatment the previous assumption doesn't hold:

- for saturated pulses the large negative coefficients make the PeakFinder fire earlier than the correct bunch crossing;

- since the BCID logic takes in account only the algorithm that fires earlier, the bunch crossing is misidentified (Fig. 6.3).

Therefore, the new decision logic, which was validated in this work of thesis, is based on the assumption that only the highly saturated signals are responsible for the early triggering of the PeakFinder.
In order to develop a new decision logic, a way to distinguish saturated pulses that the PeakFinder can manage from pulses that only SatBCID can correctly handle was found. This new logic takes the number of saturated samples into account. Then the old decision logic was modified in the following way: if the saturated samples are more than a specific number the PeakFinder is ignored and only the decision of

the SatBCID algorithm is taken into account, even if the PeakFinder fires earlier. As described in Fig. 6.4, the result is that, the Peak finder works for small pulses. Then there is an overlap region, in which both of the algorithms work. For large signals the PeakFinder is switched-off and just SatBCID is taken in account.
Thus, the logic is efficient for low energetic pulses and at the same time we keep the high efficiency in the saturation regime.
This new decision logic was studied using the calibration runs we took for the two calorimeters, using different thresholds for the number of saturated samples.

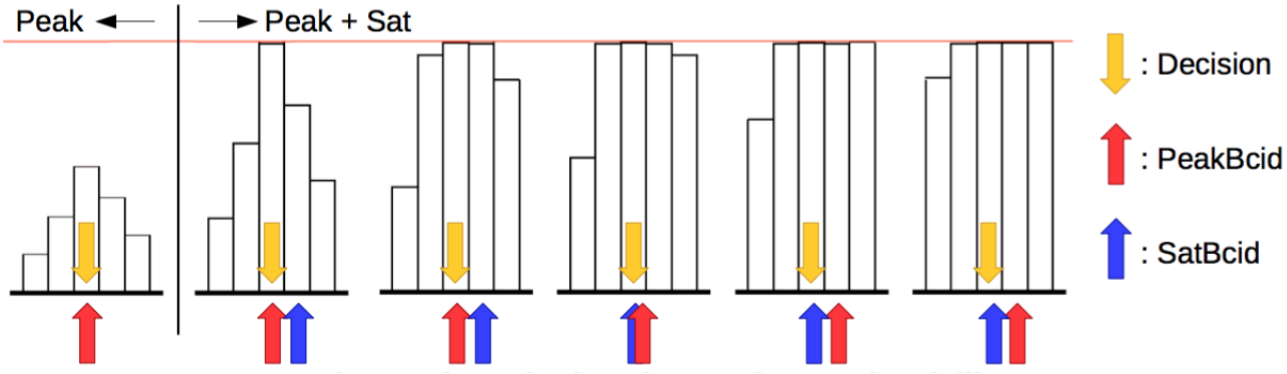

Figure 6.2: A schematic view of the old decision logic of 2015, with matched coefficients. The energy increases from left to right and the pulses get in saturation regime approximately at 255 GeV (red line). The red arrow represents the decision taken by the PeakFinder, the blu arrow stands for the decision taken by the SatBCID and the yellow arrow is the final decision taken by the decision logic. In this case the yellow arrow comes always together with the first firing algorithm arrow.

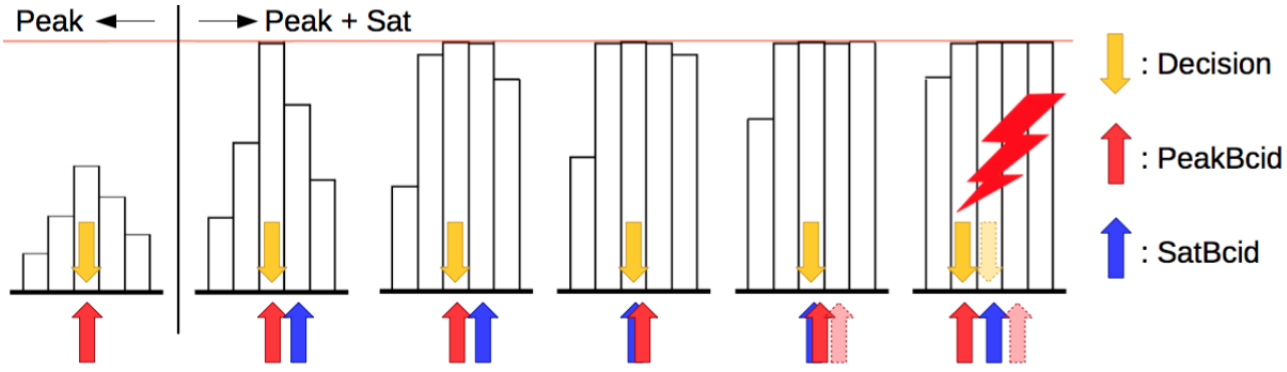

Figure 6.3: A schematic view of the old decision logic of 2015, with autocorrelation coefficients, is shown. This time the PeakFinder fires too early and causes the misidentification of the bunch crossing. In the last saturated pulse the negative AC coefficients make the PeakFinder fire too early and the decision logic takes the wrong decision.

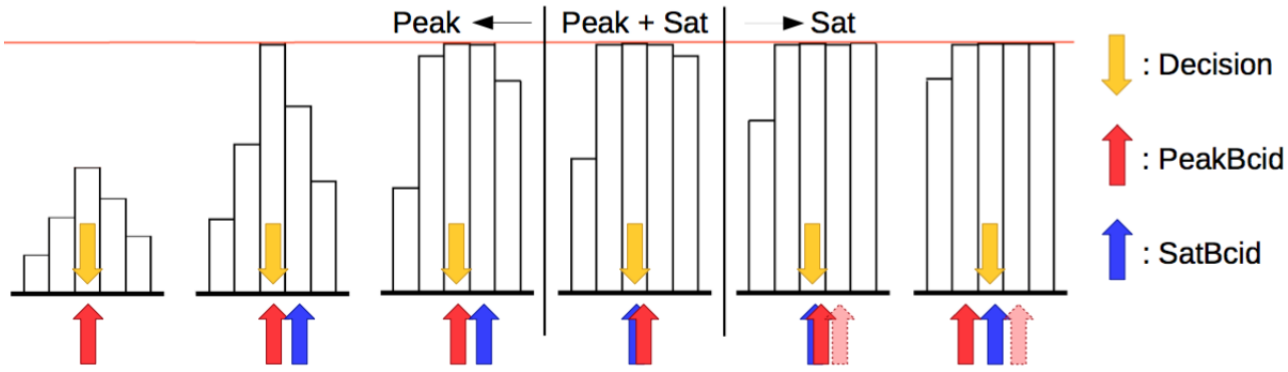

Figure 6.4: A schematic view of the new decision logic of 2016, with autocorrelation coefficients, is shown. The PeakFinder is disabled after a specific number of saturated samples (four in this case) and just the SatBCID is taken into account for the decision.

6.2 Validation Process

The new decision logic was validated using many pulser runs. In order to summarize the information coming from all the trigger towers in one single plot, the $\eta-\phi$-maps are used. These are maps showing all the trigger towers of the calorimeter as small colored squares, with color representing specific values for each trigger tower. Each of the squares is located on the $\eta-\phi$ coordinates of the corresponding trigger tower. In this way we can have a intuitive overview of what is happening in the calorimeter at "trigger tower level". The following characteristics of the events are plotted in the $\eta-\phi$-maps:

- The offline E_T, which essentially is the final transverse energy corresponding to the event seen in that trigger tower. On the other hand, in the pulser runs it is simply the energy corresponding to the amount of charge injected into the calorimeters, emulating the physical event. Whereas in normal runs it is the final estimation of the energy by the calorimeters, when the particles fly through the detector. It was used in order to see how the L1Calo trigger behaves with energy in the saturation regime;

- The number of saturated samples, which goes from 0 to 5 in 40 MHz pulses;

- The PSE (PeakFinder SatBCID ExternalBCID), which is a 3-bit word that tells if the algorithms are taking a decision or not. The external BCID is another thresholding algorithm, but its corresponding bit was always set to zero because its decision doesn't contribute to the decision logic. As a consequence, if only the PeakFinder identified the bunch crossing, the corresponding PSE 3-bit word would be (1,0,0), which converted into a decimal base is equal to four. If only SatBCID identified the BC, the PSE would be (0,1,0), which is two converted into decimal. If both of the algorithms took a decision the PSE would be (1,1,0) and it would give us six converted into decimal. If none of the algorithms took a decision the bit would be set to zero;

- the E_T^{LUT}, namely the result energy value that comes from the look-up table. This would be the energy estimated in the PreProcessor at trigger tower level, which is always between the pedestal and the saturation value;

- the ADC counts of the peak sample, that is actually the E_{LUT} before the conversion that will be realized by the LUT.

In order to find the number of saturated samples that allows to discriminate between small pulses, on which the PeakFinder can take a decision, and high saturated samples, for which the PeakFinder decision has to be ignored, many tests have been carried out. In the first ones, we started ignoring the PeakFinder after 4 or more saturated samples and then we decreased this number until inefficiencies start appearing.

6.3 Results

Before explaining the results of the new implemented decision logic, the performances of the old 2015 logic will be showed. At that time the PeakFinder was allowed to work over all the energy spectrum, therefore for some energies the triggering happened earlier and the energies were assigned to the wrong event. The following plots belong to runs taken for the LAr calorimeter and they show the EM layer (the HAD layer is shown into the Appendix A). In the following figure 6.5 the five quantities checked for the analysis are represented: the E_T, the PSE 3-bit word, the ADCs counts, the number of samples saturated and the E_T^{LUT}. It is important to compare the plots one with each other, in order to understand the behavior of the BCID procedure.

In the first energy step (6.5) the highest energies are in central barrel with $-1.2 < |\eta| < 1.2$ (slightly higher in $0.9 \leq |\eta| \leq 1.2$), while lower energies are in the electromagnetic end-cap. By looking at the third plot starting from the left, and at the bottom left one, which show respectively the ADC counts and the number of saturated samples in each trigger tower, one can see that the central barrel is saturated. The plot at bottom left shows that in the central barrel almost all the trigger towers have four saturated samples, while the towers with $|\eta| > 1.2$ have not enough energy to saturate.
In order to know the behavior of the two algorithms at trigger tower level checking the PSE and the E_T^{LUT} plots is important. Concerning the PSE plot, in the central region the towers where PeakFinder and SatBCID have both identified the correct bunch crossing are represented by the red squares. While the light-blue and the green squares mean respectively that only SatBCID has taken the right decision or that only PeakFinder has taken the right decision.
In the end, the E_T^{LUT} provides the final response regarding the efficiency of the BCID logic. The red squares at low $|\eta|$ indicate an energy above 250 GeV indeed, while the white ones represent the towers that are empty for the current event. This means that only SatBCID took the right decision in that region, but it was ignored because PeakFinder triggered earlier. This is confirmed by the fact that the light-blue squares of the PSE map have the same pattern of the white squares in the E_T^{LUT} map. By increasing the energy injected into the calorimeter we started losing more and more energy estimation in the trigger towers (Fig.6.6). In Figure 6.7 the situation is even worse. The energy is increased, as one can check monitoring the top and bottom left plots. The number of saturated samples is increased in the bottom left plot, now the trigger towers in the central region have up to 5 samples saturated. At these energy the PeakFinder started firing too early for almost all the central trigger towers, consequently the bunch crossing is misidentified and the energies assigned are lost for this particular event. By looking at the PSE plot it is clear that the current energies fall within the confidence region of the SatBCID, therefore the PeakFinder should be turned off for these energies.

In order to face this inefficiency for highly saturated pulses, it was decided to intro-

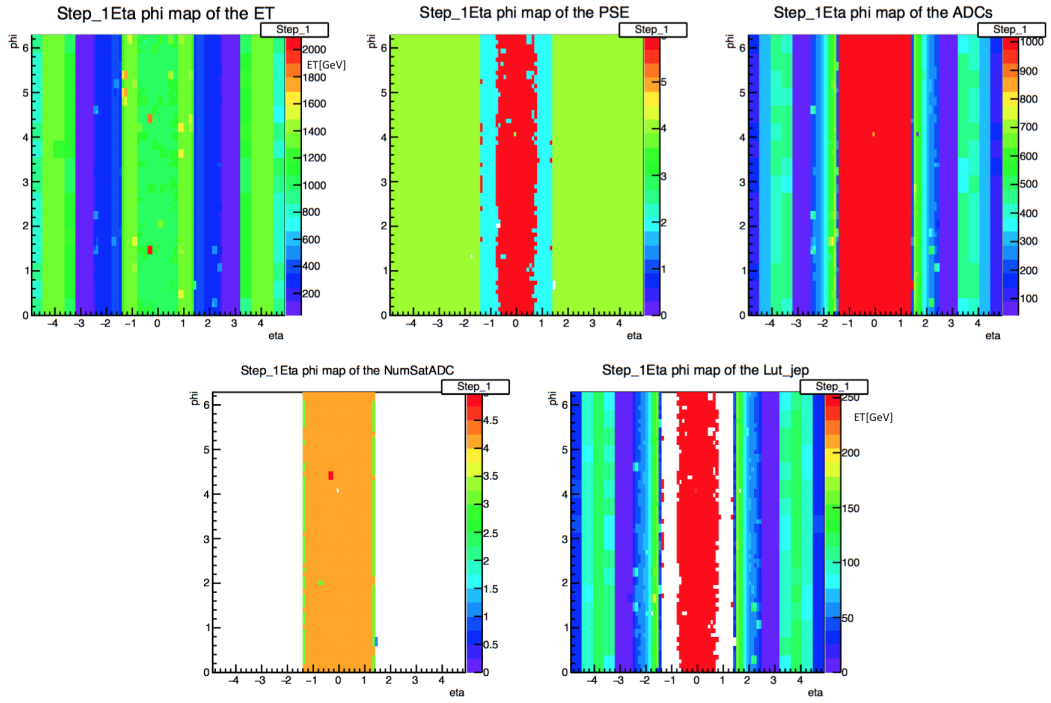

Figure 6.5: The five quantities we checked in 40 MHz pulser runs are shown in the five plots, for the lowest energy step (in the EM layer of LAr calorimeter).

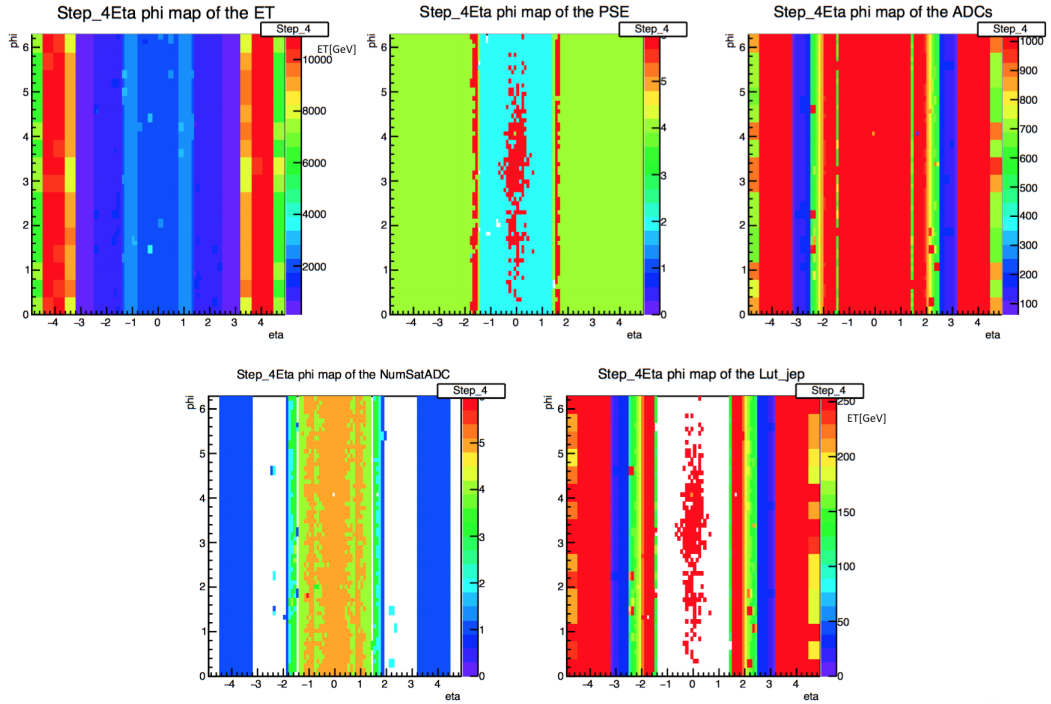

Figure 6.6: The five quantities we checked in 40 MHz pulser runs are shown in the five plots, for a middle energy step (in the EM layer of LAr calorimeter).

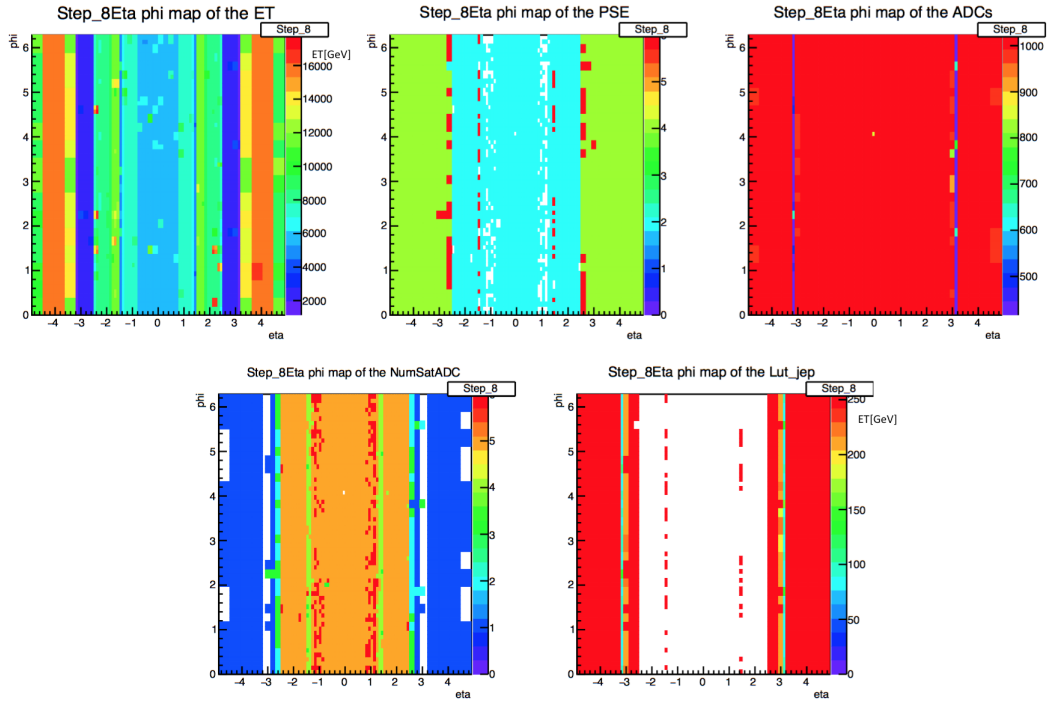

Figure 6.7: The five quantities we checked in 40 MHz pulser runs are shown in the five plots, for the highest energy step (in the EM layer of LAr calorimeter).

duce a new decision logic, which is the central part of the work carried out in this thesis. In the following plots we will show the results gained after the introduction of the new decision logic, which ignores the peak finder decision if the pulse has ≥ 4 saturated samples. The energies are the same used for the validation studies of the old decision logic.
In the first set of plots (Fig. 6.8) taken for the first energy step there is an evident change compared to Fig. 6.5. Now, in the towers with four or more saturated samples, the decision taken by the PeakFinder is ignored. Therefore, the bunch crossing is identified by the SatBCID (specialized in the peak finding for saturated signals) in almost all the central barrel towers. The advantage of ignoring the PeakFinder decision is clarified by looking at the E_T^{LUT} plot on the bottom right. It is a matter of fact that a large fraction of the towers which were empty before, now saw the energy belonging to the current event.
In the next steps (Fig. 6.9 and Fig. 6.10) energy rises and the new decision logic shows its good performance. This time the E_T^{LUT} maps are mostly full too, therefore a very good coverage is achieved thanks to the introduction of the new decision logic. The E_T^{LUT} in figure 6.10 shows still some white squares in the calorimeter region which separates the central barrel from the electromagnetic end-caps. The reason of this inefficiency is included in the plots of the PSE bit and in the number of saturated samples plot. The PSE map shows that there was not a correct decision performed by any of the algorithms, it means that for some reason SatBCID fails for these towers. The reason is that the energies and the number of saturated samples are so high that even the SatBCID algorithm is not able to identify the correct

bunch crossing. It was validated up to 4 TeV. By looking at the energy, one can see that the event energy is well above that threshold and at some point the SatBCID is expected to start failing for such high energies.

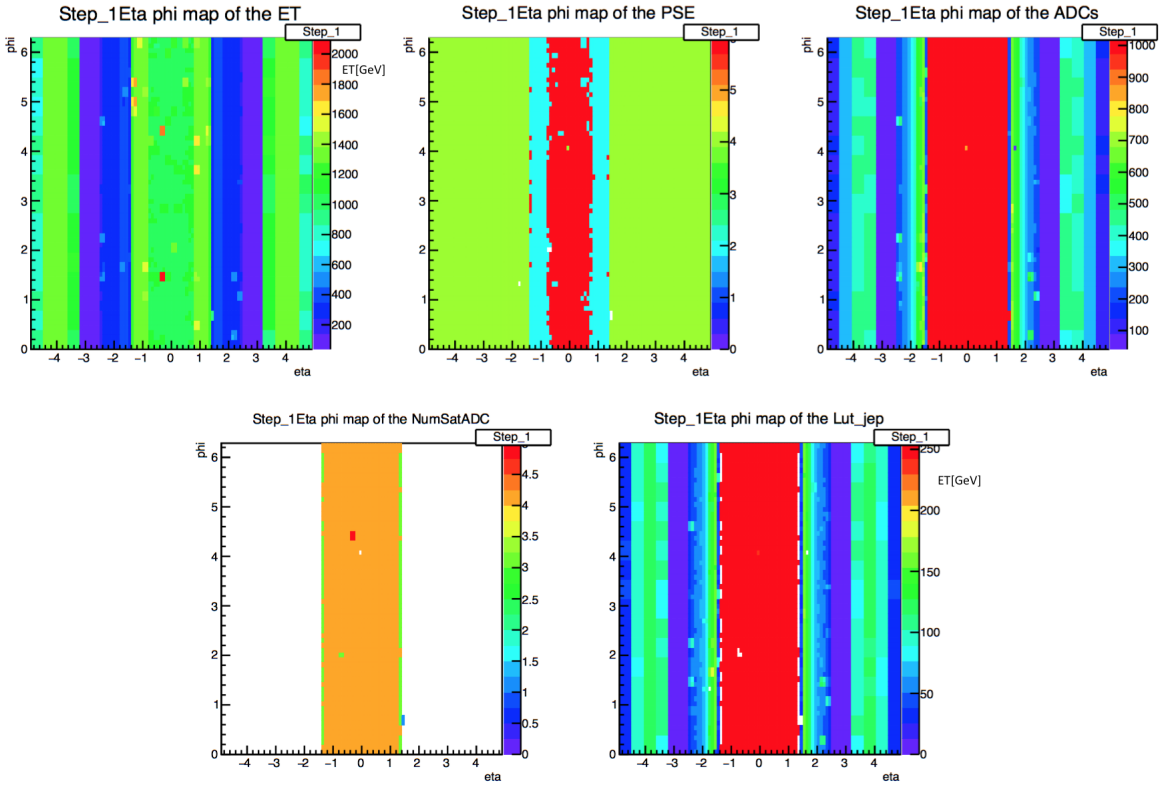

Figure 6.8: The five quantities we checked in 40 MHz pulser runs with the new decision logic are shown in the five plots, where the PeakFinder stops working at 4 saturated samples. It is for the lowest energy step (in the EM layer of LAr calorimeter).

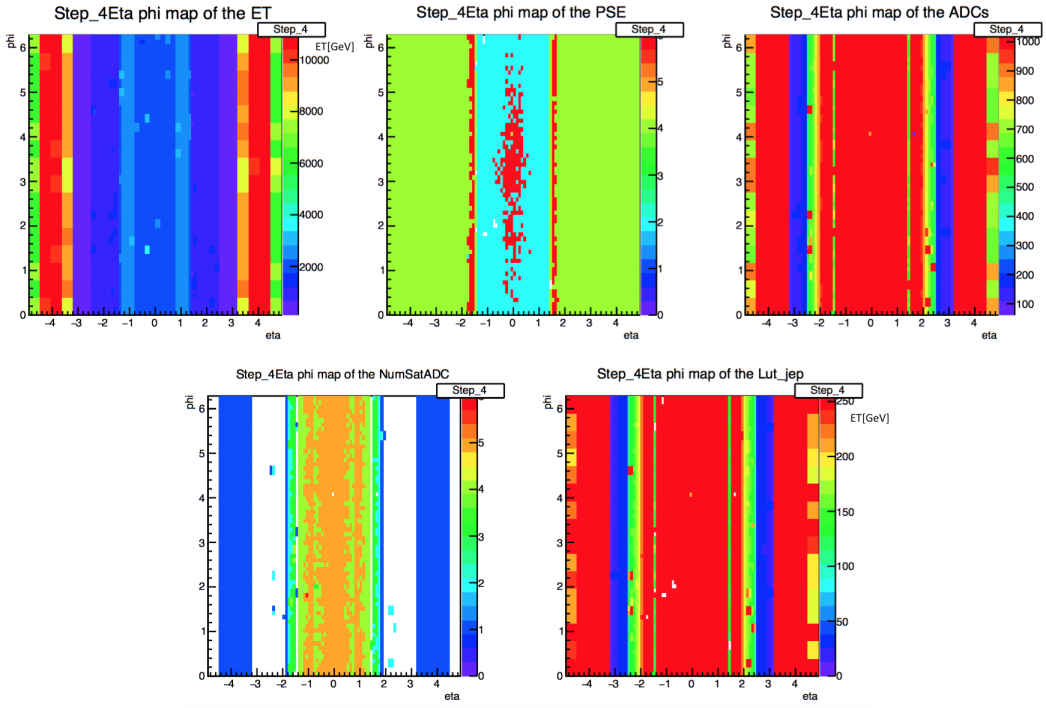

Figure 6.9: The five quantities we checked in 40 MHz pulser runs with the new decision logic are shown in the five plots, where the PeakFinder stops working at 4 saturated samples. It is for a middle energy step (in the EM layer of LAr calorimeter).

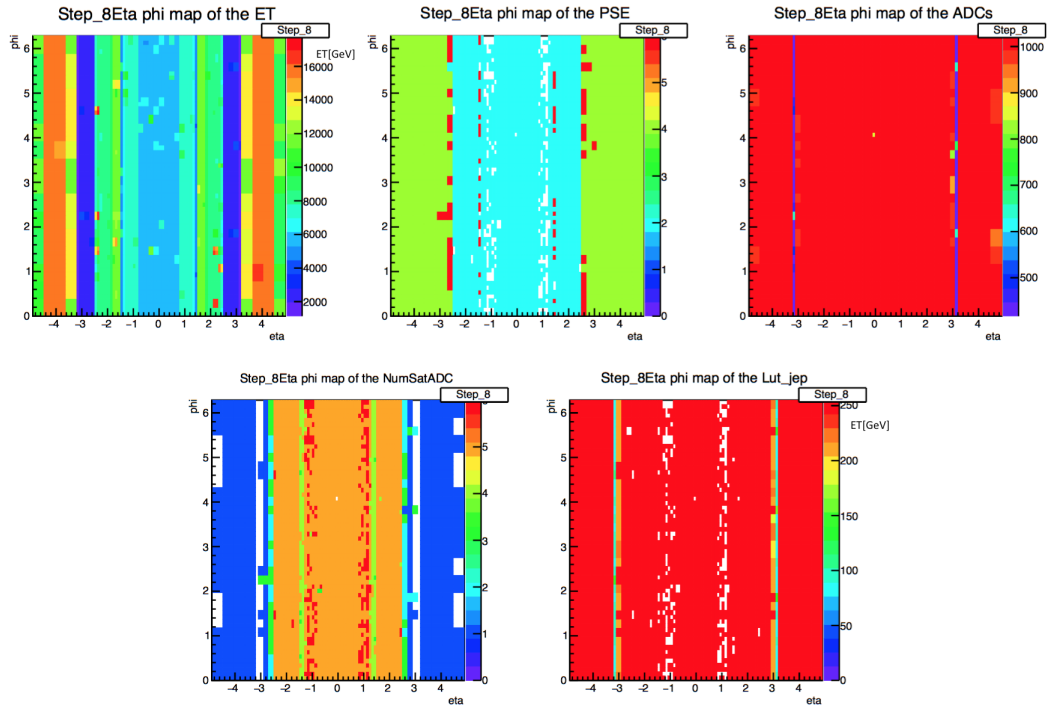

Figure 6.10: The five quantities we checked in 40 MHz pulser runs with the new decision logic are shown in the five plots, where the PeakFinder stops working at 4 saturated samples. It is for the highest energy step (in the EM layer of LAr calorimeter).

In order to check if the optimal number of samples for the decision logic was even lower than 4, new pulser runs have been taken stopping the PeakFinder from working after 3 or more saturated samples. The result are shown in the following pictures.

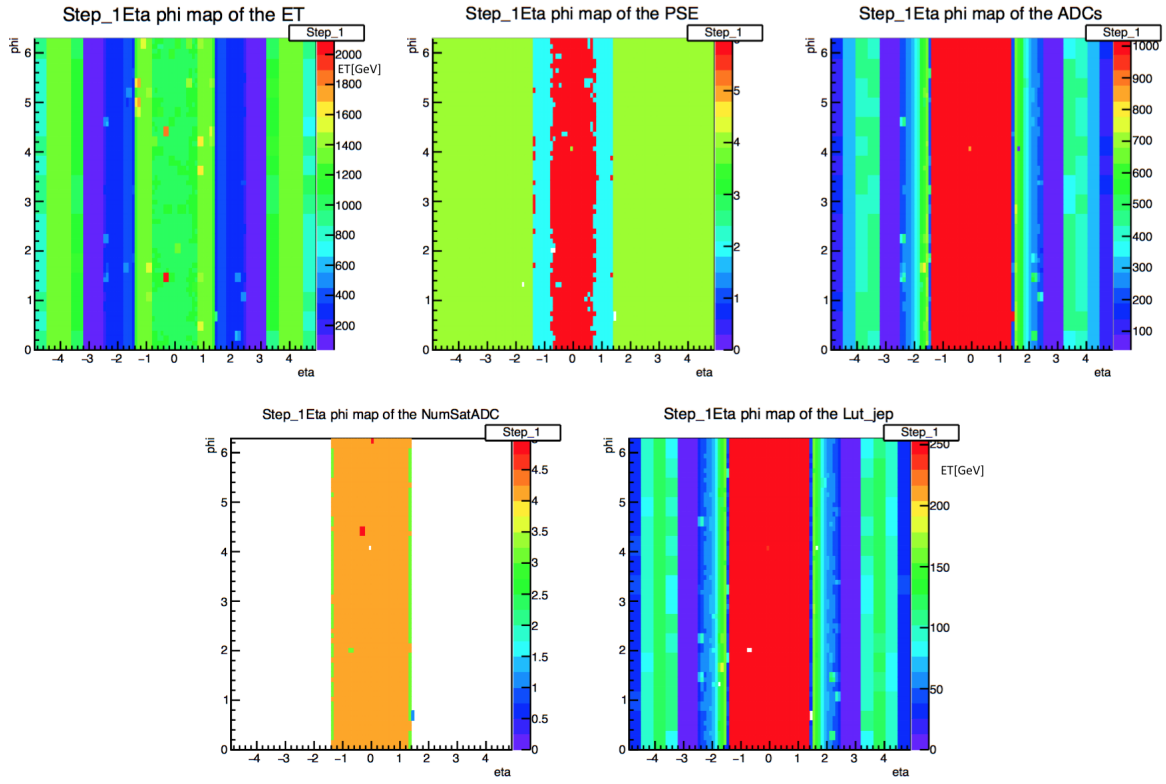

Figure 6.11: The five quantities we checked in 40 MHz pulser runs with the new decision logic are shown in the five plots, where the PeakFinder stops working at 3 saturated samples. It is for the lowest energy step (in the EM layer of LAr calorimeter).

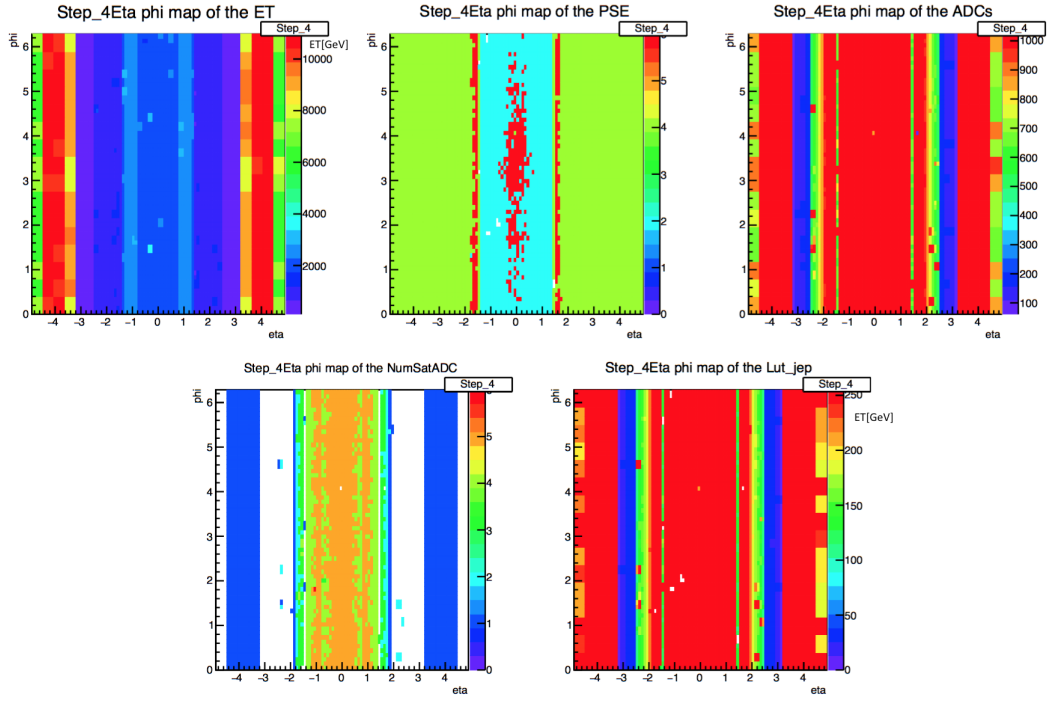

Figure 6.12: In the five plots are shown the five quantities we checked in 40 MHz pulser runs, where PeakFinder stops working at 3 saturated samples. It is for a middle energy step (in the EM layer of LAr calorimeter).

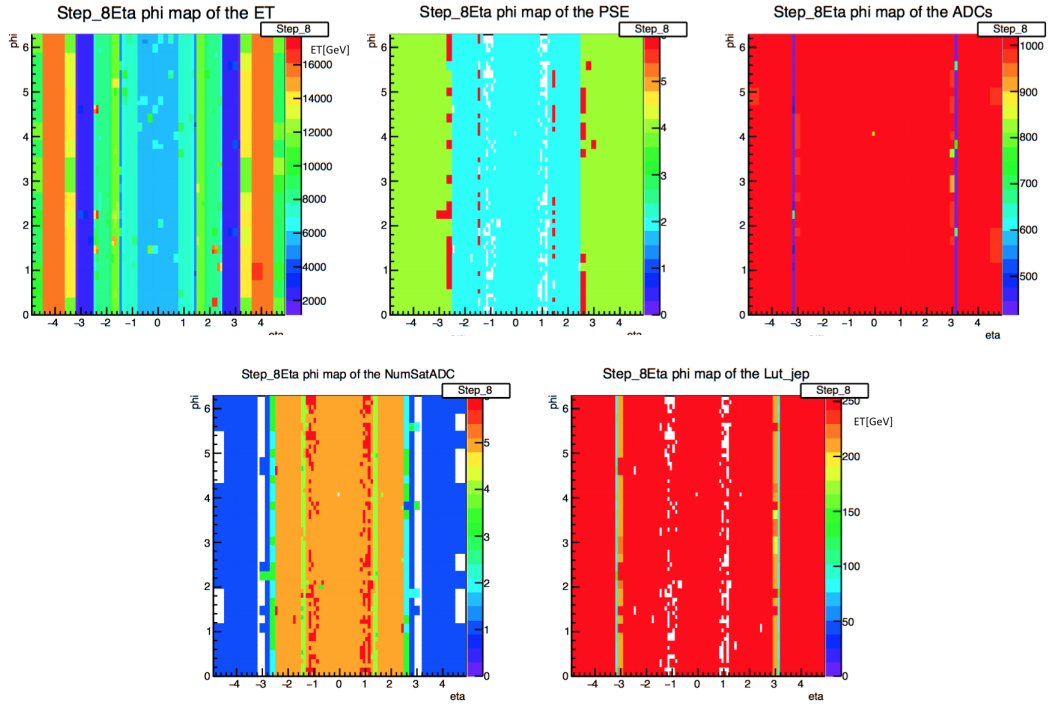

Figure 6.13: In the five plots are shown the five quantities we checked in 40 MHz pulser runs, where PeakFinder stops working at 3 saturated samples. It is for the highest energy step (in the EM layer of LAr calorimeter).

Since there were no improvements passing from four samples to three samples, we decided to let the PeakFinder work longer in order to catch low saturated pulses. Therefore the new decision logic, which was validated during this thesis, works ignoring the PeakFinder decision for four or more saturated samples.

To be thorough we will show the same plots done for the hadronic layer of Tile calorimeter. The energies are different because we switched to the usual energy range of the Tile calorimeter. We will start showing plots representing the old decision logic, then plots showing the logic in which the PeakFinder was ignored with $\geq$4 saturated samples and at the end the plots for the decision logic in which the PeakFinder was stopped for $\geq$3 saturate samples. The result is the same as before and the old logic doesn't work (see Fig. 6.16) for high energies. By looking at the E_T map and at the number of saturated samples map one can see that the energies are reduced. In the first energy step the signals are not saturated at all (not even one sample is saturated), therefore the PeakFinder works fine (PSE map in Fig. 6.14) and the E_T^{LUT} is almost completely full. Things change when the energy increases: the samples start to saturate and the PeakFinder starts failing. It is made clear by looking at the PSE and E_T^{LUT} in Fig. 6.16 that the PeakFinder is firing one BC earlier then the correct one. In the PSE map except for a few towers the only working algorithm is the SatBCID, but with the old decision logic its decision is ignored because the PeakFinder triggers earlier. Therefore, the final E_T^{LUT} map is almost empty.

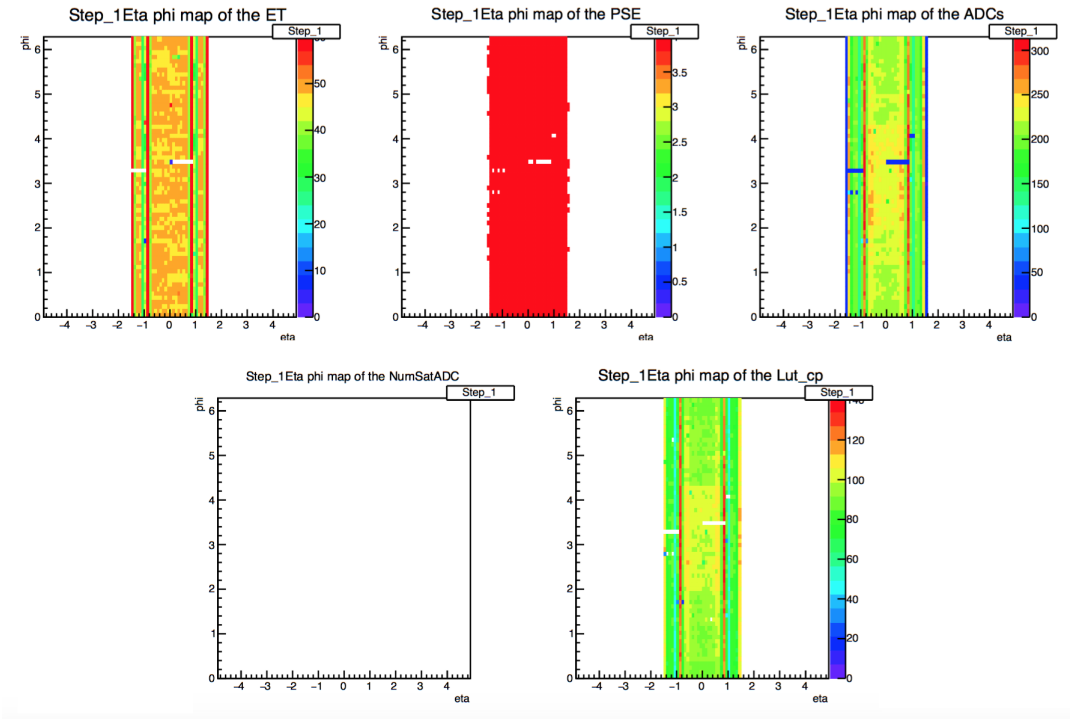

Figure 6.14: The five quantities we checked in 40 MHz pulser runs are shown in the five plots, for the lowest energy step (in the HAD layer of Tile calorimeter).

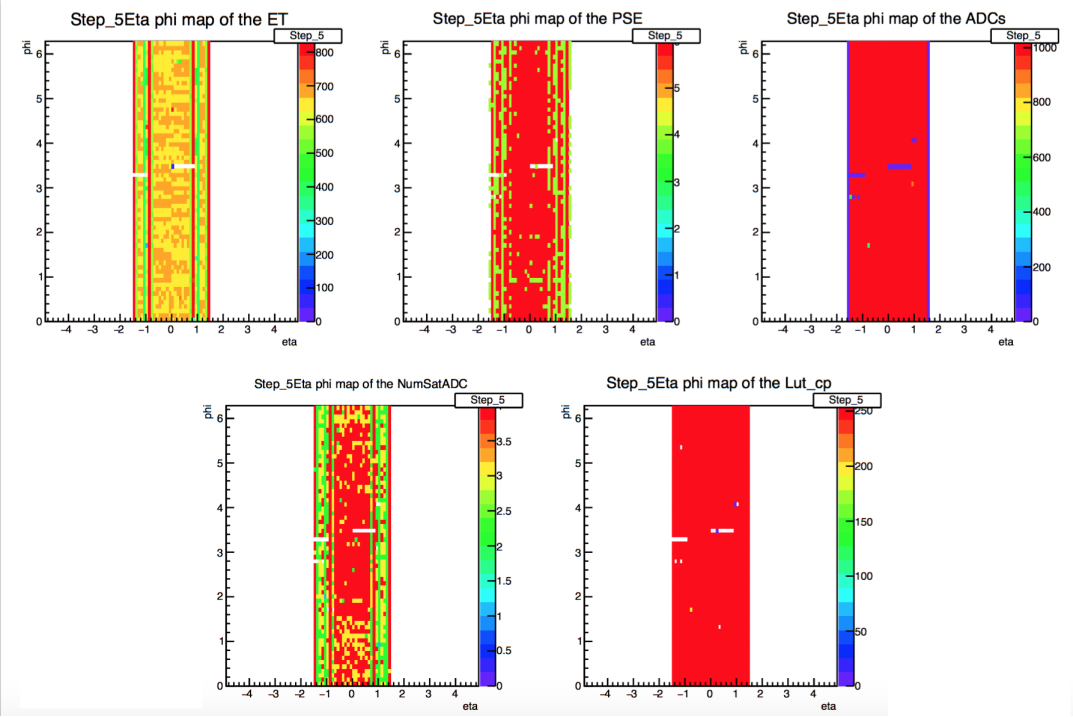

Figure 6.15: The five quantities we checked in 40 MHz pulser runs are shown in the five plots, for the middle energy step (in the HAD layer of Tile calorimeter).

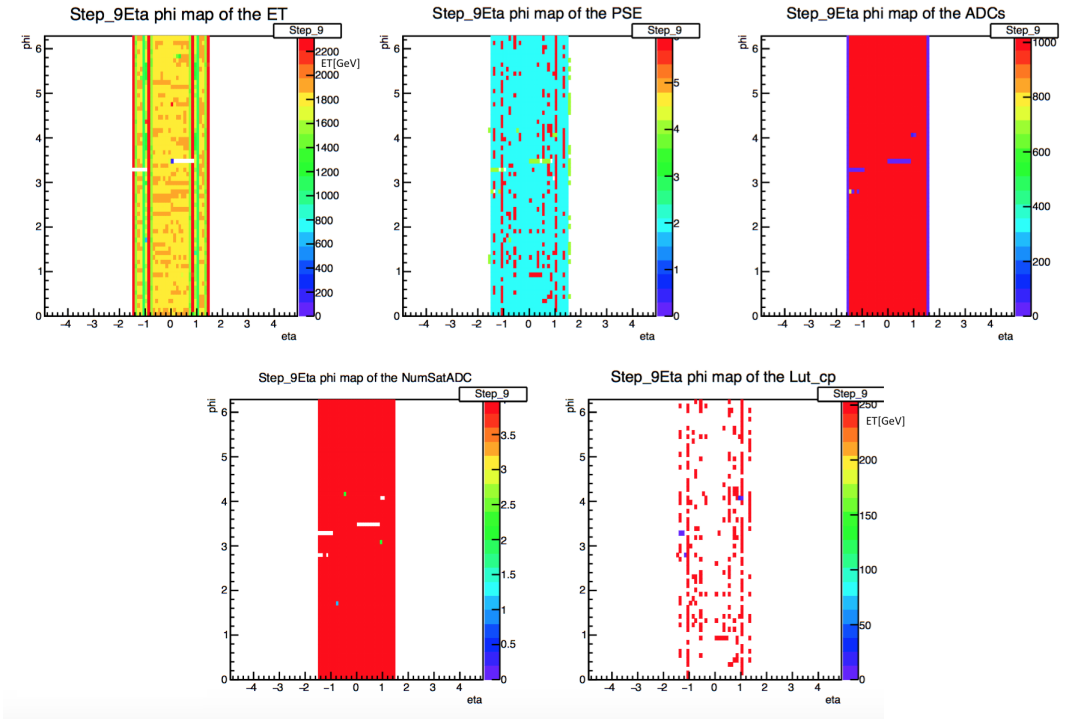

Figure 6.16: The five quantities we checked in 40 MHz pulser runs are shown in the five plots, for the highest energy step (in the HAD layer of Tile calorimeter).

A better efficiency is achieved ignoring the PeakFinder decision after 4 saturated samples. In Fig. 6.19 there is a big improvement, which could be understood by looking at the E_T^{LUT}. If the SatBCID works alone without the bias of the PeakFinder on the final decision, it will trigger on the correct bunch crossing, as expected.
A great efficiency was achieved for the Tile calorimeter and for the Liquid Argon Calorimeter turning off the PeakFinder after four saturated samples.

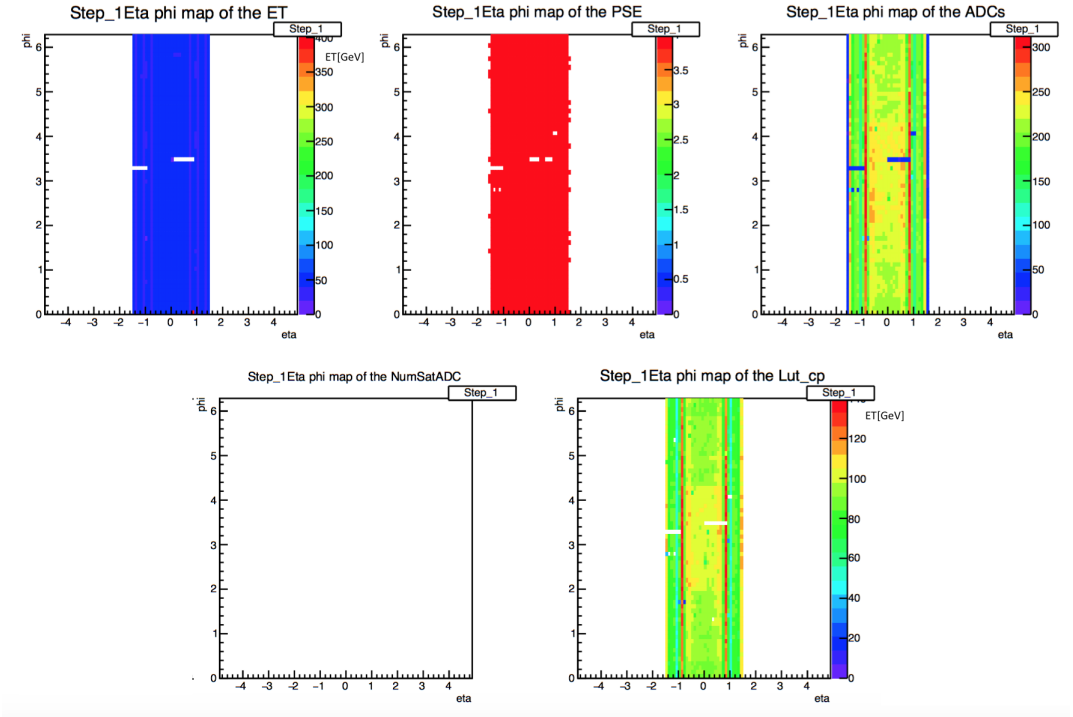

Figure 6.17: The five quantities we checked in 40 MHz pulser runs are shown in the five plots, for the lowest energy step (in the HAD layer of Tile calorimeter).

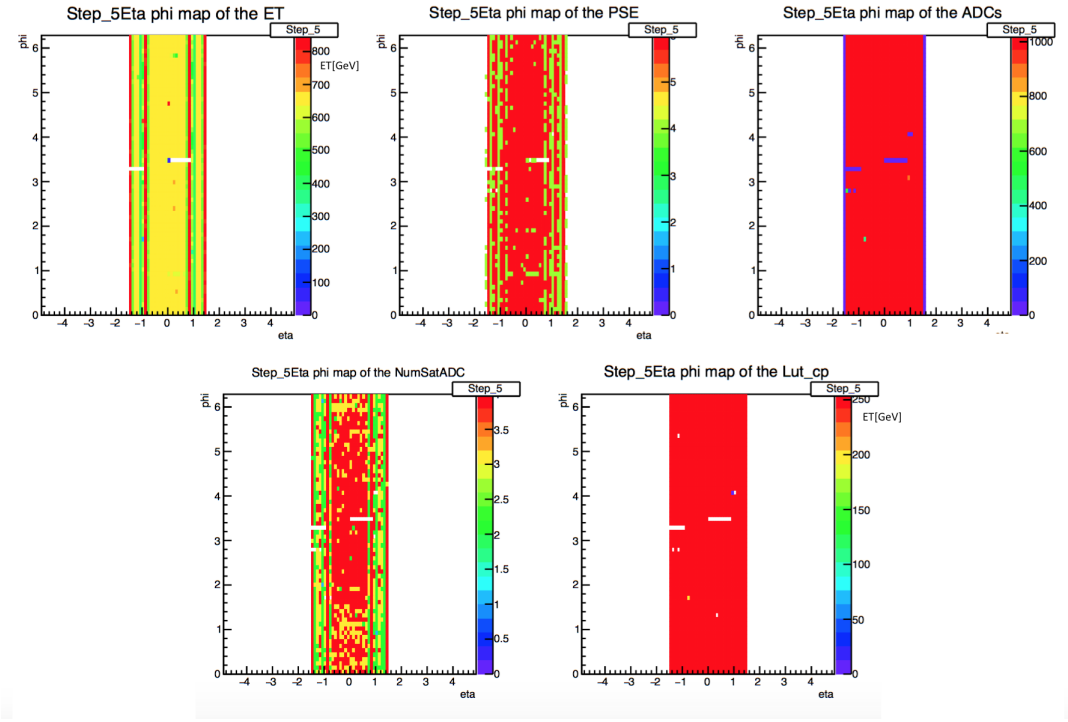

Figure 6.18: The five quantities we checked in 40 MHz pulser runs are shown in the five plots, for the middle energy step (in the HAD layer of Tile calorimeter).

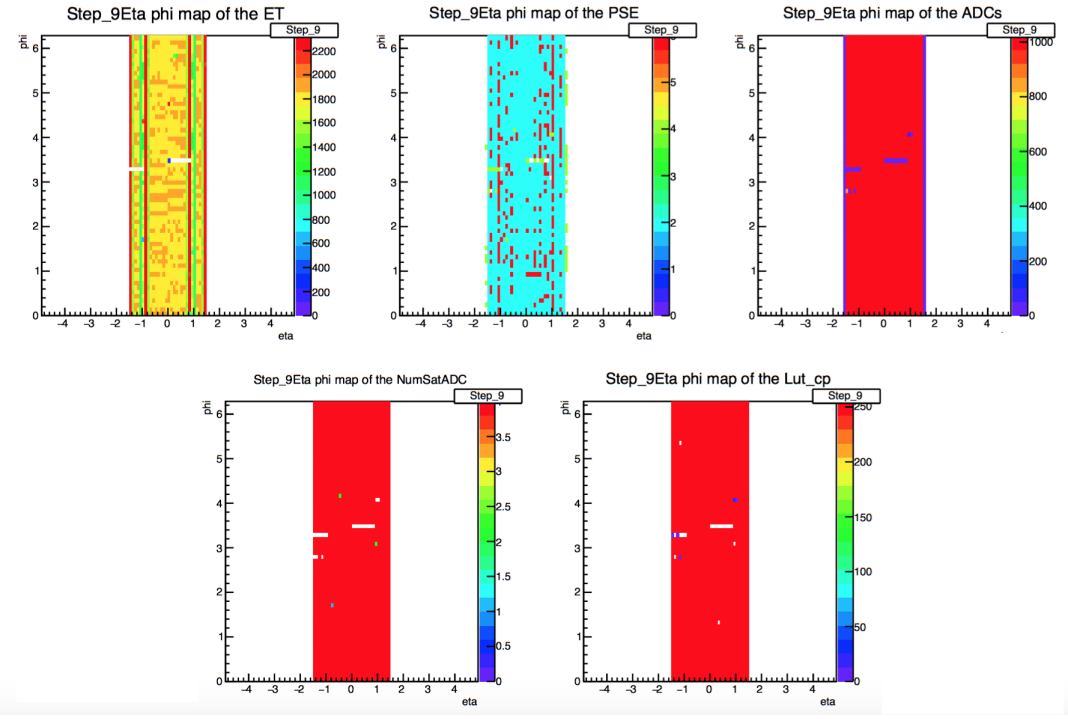

Figure 6.19: The five quantities we checked in 40 MHz pulser runs are shown in the five plots, for the highest energy step (in the HAD layer of Tile calorimeter).

In this case too the PeakFinder stopped at three saturated samples doesn't work because we start missing middle energy events, that could be identified only by PeakFinder (see Fig. 6.21). The PeakFinder should be allowed to work as much as possible, in such a way to handle the normal sized signals, which are hard for the SatBCID.
However, in the Tile physical runs a better efficiency is achieved turning off the PeakFinder after three or more saturated samples. It was seen that in physical runs the PeakFinder stopped at four saturated samples caused indeed early triggering. This discrepancy is probably due to the different shapes which we got in physical and calibration runs, as already mentioned in chapter five.

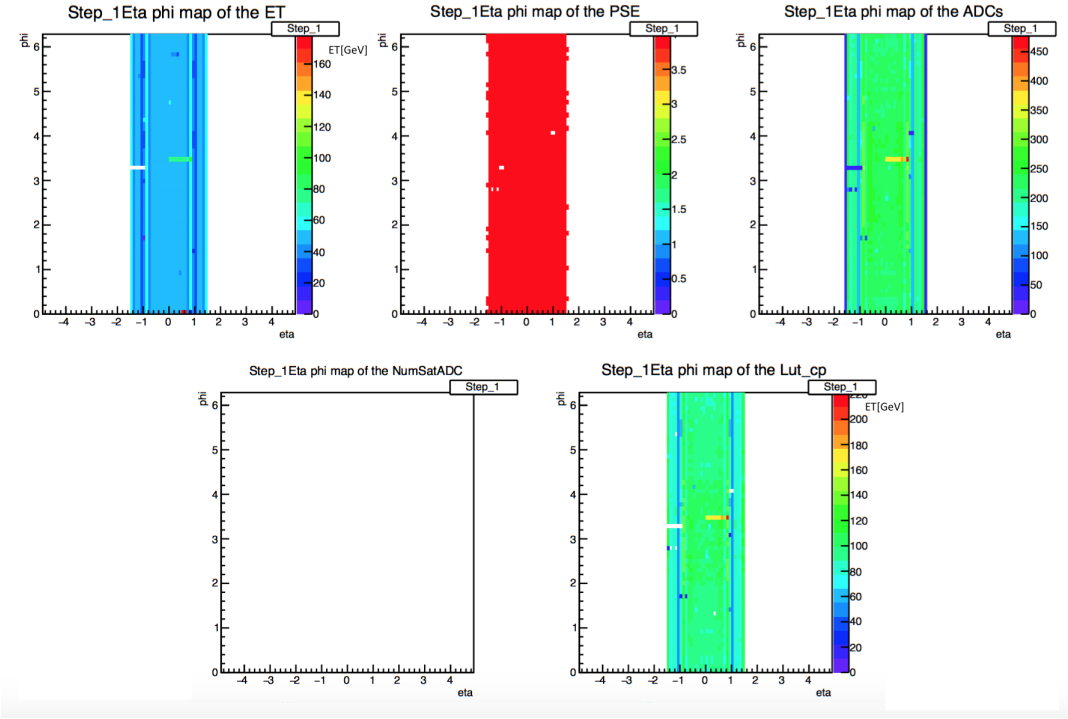

Figure 6.20: The five quantities we checked in 40 MHz pulser runs are shown in the five plots, for the lowest energy step (in the HAD layer of Tile calorimeter).

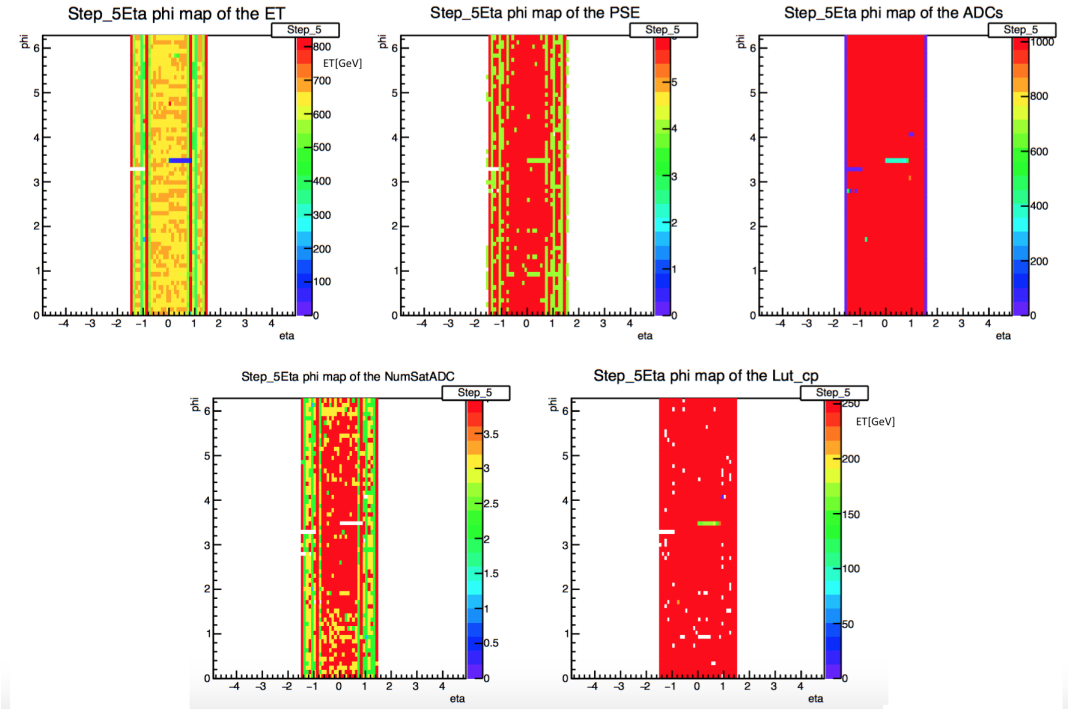

Figure 6.21: The five quantities we checked in 40 MHz pulser runs are shown in the five plots, for the middle energy step (in the HAD layer of Tile calorimeter).

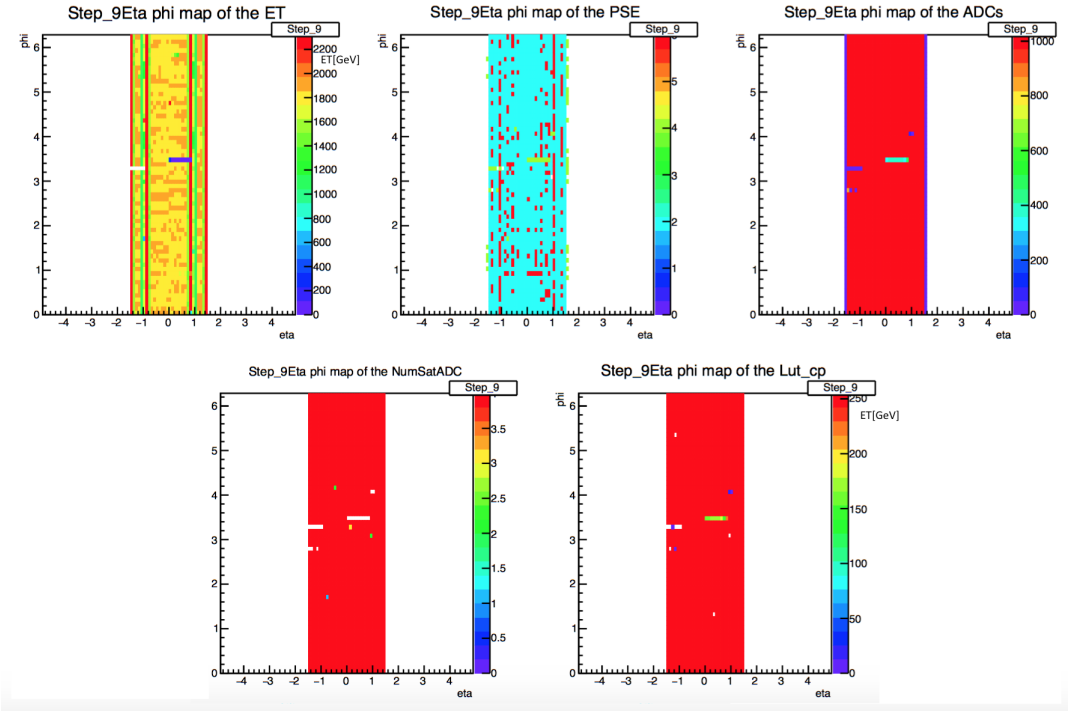

Figure 6.22: The five quantities we checked in 40 MHz pulser runs are shown in the five plots, for the highest energy step (in the HAD layer of Tile calorimeter).

Chapter 7

The Updated Saturated BCID Algorithm

Since the center of mass energy available at the LHC was increased in 2015 (during the first long shutdown), the Level-1 calorimeter trigger needed a new BCID algorithm that could handle these energies. In case of extreme saturation, neither the 40 MHz SatBCID nor the PeakFinder are able to find the peak sample. Therefore, the SatBCID working at 40 MHz was upgraded and a new algorithm was introduced, called Saturated BCID at 80 MHz*(Sat80)*.

7.1 The Algorithm Design

As the name suggests, the new BCID algorithm uses 80 MHz sampling. This digitizing speed allows us to have a finer sampling of the pulses injected into the calorimeter towers. Therefore, the rising edge of the signal can be measured in a better way even if the signal is highly saturated. It is a big improvement compared to the previous SatBCID at 40 MHz. After the upgrade of the LHC, the center of mass energy of the events was increased. Thus, we could have so energetic events that all the five 40 MHz samples were saturated. Since the algorithm working with thresholds needs at least one non-saturated sample, these events would be misidentified. In the figure 7.1 we can see a schematic view of the improvement. What happens in the PPr during the digitization process is that one 80 MHz sample is placed between each pair of 40 MHz samples. In the following, the design of the new Sat80 algorithm will be explained. It is based on four decision branches

1. if (s-1 $>$ high AND s-1.5 $>$ low) $\rightarrow$ BCID = s;
2. if (s-1 $>$ high AND s-1.5 $<$ low) $\rightarrow$ BCID = s+1;
3. if (s-1 $<$ high AND s-0.5 $>$ high) $\rightarrow$ BCID = s+1;
4. if (s-1 $<$ high AND s-0.5 $<$ high) $\rightarrow$ BCID = s +2.

In these branches s-0.5 stands for one 80 MHz sample to the left of the first saturated sample s. We used 0.5 and 1.5 because the samples are calculated always in 40 MHz units, so they indicate samples between the 40 MHz ones. The two thresholds (High

and Low) have to be calculated at trigger tower level in order to be optimized for the new algorithm (Fig. 7.2).

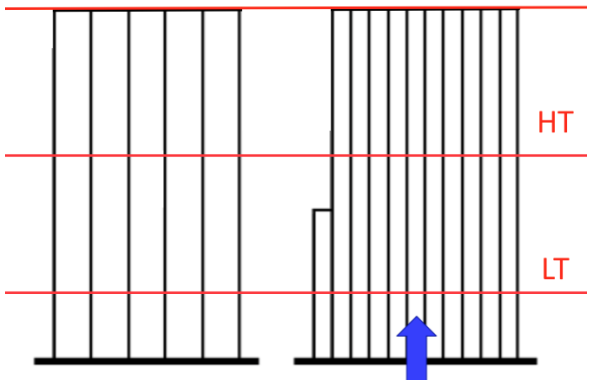

Figure 7.1: On the left side of the figure a signal digitized with 40 MHz speed is depicted. This cannot be handled by SatBCID working at 40 MHz because all the samples are saturated. On the right side there is the same pulse digitized in 80 MHz, ready to be analyzed by the Sat80. The blue arrow identifies the s+2 sample as the correct bunch crossing, because in this case the signal is in the fourth branch of the logic shown above.

7.2 Validation Process

Following the same method used for the validation of the new decision logic, we took calibration runs for the two calorimeters. In figure 7.3 we show a common pulse shapes at 80 MHz we got from pulser runs, for a saturated event and for a non-saturated event. For the Sat80 algorithm we looked at an information stored in the xAOD of pulser runs called RHL 3-bit. This is a 3-bit that tells us if the Sat80 took a decision or not, as the PSE 3-bit . Three information are stored in the RHL 3-bit:

- R stands for "result" and tells if the algorithm takes a decision for the BCID of the current pulse;
- H stands for "high threshold" and tells if the high threshold was passed by the pulse;
- L stands for "low threshold" and tells if the low threshold was passed by the pulse;

During the analysis we ignored the H and L contributions, only taking care about the R one. So the only two results we could have from the RHL 3-bit, after a decimal conversion, were 4, if there was a decision, or 0, if there was not. By studying the usual $\eta - \phi\, maps$ of the R bit, it is possible to understand if the Sat80 is working or not at trigger tower level.

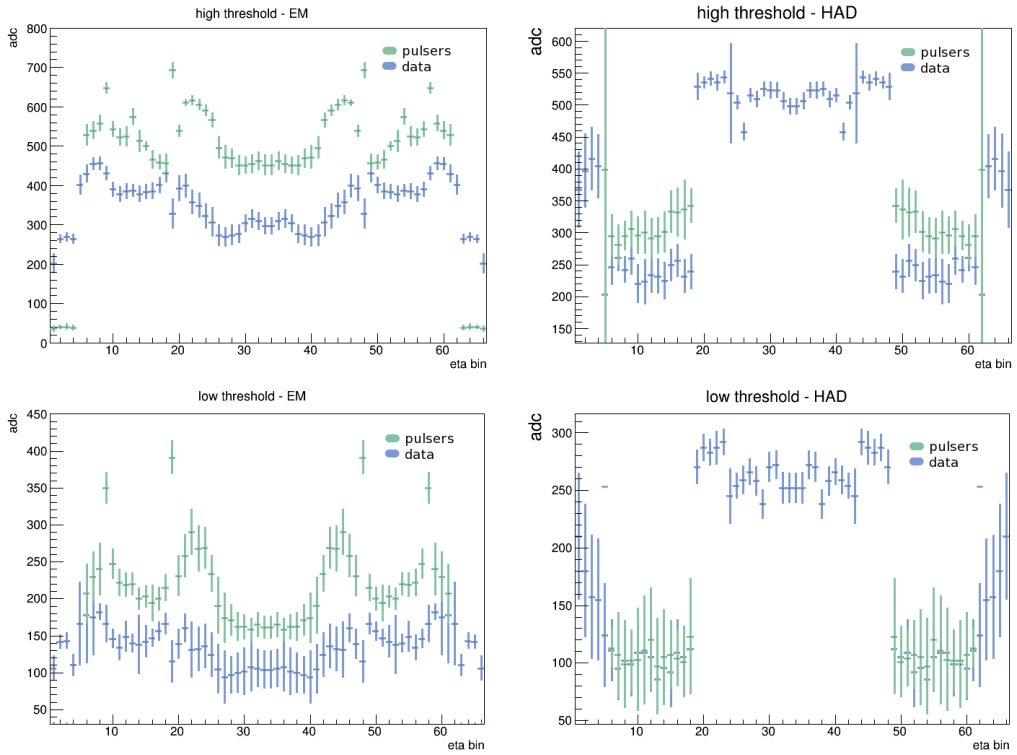

Figure 7.2: The picture shows the averages on η of the thresholds for the EM and HAD layers (LAr) [23].

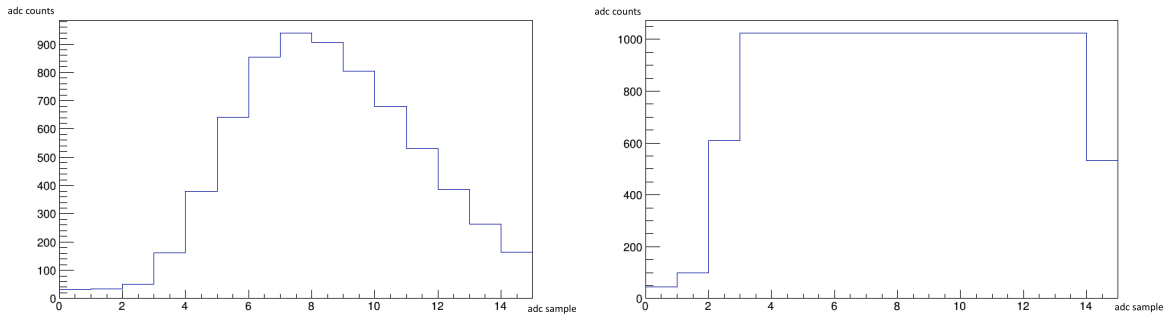

(a) (b)

Figure 7.3: In the picture one can see a non saturated pulse in 80 MHz (a) and a highly saturated one (b), both of them are from a calibration run used for the validation of the Sat80 algorithm.

7.3 Results

Now maps of the result bit will be shown for the calorimeter towers. The same decision logic as before was used, and it stops the PeakFinder for a number of saturated slices ≥ 4. In the following we show the data taken from the same pulser runs, for the EM layer of the LAr calorimeter. By looking at the Sat80 performance for pulser runs we found out an inefficiency at high energies, for which this algorithms is designed. In Fig. 7.4 one can see that the Sat80 algorithm works well in all the central barrel where the energies are high enough to produce saturation. Outside the barrel the algorithm didn't fire indeed, this happens because the energy is so low that the saturation regime is not reached. Increasing the energy (Fig. 7.5) a larger number of towers starts saturating, at the same time the algorithm shows inefficiencies and white strips modulated in the η coordinate start appearing. This pattern modulated in η is even more present in the higher energy steps as for example in (Fig. 7.6). In this figure inefficiencies are shown, mostly in the region $-1.2 < \eta < 1.2$. The modulation along η is due to the fact that the towers at the same η have the same number of calorimeter cells inside. Thus, the shaping of the signals produced by the charge injection system is very similar. Therefore it can happen that the algorithm doesn't work along a whole η strip.
This inefficiency could be due to the fact that at high energies the charge injection system produces pulses that are not reliable as for low energy signals. We tried to figure it out in the next paragraph.

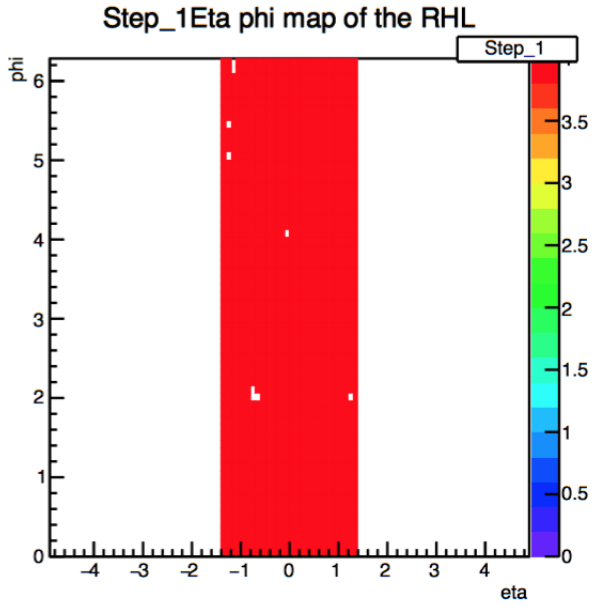

Figure 7.4: In the plot the result bit is shown over all the the trigger towers for the EM layer of the LAr calorimeter. At low energies (the same as for Fig. 6.8) the Sat80 provides good coverage.

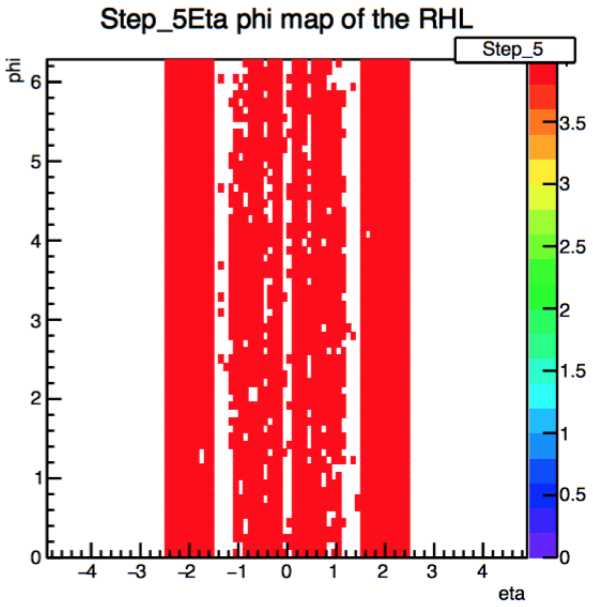

Figure 7.5: In the plot the result bit is shown over all the the trigger towers for the EM layer of the LAr calorimeter. At medium energies (the same as for Fig. 6.9) the Sat80 starts failing.

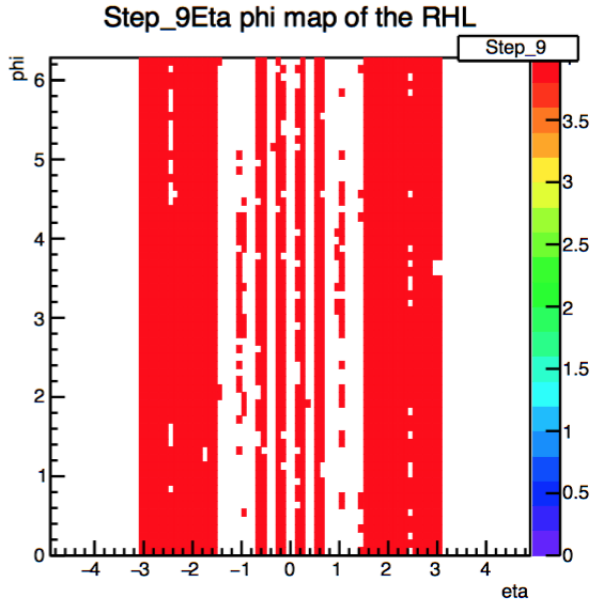

Figure 7.6: In the plot the result bit is shown over all the the trigger towers for the EM layer of the LAr calorimeter. At high energies (the same as for Fig. 6.10) the Sat80 shows a inefficiency mostly in the central barrel.

7.4 Emulating the Algorithm

In order to understand if it is possible to validate the Sat80, an emulation logic was designed, which is a software that mimics the algorithm behavior. For this, new custom thresholds were derived from pulser runs and given as an input to the emulation logic. This was done in order to make thresholds as compatible as possible with pulser runs. Consequently, the emulation logic takes these new thresholds together with digitized samples of the signals and makes a decision, emulating the algorithm. In the following plots (Fig. 7.7, Fig. 7.8, Fig. 7.9) the behavior of the emulation logic is shown, for the same energy steps showed in the previous section.

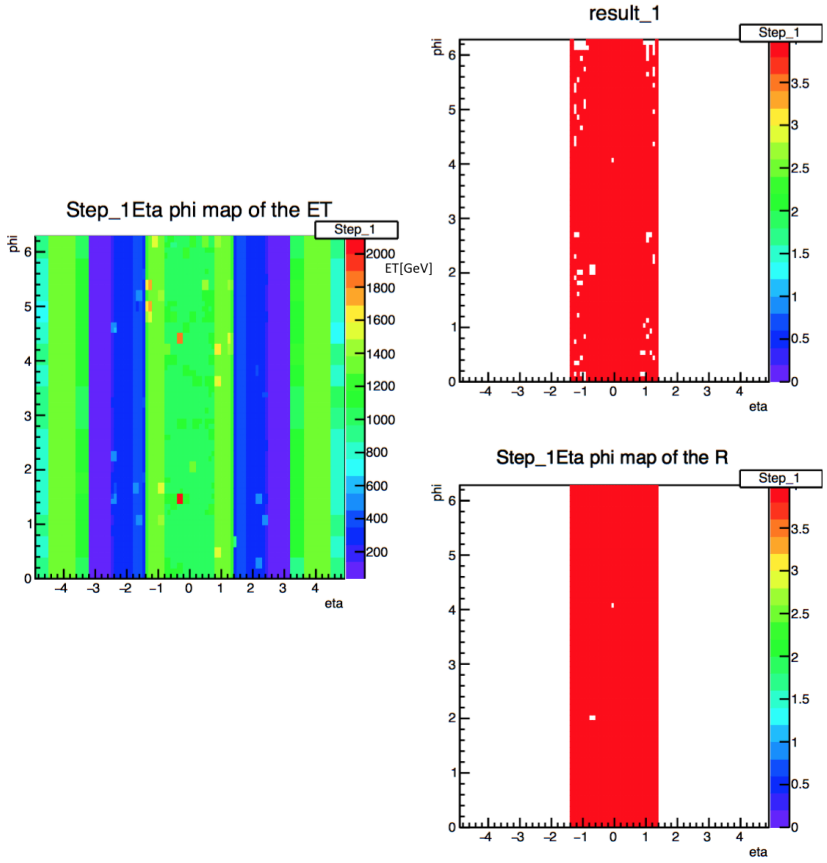

Figure 7.7: In the top right plot (*result_1*) the emulation logic response for the lowest energies is shown (LAr EM layer). On the left and on the bottom the transverse energy and the result bit of the RHL 3-bit are plotted. The latter worked with the old thresholds calibrated on the physical pulse. All the plots refers to lowest energy step.

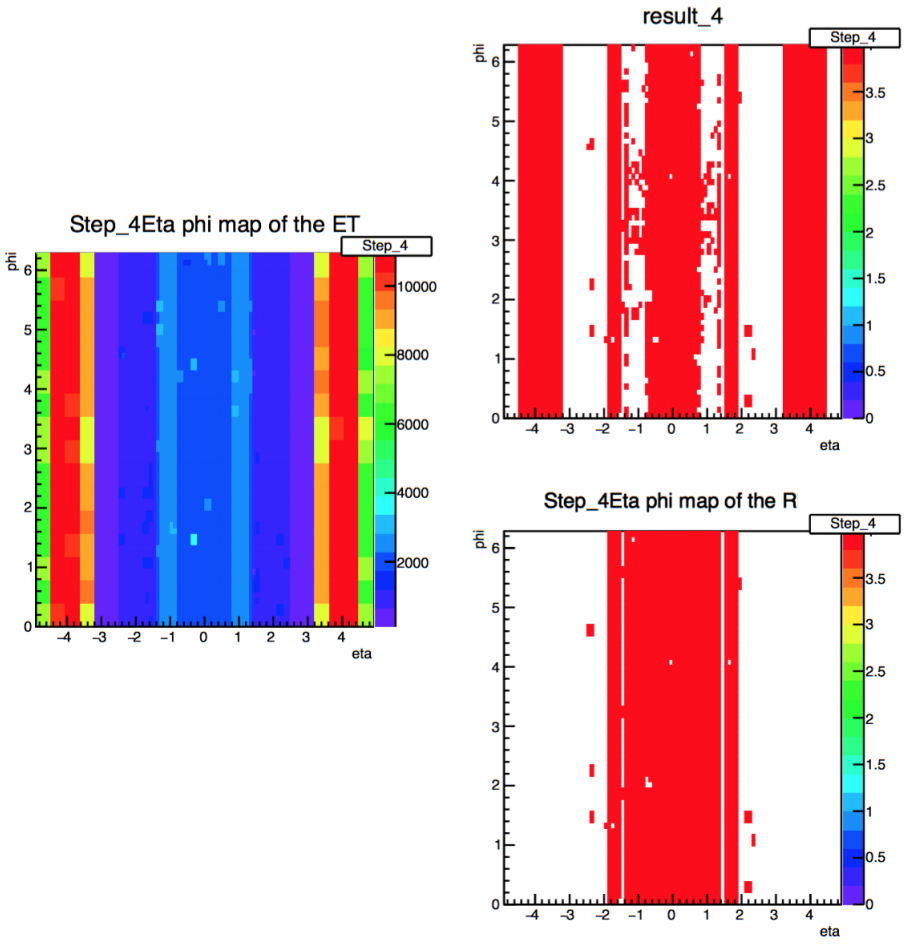

Figure 7.8: In the top right plot (*result_4*) the emulation logic response for the lowest energies is shown (LAr EM layer). On the left and on the bottom the transverse energy and the result bit of the RHL 3-bit are plotted. The latter worked with the old thresholds calibrated on the physical pulse. All the plots refers to middle energy step.

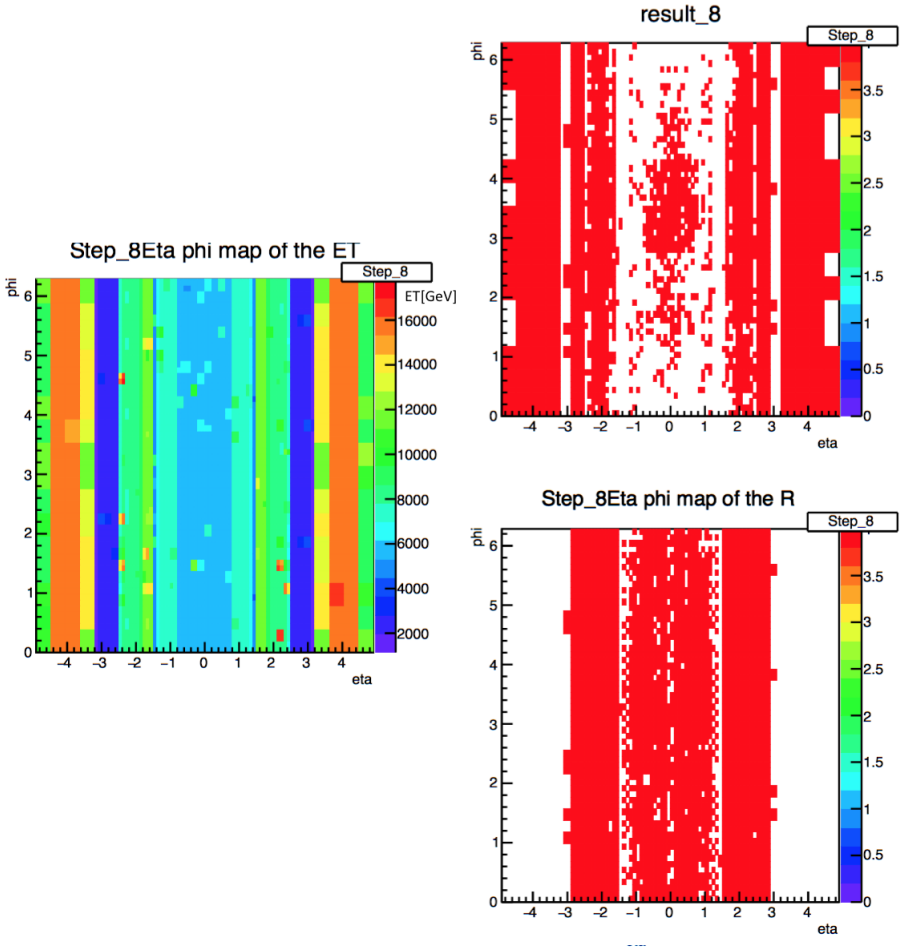

Figure 7.9: In the top right plot (*result_8*) the emulation logic response for the lowest energies is shown (LAr EM layer). On the left and on the bottom the transverse energy and the result bit of the RHL 3-bit are plotted. The latter worked with the old thresholds calibrated on the physical pulse. All the plots refers to highest energy step.

As one can see in the figures 7.7, 7.8 and 7.9 the algorithm is not working correctly even if the thresholds are optimized on pulser runs. However, the thresholds for one trigger towers are derived assuming the linear behavior for all the ADC values as a function of the energy measured by the calorimeters. Therefore in order to figure out this large inefficiency, the relationship between ADC counts and energy was checked for pulser runs. The single trigger towers were picked up and their ADCs have been studied as function of the calorimeter transverse energy. In the following plots (Fig. 7.10, Fig. 7.11, Fig. 7.12, Fig. 7.13) examples taken for one trigger tower in the central barrel of the LAr calorimeter are displayed. The points represent the ADC counts/E_T correlation for the 2000 events stored in the xAOD, looking at one particular trigger tower.

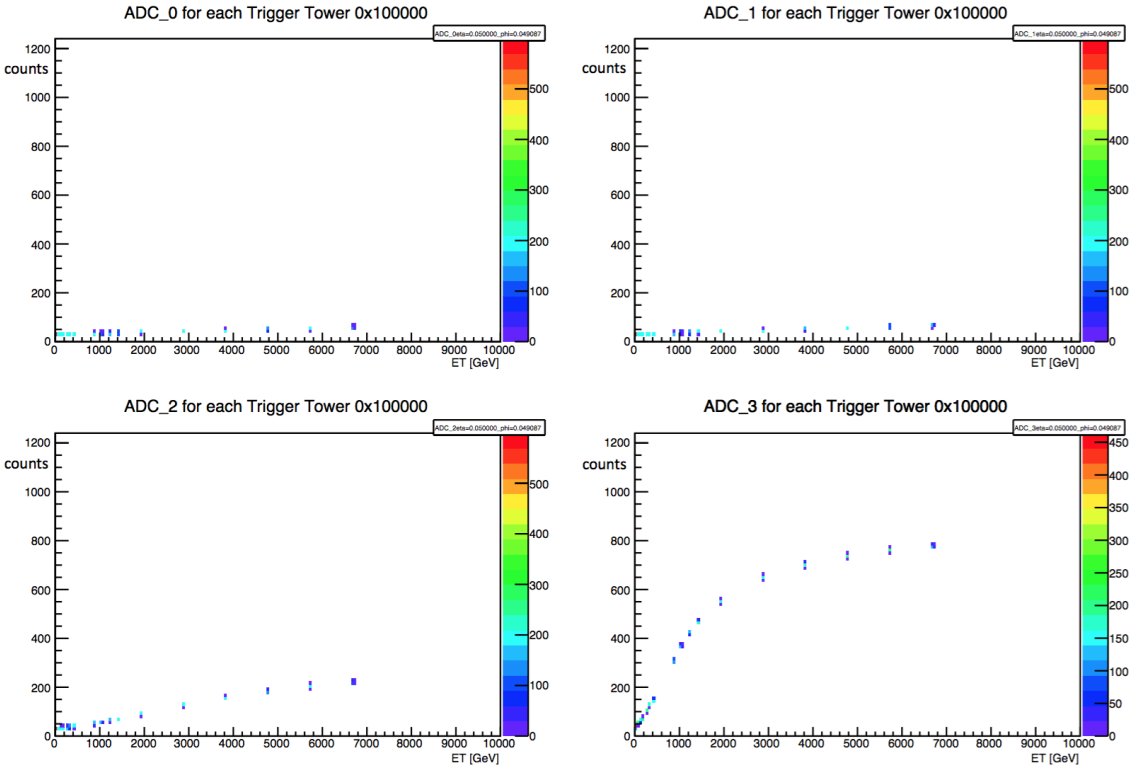

Figure 7.10: In this plots four ADC sample curves are shown. The colored scale on the right side shows the number of the events present in the same 2-D bin.

Especially by looking at fig. 7.10 and 7.11 one can immediately see the nonlinearity of the curves before saturation. In the two bottom plots of fig. 7.10, ADC_2 and ADC_3 have two turning points: the first around 1000 GeV and the other around 3500 GeV. They are not due to saturation effects, because they are far away from the saturation regime. The assumption of the linear behavior doesn't hold for so energetic pulses. It is probably due to an intrinsic characteristic of the pulser system at high energies. By looking at the previous plot we could conclude that validating the Sat80 algorithm is not possible using pulser runs. It is not possible to extract thresholds with the ADC nonlinear behaviors, then the fundamental as-

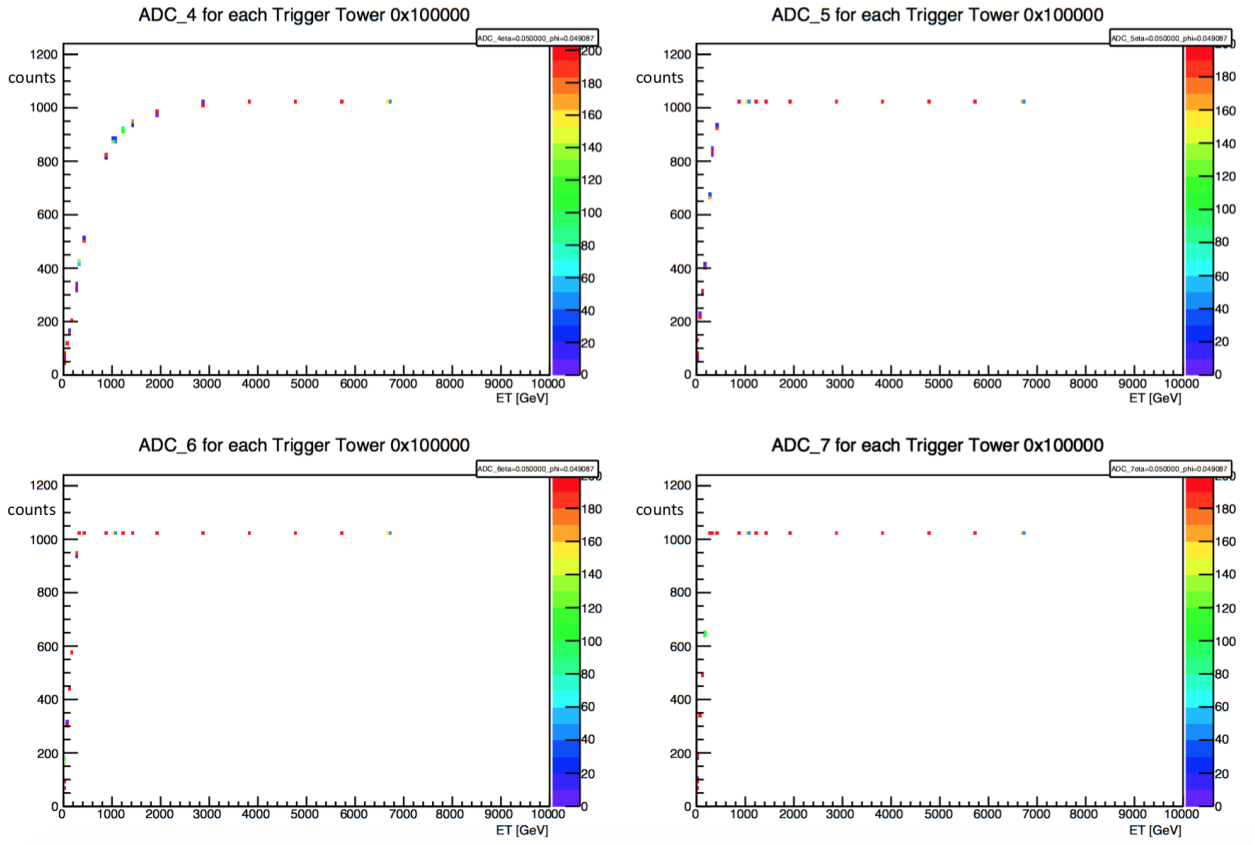

Figure 7.11: In this plots four ADC sample curves are shown. The colored scale on the right side shows the number of the events present in the same 2-D bin.

sumption of the algorithm doesn't hold anymore. Therefore, the validation of the Sat80 for the highest energies can be performed only using physical runs.
The last two figures 7.12 and 7.13 show the typical turning point when the energies in the samples are high enough to get in the digital saturation regime. In this plots the nonlinear behavior is due to the saturation of the ADCs and the more the energy increases the more the turing point is narrow and abrupt.

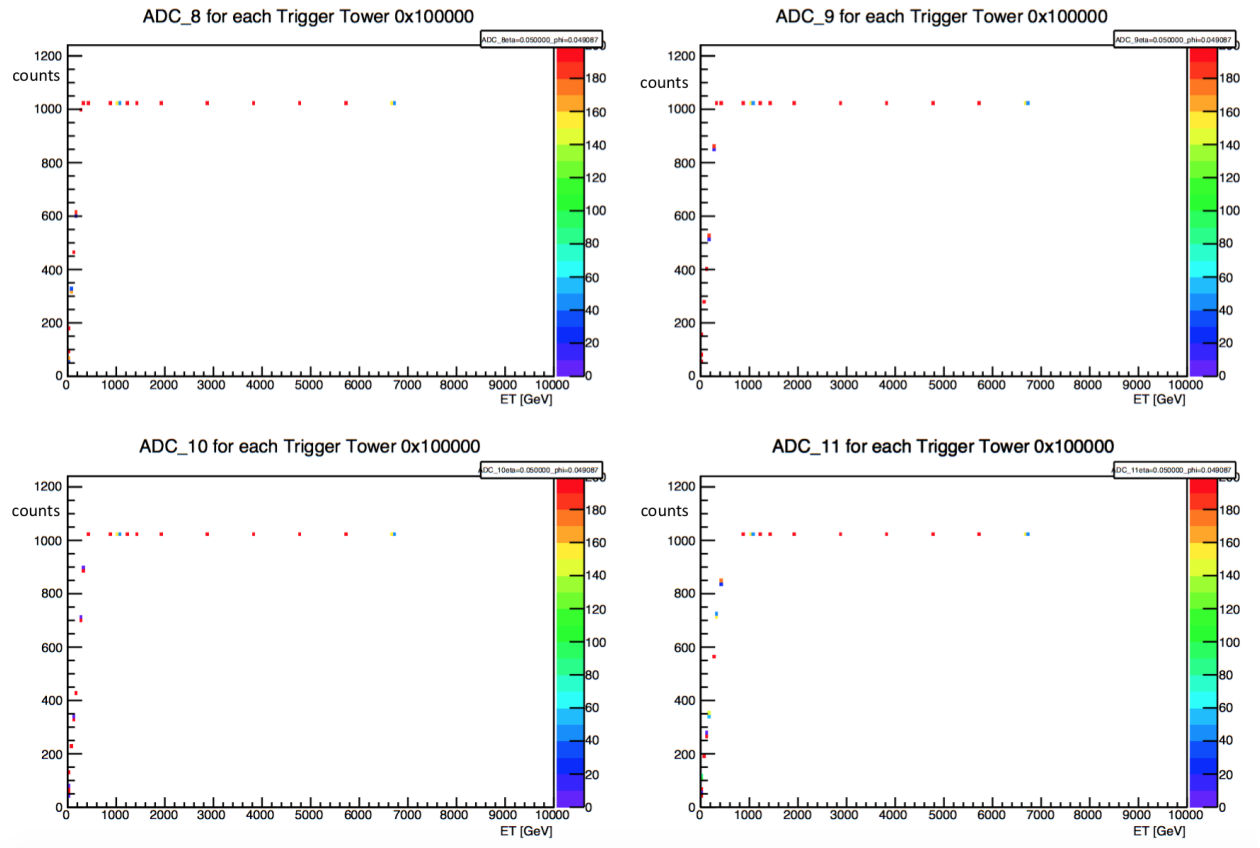

Figure 7.12: In this plots four ADC sample curves are shown. The colored scale on the right side shows the number of the events present in the same 2-D bin.

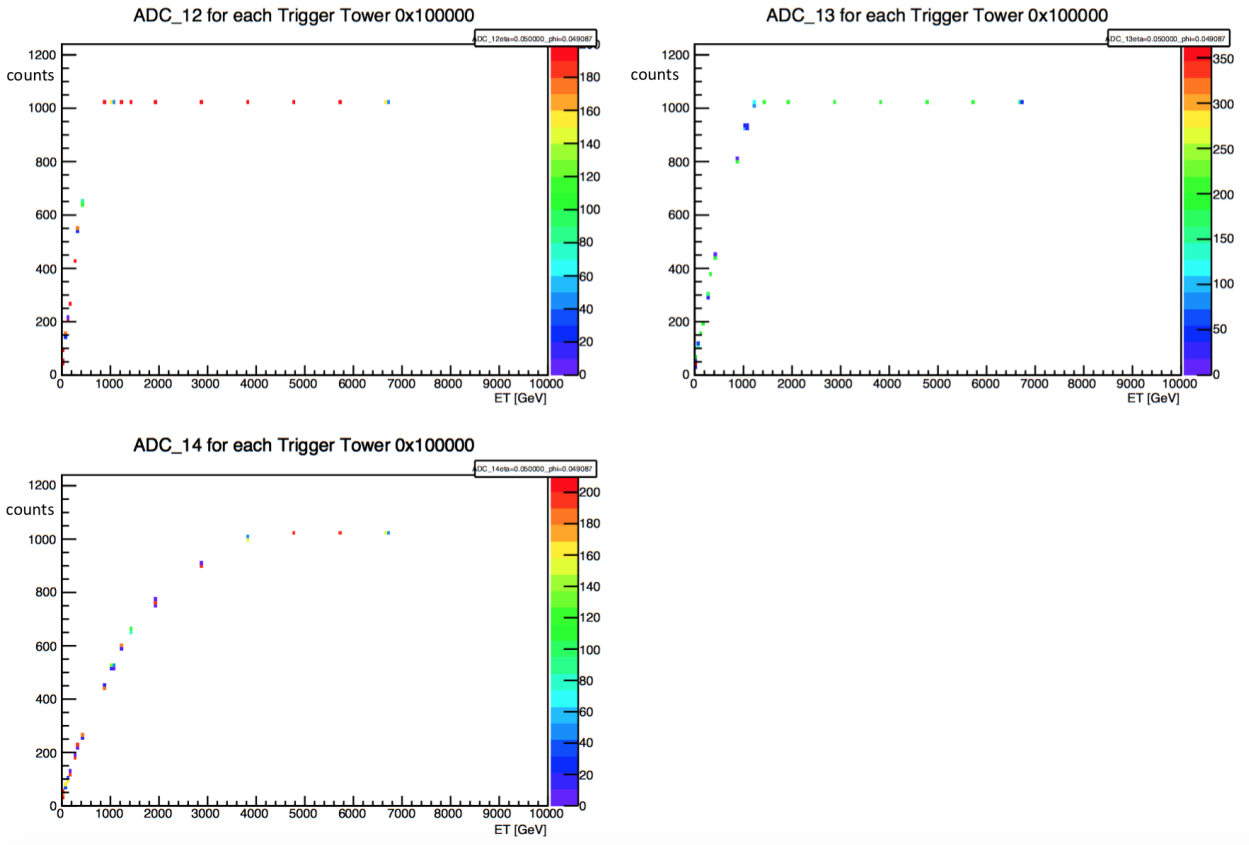

Figure 7.13: In this plots four ADC sample curves are shown. The colored scale on the right side shows the number of the events present in the same 2-D bin.

Chapter 8

Conclusions

In this thesis I worked on the Level-1 Calorimeter Trigger system of the ATLAS detector. In particular we carried out studies on the working principle of the two algorithms responsible for the bunch crossing identification at L1Calo. The whole system was tested, optimized and validated by means of calibration runs, called pulser runs. They were produced by the charge injection system of the two calorimeters, which emulates the physical pulses by injecting charges directly into the calorimeter cells. This system was used in order to check the L1Calo behavior indeed, especially at highly saturated regime. The calibration run data were analyzed using ATHENA framework and the software ROOT. I tested also the also the discrepancy between the physical signal and the calibration run pulse. As expected, it was found that pulse shapes are not exactly the same for physics runs and for pulser runs. This discrepancy grows for very high energies and also by moving on the η coordinate.

Furthermore in this thesis I validated a new decision logic, which combines the two bunch crossing identification algorithms (PeakFinder and Saturated BCID),up to highly saturated regime (7-8 TeV). It was developed in order to handle the highly saturated pulses, which caused a small inefficiency. It combines the high precision of the PeakFinder algorithm for the BCID on normal sized signals, with the high efficiency of the SatBCID working at 40 MHz for highly saturated pulse. A new variable was introduced into the logic: the number of saturated samples, which quantifies the saturation level of the signal. I found out that switching off the PeakFinder decision at 4 or more saturated samples, a better efficiency in the BCID was achieved. The liquid argon and the tile calorimeter were checked over a large energy spectrum. A good trigger towers coverage was achieved with this new set-up. This new decision logic is now online in the Level-1 Calorimeter Trigger and it is the main result of the studies conducted in this Master Thesis work, because it will allow the L1Calo to work fine up to very high energies.

Another study that I carried out was the validation of the Saturated BCID working at 80 MHz. We used pulser runs with the same energies as before in order to check the improvement led by this new algorithm with a doubled digitization speed. Unfortunately we discovered that for the highest energies the charge injection system does not reproduce correctly the signal shape. The height of the digitized samples

is not linearly correlated with the energy anymore, but it has strong deviation especially in the early samples. Without the hypothesis of the linear behavior as a function of the energy, this algorithm can't be correctly calibrated. Therefore, the algorithm couldn't be validated using pulser runs at these energies and so physics runs had to be used.
However, further studies on the algorithm behavior with pulser runs will be done, considering also the functional behavior of the ADC curves depending on the spacial coordinates. In this direction fit studies will be performed in the next works which will be conducted on that topic.

Appendix A

HAD layer of the LAr calorimeter

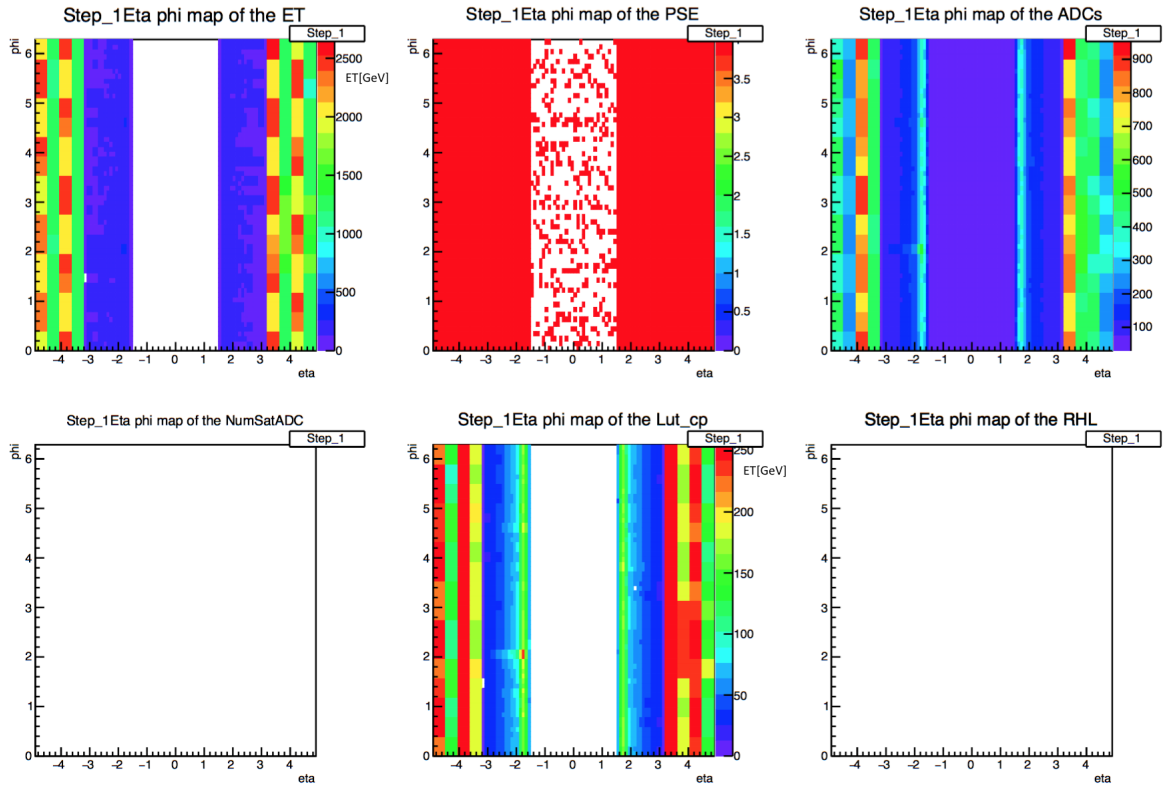

Figure A.1: Starting from the top left, the six quantities shown in the picture are: the transverse energy E_T, the PSE 3-bit, the ADCs counts, the number of saturated samples, the E^T_{LUT} and the result bit from the RHL 3-bit. These $\eta - \phi$ maps are taken from pulser runs referring to the hadronic layer of the LAr calorimeter. In this case the lowest energy step of the run is shown, and as one can see the energy is not high enough to produce the saturation of the samples. The PeakFinder worked always in this calibration run.

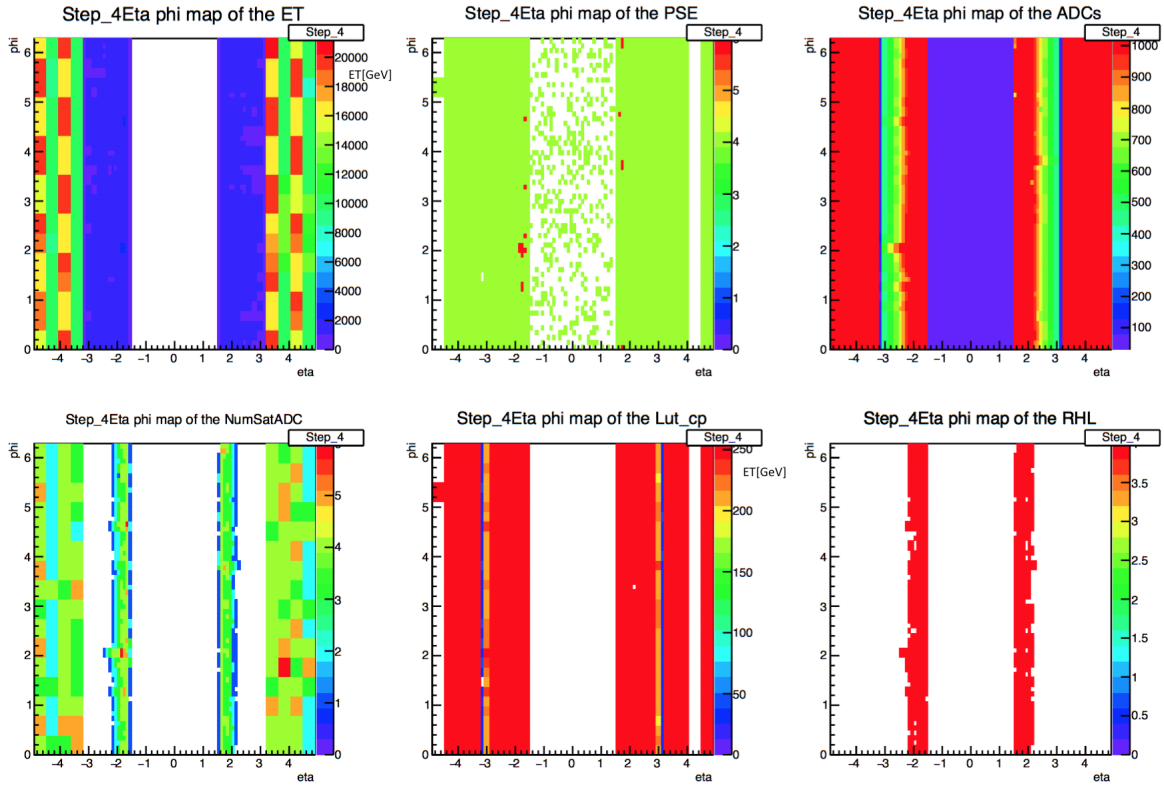

Figure A.2: Starting from the top left, the six quantities shown in the picture are: the transverse energy E_T, the PSE 3-bit, the ADCs counts, the number of saturated samples, the E^T_{LUT} and the result bit from the RHL 3-bit. These $\eta - \phi$ maps are taken from pulser runs referring to the hadronic layer of the LAr calorimeter. In this case the medium energy step of the run is shown, the samples start saturating and the SatBCID starts working too. The PeakFinder worked always in this calibration run.

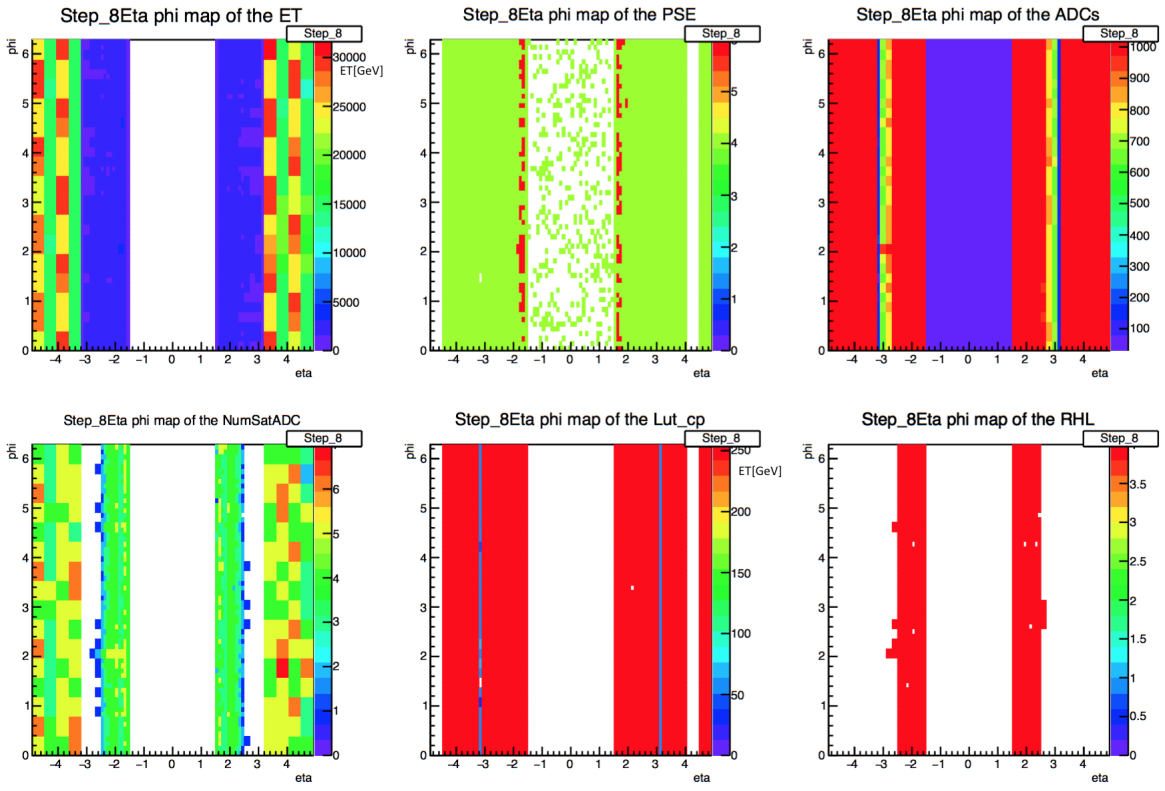

Figure A.3: Starting from the top left, the six quantities shown in the picture are: the transverse energy E_T, the PSE 3-bit, the ADCs counts, the number of saturated samples, the E^T_{LUT} and the result bit from the RHL 3-bit. These $\eta - \phi$ maps are taken from pulser runs referring to the hadronic layer of the LAr calorimeter. In this case the highest energy step of the run is shown, the samples are saturated. The PeakFinder worked always in this calibration run.

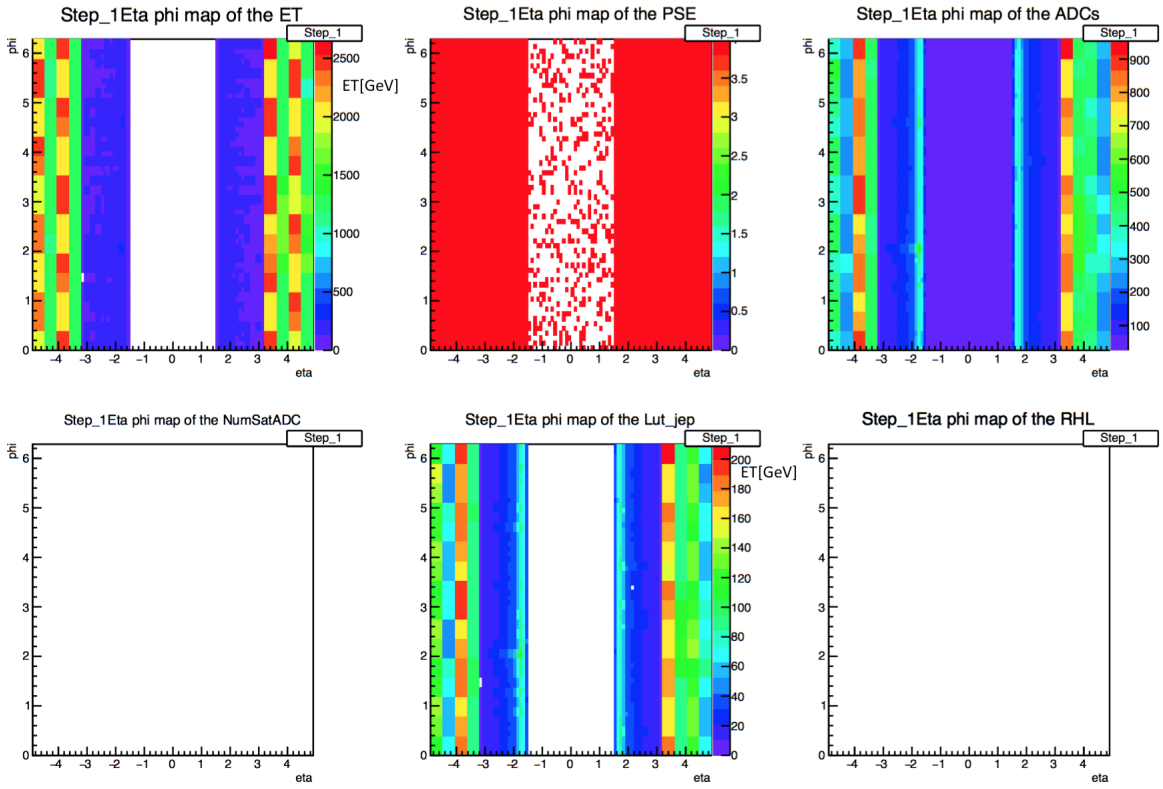

Figure A.4: Starting from the top left, the six quantities shown in the picture are: the transverse energy E_T, the PSE 3-bit, the ADCs counts, the number of saturated samples, the E^T_{LUT} and the result bit from the RHL 3-bit. These $\eta - \phi$ maps are taken from pulser runs referring to the hadronic layer of the LAr calorimeter. In this case the lowest energy step of the run is shown, and as one can see the energy is not high enough to produce the saturation of the samples. The PeakFinder worked for less than 4 saturated samples in this calibration run.

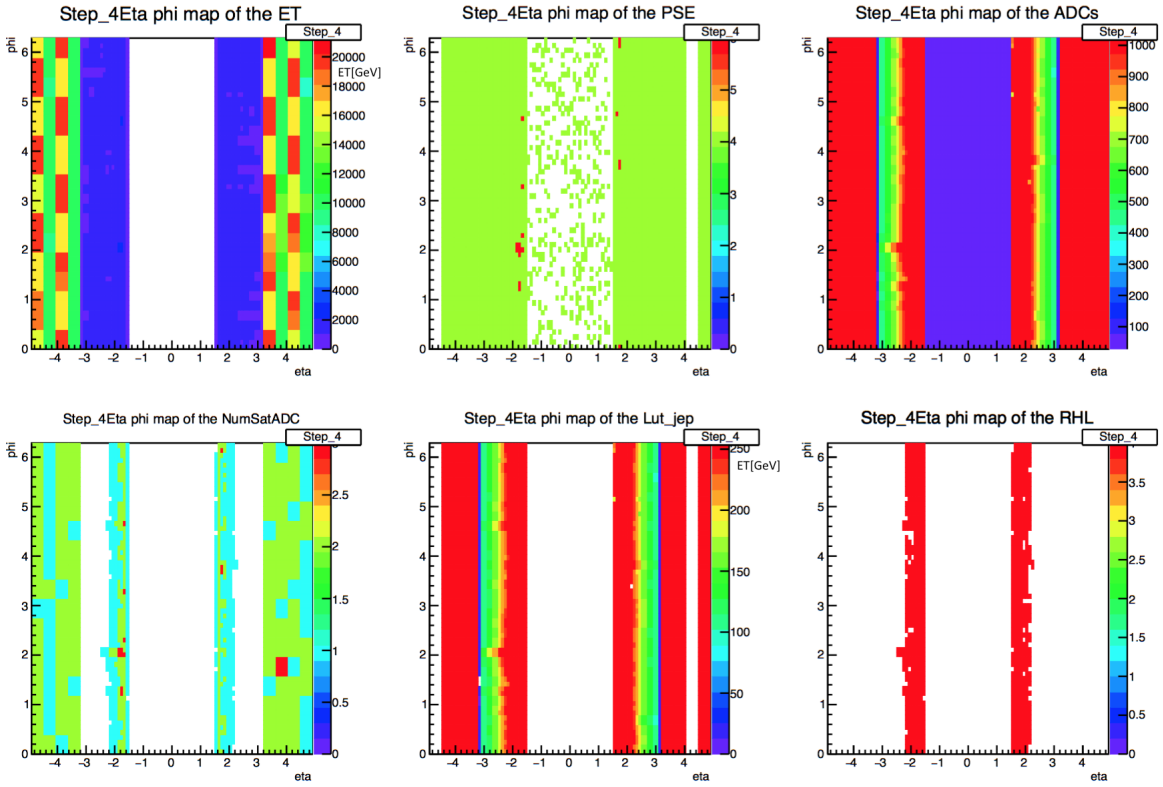

Figure A.5: Starting from the top left, the six quantities shown in the picture are: the transverse energy E_T, the PSE 3-bit, the ADCs counts, the number of saturated samples, the E^T_{LUT} and the result bit from the RHL 3-bit. These $\eta - \phi$ maps are taken from pulser runs referring to the hadronic layer of the LAr calorimeter. In this case the medium energy step of the run is shown, the samples start saturating and the SatBCID starts working too. The PeakFinder worked for less than 4 saturated samples in this calibration run.

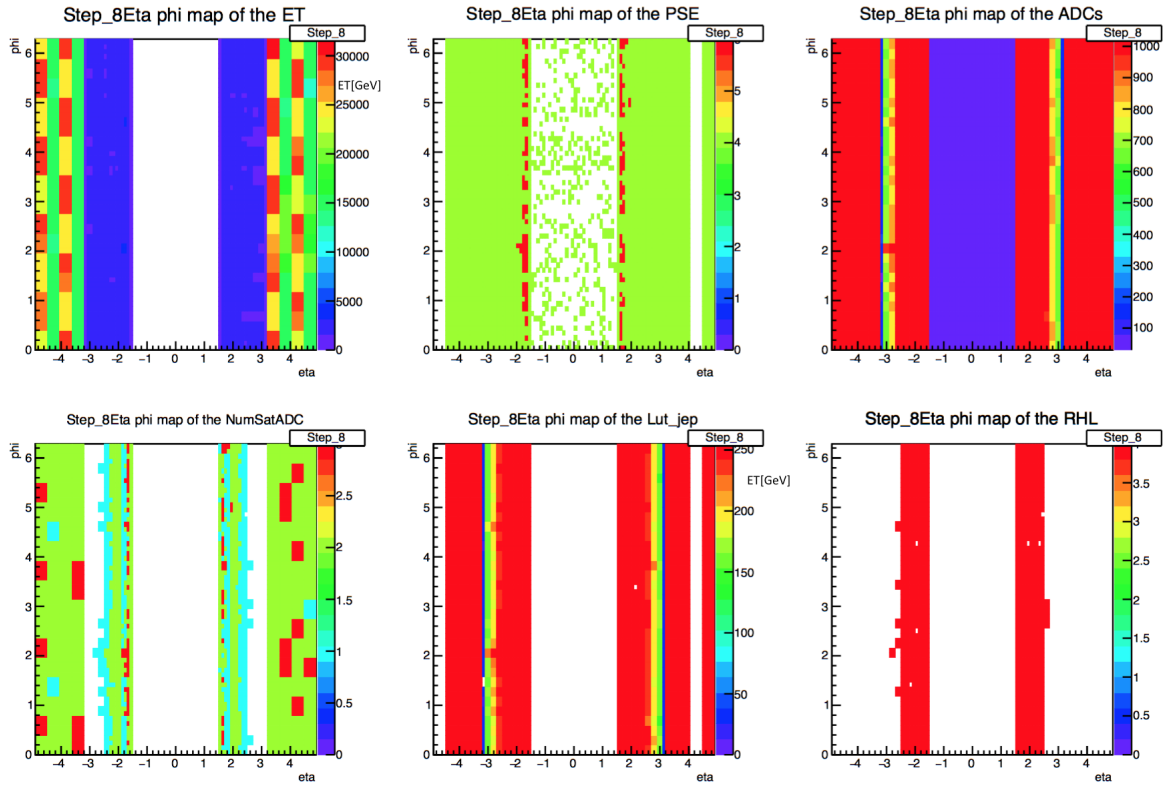

Figure A.6: Starting from the top left, the six quantities shown in the picture are: the transverse energy E_T, the PSE 3-bit, the ADCs counts, the number of saturated samples, the E^T_{LUT} and the result bit from the RHL 3-bit. These $\eta - \phi$ maps are taken from pulser runs referring to the hadronic layer of the LAr calorimeter. In this case the highest energy step of the run is shown, the samples are saturated. The PeakFinder worked for less than 4 saturated samples in this calibration run.

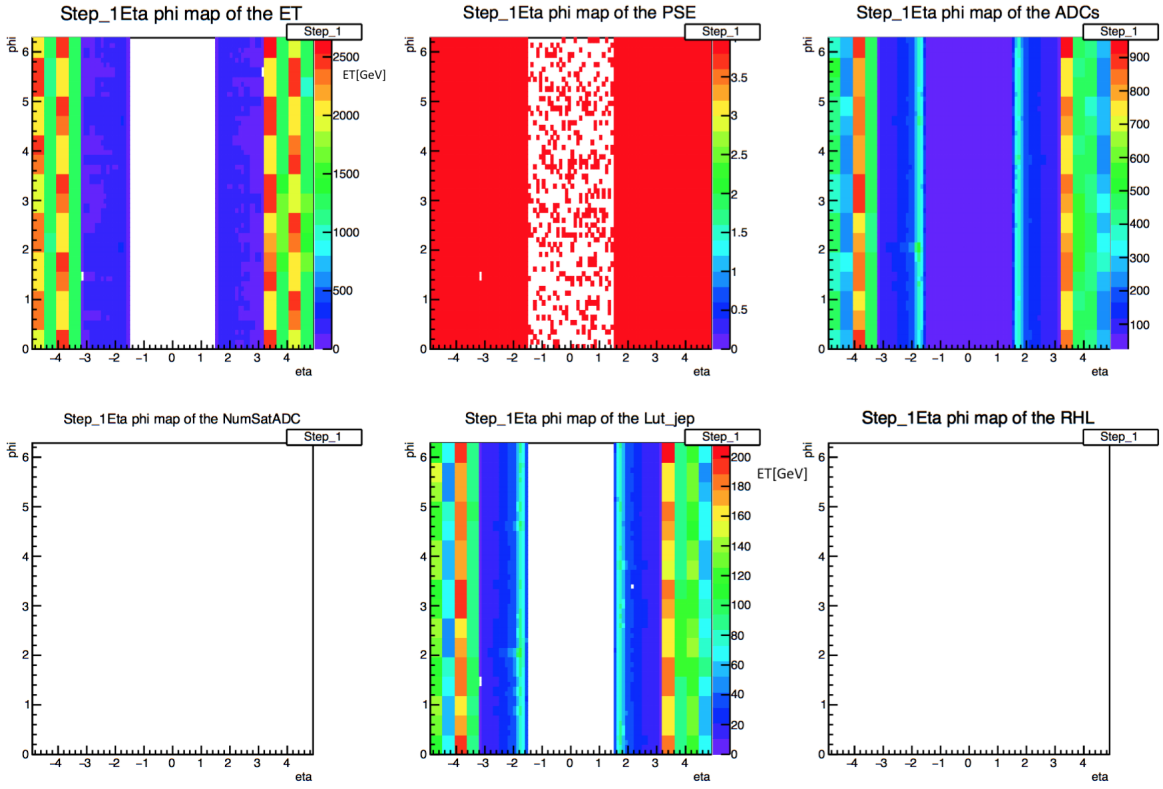

Figure A.7: Starting from the top left, the six quantities shown in the picture are: the transverse energy E_T, the PSE 3-bit, the ADCs counts, the number of saturated samples, the E^T_{LUT} and the result bit from the RHL 3-bit. These $\eta - \phi$ maps are taken from pulser runs referring to the hadronic layer of the LAr calorimeter. In this case the lowest energy step of the run is shown, and as one can see the energy is not high enough to produce the saturation of the samples. The PeakFinder worked for less than 3 saturated samples in this calibration run.

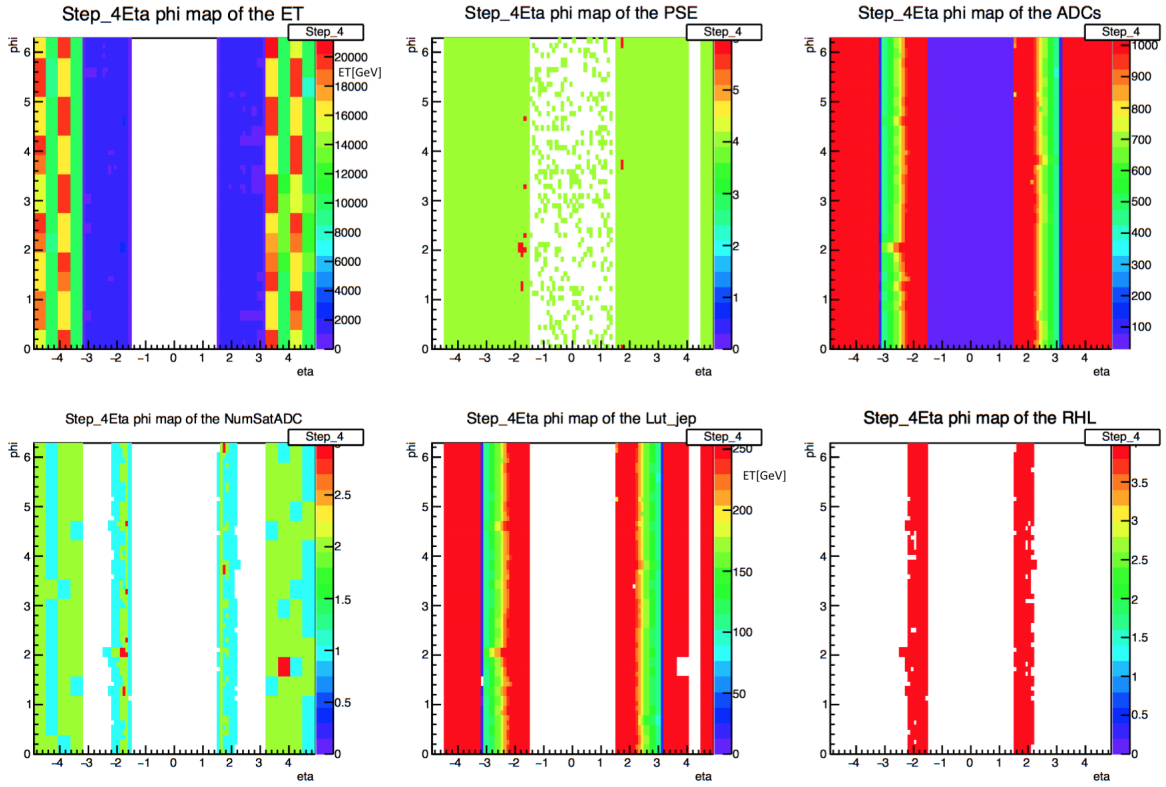

Figure A.8: Starting from the top left, the six quantities shown in the picture are: the transverse energy E_T, the PSE 3-bit, the ADCs counts, the number of saturated samples, the E^T_{LUT} and the result bit from the RHL 3-bit. These $\eta - \phi$ maps are taken from pulser runs referring to the hadronic layer of the LAr calorimeter. In this case the medium energy step of the run is shown, the samples start saturating and the SatBCID starts working too. The PeakFinder worked for less than 3 saturated samples in this calibration run.

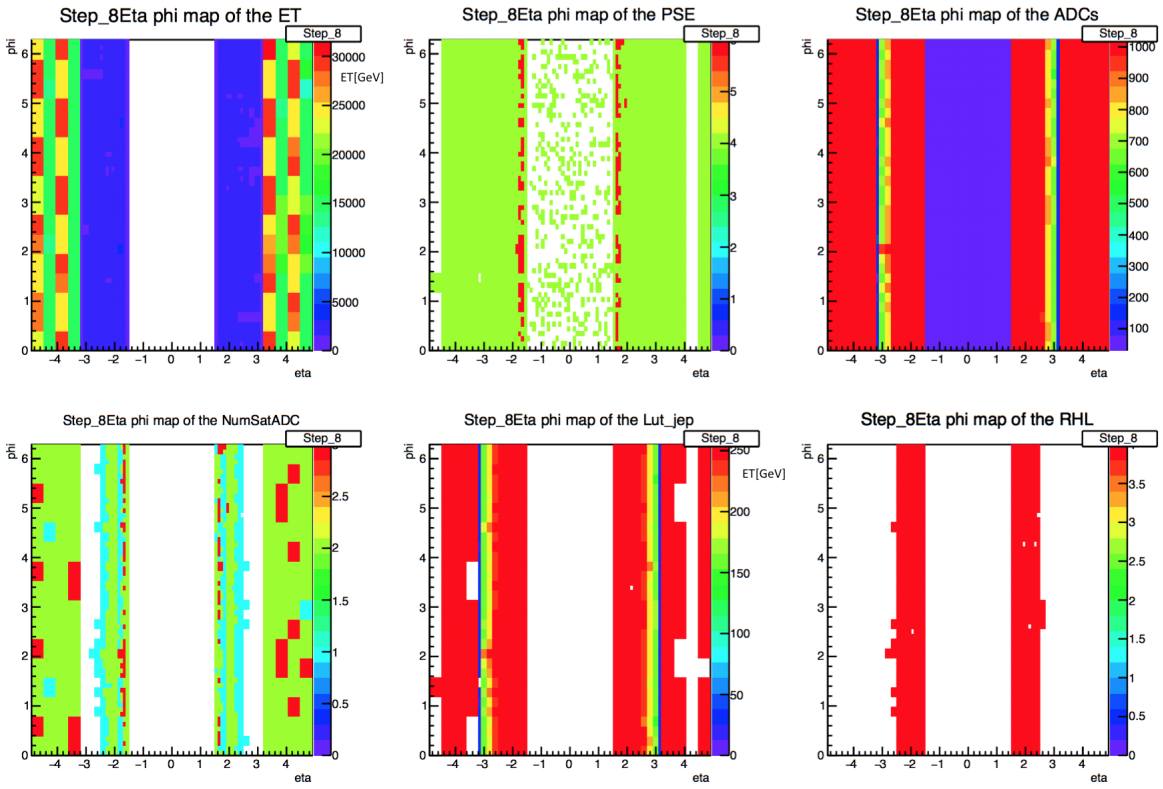

Figure A.9: Starting from the top left, the six quantities shown in the picture are: the transverse energy E_T, the PSE 3-bit, the ADCs counts, the number of saturated samples, the E^T_{LUT} and the result bit from the RHL 3-bit. These $\eta - \phi$ maps are taken from pulser runs referring to the hadronic layer of the LAr calorimeter. In this case the highest energy step of the run is shown, the samples are saturated. The PeakFinder worked for less than 3 saturated samples in this calibration run.

Appendix B

New Tile ADC correlation plots

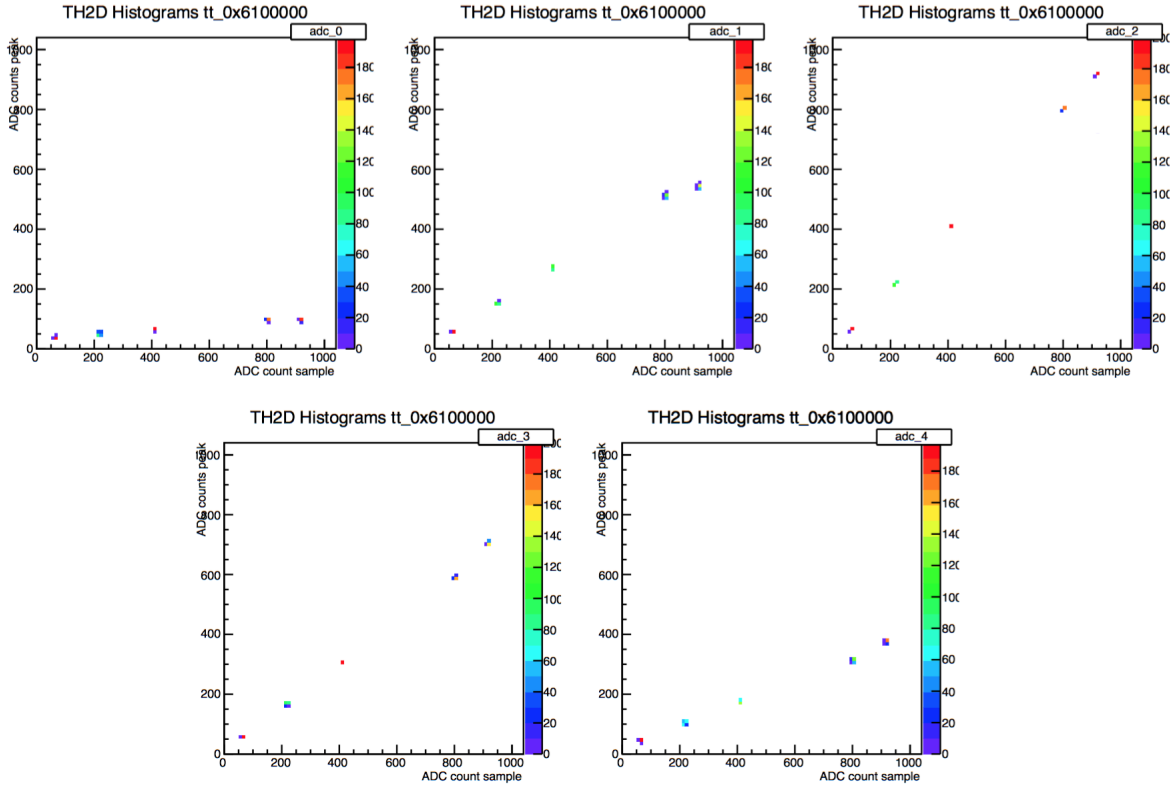

Figure B.1: The ADC counts correlation after having discarded the mistimed events is shown in this picture. In the top right box the position of the ADC sample is indicated. One can easily see that the double edge is disappeared. Therefore, we found that that few nonlinear events were due to a timing anomaly for Tile.

Bibliography

[1] ALICE Collaboration, *The ALICE experiment at the CERN LHC*, JINST 3 (2008), S08002.

[2] A. Bazan at all, *The Athena Data Dictionary and Description Language*, 2003.

[3] ATLAS Collaboration, *The ATLAS Experiment at the CERN Large Hadron Collider*, JINST 3 (2008) S08003.

[4] The ATLAS TDAQ Collaboration, *The ATLAS Data Acquisition and High Level Trigger system*, JINST 11 (2016), P06008.

[5] ATLAS Collaboration, *The ATLAS Calorimeter Performance*, 1997.

[6] CMS Collaboration, *The CMS experiment at the CERN LHC*, JINST 3 (2008),S08004.

[7] The ATLAS Collaboration, *Observation of a new particle in the search for the Standard Model Higgs boson with the ATLAS detector at the LHC*, arXiv:1207.7214 (31 August 2012).

[8] Private communication, Falk Bartels Bachelor Thesis (KIP Web) .

[9] The ATLAS L1Calo Collaboration, *The ATLAS Level-1 Calorimeter Trigger*, JINST 3 (2008), P03001.

[10] Martinez, Besson and Morange *Update on the study and validation of the BCID of the L1Calo at vary high transverse energies*, 2012.

[11] Marek Palka on behalf of the ATLAS collaboration *Operation of the enhanced ATLAS First Level Calorimeter Trigger at the start of Run-2*, (2016) JINST 11.

[12] The ATLAS L1Calo Collaboration, *The ATLAS Level-1 Calorimeter Trigger: PreProcessor implementation and performance*, (2012) JINST 7 .

[13] Lyndon Evans and Philip Bryant, *LHC machine*, JINST 3 (2008) S08001.

[14] CERN PublicWebPages, *The accelerator complex*, http://public.web.cern.ch/public/en/Research/AccelComplex-en.html, 2010.

[15] Steven Weinberg, *Conceptual foundation of the unified theory of weak and electromagnetic interactions*, (1979) Reviews of Modern Physics, Vol. 52 No. 3 .

[16] Steven Weinberg, *Gauge unification of fundamental forces*, (1979) Rev. Mod. Phys. 52, 525 .

[17] SL Glashow, *Toward a Unified Theory: Threads in a Tapestry*, (1980), Science 19 Dec 1980:Vol. 210, Issue 4476.

[18] G.Barnad *GAUDI - A Software Architecture and Framework for building HEP Data Processing Applications.*

[19] Murray Gell-Mann, *Symmetries of Barion and Mesons*, (1962) Phys. Rev. 125 .

[20] P.W. Higgs, *Broken symmetries and the masses of gauge bosons*, (1964) Phys. Rev. Lett. 13, 508.

[21] LHCb Collaboration, *The LHCb Detector at the LHC*, JINST 3 (2008), S08005.

[22] The ATLAS L1Muon Collaboration, *The Level-1 Trigger Muon Barrel System of the ATLAS experiment at CERN*, (2009) ATLAS-DAQ-PUB 2009-001.

[23] Private communication, Claire Antel PhD thesis in progress, 2016.

[24] TOTEM Collaboration, *The TOTEM experiment at the CERN LHC*, JINST 3 (2008), S08007.

Acknowledgements

"Sento la vita che mi scoppia dentro al cuore,
cammina l'uomo quando sa bene dove andare."
Il popolo canta la sua liberazione, Claudio Chieffo

There are many people which I am grateful to, for the help they gave me during this work.
First of all, I would like to thank my supervisors, Prof. Anna Di Ciaccio and Prof. Hans-Christian Schultz-Coulon. Their joined work and patronage allowed me to carry out this master thesis.
I am also very thankful to Dr. Martin Wessel, Dr. Rayner Stamen, Sebastian Weber and all the Master and PhD students of the KIP ATLAS group. They taught me a lot and gave me constant help in the realization of this final work. Moreover, they treated me as a part of the group from the beginning of my work and they supported me in the initial difficulties. Their guidance makes me discover different scenarios of the modern particle physics I would hardly approached alone.
An heartfelt thanks to my family, especially to my parents. Without the education, inspiration and support they gave me over all these years I would never reached this goal.
I would also like to thank all the friends near and far that accompanied me during this year abroad: Veronica, Michael, Massimo, Carol, Maria Concetta, Aldo, Roberto, Elisabetta, Andrea, Ester and many others. Thanks to their everyday encouragement and company I have never lost the right way.